Primordial Magnetic Fields And Early Structure Formation In The Universe

Thesis submitted to

Jawaharlal Nehru University, New Delhi (India)

for award of the degree of

Doctor of Philosophy

Kanhaiya Lal Pandey

Raman Research Institute
Bangalore - 560 080 (India)

(2013)

Primordial Magnetic Fields And Early Structure Formation In The Universe

by

Kanhaiya Lal Pandey

under the supervision of

Prof. Shiv K. Sethi

A Thesis for the degree of

Doctor of Philosophy

Raman Research Institute
Bangalore - 560 080 (India)

(2013)

DECLARATION

I hereby declare that the work reported in this thesis entitled "**Primordial Magnetic Fields And Early Structure Formation In The Universe**" has been independently carried out by me at the *Raman Research Institute, Bangalore,* under the supervision of *Prof. Shiv K. Sethi*. The subject matter presented in this thesis has not previously formed the basis of the award of any degree, diploma, associateship, fellowship or any other similar title.

Prof. Shiv K. Sethi
(Thesis Supervisor)

Kanhaiya L. Pandey
(The Candidate)

Astronomy & Astrophysics Group
Raman Research Institute
Bangalore 560 080
India.

CERTIFICATE

This is to certify that the thesis entitled "**Primordial Magnetic Fields And Early Structure Formation In The Universe**", submitted by *Kanhaiya L. Pandey* for the award of the degree of Doctor of Philosophy of Jawaharlal Nehru University, is his original work. This has not been published or submitted to any other University for any other degree or diploma.

Prof. Ravi Subrahmanyan
(Director)

Prof. Shiv K. Sethi
(Thesis Supervisor)

Astronomy & Astrophysics Group
Raman Research Institute
Bangalore 560 080
India.

Acknowledgements

I believe that the success of any project depends largely on the encouragement and guidance of many, and I must admit that this thesis would not have been possible without the kind support and help of many individuals and organizations. I am writing this section to take an opportunity to express my gratitude to all those people who have been helpful in the successful completion of this thesis work.

First of all I would like to thank RRI as an organization for providing me a place and a nice healthy academic atmosphere to work here as a PhD student. It has been a really good experience to be in RRI. I express my gratitude to all of them who have / had been involved in the establishment and nurturing of this institute.

My Special thanks of gratitude to Shiv for being my thesis adviser and giving me timely suggestions and support. He has been a great teacher all along, I benefited immensely from his constructive criticism and suggestions. I have learnt a lot from him and most importantly how to be patient. He has always encouraged me to think in new ways and gave me a lot of freedom. I would like to convey my sincere regards and respect for his valuable involvement during the period of my graduate research. I would also like to thank Bhargavi for her kind hospitality and delicious food, which I get whenever I go to Shiv's home.

I thank the members of my supervisory committee, Biman, Sam, Ravi and Dwarka for the fruitful academic discussions, and practical advices which helped me a lot all along. I must also thank all the faculty members of our astro floor, Sridhar, Biswajit, Ramesh, Uday, Shukre, CRS and Laxmi for all the help, support, encouragement and several valuable scientific discussions on various occasions.

I would also like to express my gratitude to Desh, Sesh and Srikanth for all their support, help and encouragement, for many valuable academic / non-academic discussions and even more importantly for their friendly gesture all along.

I thank all my collaborators, especially Dr. Zoltán & Dr. Kahniashvili for all the scientific discussions, help and encouragement.

Thanks to Vidya for her support and care, her immense patience, and prompt and timely help for any administrative issue. I must thank Laxamamma and Hanumatappa also for 3 o'clock tea and all other assistance. Thanks to the very supportive RRI administration, Krishna, Marisa and Radha for being very proactive in their help, the computer department, Jacob, Krishnamurthy, Nandu and Sridhar for their timely assistance with the computer related problems, our canteen people for providing healthy food, our very friendly library staff members for maintaining the library in a very efficient manner, es-

pecially Kiran, Nagraj, Manjunath, Meera, Geetha and Vrinda for all the help in library related matters. Many thanks to the housekeeping staff of RRI for making my stay in RRI a pleasant and enjoyable experience. I thank our hostel-mess cooks Yashodamma, Ratnamma, Padmaji, Mangalaji and other staff for healthy food and environment at the hostel.

I must also thank all my friends at RRI who made my stay in RRI memorable. I really enjoyed their company all along. Many many thanks to my old friend Laxmi Narayan Tripathi (IISc), who has been like a family member for me here in Bangalore, for all his help and support. I thank Yogesh, Wasim, Peyush, Ruta, Kshitij, Shashikant, Poonam, Siddharth, Chetana, Raman, Harsha, Samarth, Sharanya, Nithya, and Harshal for various valuable discussions with them through which I developed my understanding of various topics in astrophysics and other related subjects. I thank Nishant, Mamta, Giri, Pragya, Madhukar, Chandreyee, Nipanjana, Mahavir, Jagdish, Lijo and Nazma for all the help and companionship. I would also like to thank my hostel friends Satyam, Rakesh, Bharat, Suresh, RK and JK for introducing sports into my daily routine and also thanks to Radhika, Renu and Santosh especially for letting me grab some of their food on many Sundays, what they cooked for themselves. Let me thank all my old, new, Facebook and non-Facebook friends here collectively, for all the wishes, comments, tagging, liking & sharing, which made my leisure times happy and joyful.

Last, but certainly not the least, I wish to thank and express my gratitude towards my beloved parents. They took care of all the family responsibilities on their own so that I can concentrate fully on my research work without any hassle. I must also thank Gayatri bua for taking care of my parents, whenever they needed it, during my absence at home. Without their moral and practical support throughout, I would not have been able to complete this task.

Now finally, in memory of my grandfather who, to me, was a very simple, easy going, down to earth, a thoughtful person, and who was a great admirer of the slogan “Jai Jawan, Jai Kisan, Jai Vigyan”, I would like to dedicate this thesis to the whole community of the farmers, whose contribution to the humanity is immense but ironically the least rewarded.

Preface

This thesis contains the study of the implications of the primordial magnetic fields for early structure formation in the Universe and the bounds on primordial magnetic field parameters coming from various cosmological observables such as, cosmic microwave background polarization, large scale structure formation, weaklensing shear, and Lyα opacity.

Based on recent observations of magnetic fields in the cosmos, indicating their presence in clusters, super-clusters, even in the intergalactic medium and high redshift galaxies, it is now commonly believed that magnetic fields exist in the whole universe quite ubiquitosly. These cosmic magnetic fields in turn indicates the existence of magnetic fields in the early universe, which would have been generated in the very early universe, possibly during the inflation or other early phase transitions in the Universe. The existence of magnetic fields in the early universe can alter the course of structure formation in several ways. One of those is the extra matter perturbations (over and above inflationary matter perturbations) sourced by the existence of these primordial magnetic fields during recombination era. After recombination these matter perturbations also would grow and take part in the structure formation. This can lead to extra power in the matter power spectrum at scales around $\sim$ 1–10 h Mpc^{-1}. At the other hand presnce of sufficiently strong magnetic fields can even lead to heating of the ambient medium via decay of magnetic field energy due to ambipolar diffusion and decaying turbulence in the medium, and therefore affect the structure formation as thermal history plays an important role in this process. Thus we see that the existence of the primordial magnetic fields can influence the matter distribution in the univesre. And therefore the cosmological probes of the matter distribution in the universe are expected to have signatures of the existence of primordial magnetic fields. Using these observables we can actually probe the existence of primordial magnetic fields and put bounds on the physical parameters related to them. These were the main motivation behind this thesis work.

Following is the summary of the actual thesis work,

$*$ **Implications of primordial magnetic fields for early structure formation**

- **Formation of supermassive black holes (SMBH) at very high redshifts:** This work is about the investigation of possible role of primordial magnetic field to solve the puzzle of the formation of early super massive black holes posed by some SDSS observations of early (z $\simeq$ 6) bright quasars. Many models have been proposed to solve this mystery based on super-Eddington accretion or hierarchal merger models.

All the models make very optimistic assumptions and have their own share of problems. Presence of magnetic field also affects the course of thermal and dynamical evolution of collapsing gas because of the dissipation of the magnetic field energy in the medium. Our work suggests that if the magnetic field strength is above a critical value ($\sim$ 3.5 nG), it can actually lead to the formation of more massive stars $\simeq 10^4$ $M_\odot$. The black holes left behind after the death of these stars will have enough time to accrete gas to become a 10^8 $M_\odot$ SMBH by the redshift of 6–8. This model avoids many of the odd assumptions which are required in other models. Though this model requires a larger magnetic field value than the available bounds on primordial magnetic fields and relies on metal-free primordial gas, these value of magnetic fields are allowed under $\sim$ 2–3 σ upward fluctuation of the Gaussian random primordial magnetic fields which is sufficient to account for the number of high redshift quasars observed. Metal-free gas is not a bad assumption for the primordial gas at the redshift of z $\sim$ 15. Over all this model presents a plausible novel mechanism to form high redshift supermassive black holes.

$*$ **Bounds on primordial magnetic fields coming from various cosmological parameters**

- **Cosmic Microwave Background Polarization & Large Scale Structure formation:** In this work we have studied the limits on primordial magnetic field coming from various cosmological probes such as, Faraday rotation of Cosmic Microwave Background (CMB) polarization plane and statistics of large scale structures in the universe. The presence of primordial magnetic field during recombination causes a rotation of the CMB polarization plane due to the Faraday effect. The rotation angle is proportional to the magnetic field strength. Primordial magnetic field can also induce formation of structures in the Universe. Unlike the ΛCDM matter power spectrum, the magnetic field induced matter power spectrum increases at small scales (up till a cut-off at magnetic Jeans scale) and it plays an important role in the formation of the first structures in the Universe also. The smallest structure to collapse at $z \simeq 10$ in the ΛCDM model are 2.5σ fluctuations of the density field as opposed to the magnetic field case where 1σ collapse is possible. This means the number of collapsed halo is more abundant in the later case. This result is crucial in finding the bounds on the strength of primordial magnetic field, since the WMAP results suggests that the Universe reionized at z = 10, combining these two one can put bounds on the primordial magnetic field strength. From the analysis in this work we find that the range of the acceptable values of magnetic field strength is below 1-3 nG.

- **Cosmological weak lensing shear:** In this work we have calculated a theoretical estimate of shear power spectrum and the shear correlation functions, taking into account the effect of primordial magnetic fields on matter power spectrum. Comparing this result with the CFHTLS weak lensing data (Fu et al., 2008), we have found limits on primordial magnetic fields which are much stronger ($\sim$ 0.5 nG for the spectral index value $n_B = -2.8$ under the confidence level of 5σ) in comparison to the existing limits on primordial magnetic fields coming from CMB data.
- **Lyα effective optical opacity:** This work is an extension of the previous work, with the same motive but this time the observable is the line of sight distribution of Lyα clouds. We have simulated one dimensional distribution of Lyα absorbers along the line of sight and calculated effective Lyα opacity as function of redshift. Using observed data of effective Lyα opacity from Faucher-Giguère et al. (2008) we have calculated bounds on primordial magnetic field, which turned out to be even stronger than our previous estimates ($B_0 \sim 0.2 - 0.3$ nG for n_B = -2.8 with the confidence level of 5σ). In this analysis we have considered two cases, one when the magnetic field induced perturbations are uncorrelated with inflationary perturbations, and the other is when they are correlated, though the final results (bounds on B_0) are not very different for both the cases.

The work presented in this Thesis has been already published, the details of which are as following :

Publications

1. Supermassive Black Hole Formation At High Redshifts Through A Primordial Magnetic Field, Shiv K. Sethi, Zoltan Haiman, Kanhaiya L. Pandey 2010, *ApJ* 721, 615

2. Primordial Magnetic Field Limits From Cosmological Data, Tina Kahniashivili, Alexander G. Tevzadze, Shiv K. Sethi, Kanhaiya L. Pandey, Bharat Ratra 2010, *PRD* 82, 083005

3. Theoretical Estimates Of Two-point Shear Correlation Functions Using Tangled Magnetic Fields, Kanhaiya L. Pandey, Shiv K. Sethi 2012, *ApJ* 748, 27

4. Probing Primordial Magnetic Fields Using Lyα Clouds, Kanhaiya L. Pandey, Shiv K. Sethi 2012, *ApJ* 762, 15

Contents

List of Figures

List of Tables

1 Introduction

1.1 Magnetic Fields In The Universe

Magnetic field is another manifestation of electromagnetic force field, which is one of the four fundamental forces (others are gravitational, weak & strong nuclear forces) in the universe known to humankind by now, and after strong nuclear force the second strongest amongst them. Since the universe as we know it today, is charge neutral globally as well as locally, we do not need to worry about the electrical forces but, whenever we encounter plasmas, which is very common in astrophysical systems, magnetic field effects come into the picture. In most of the cases these magnetic fields are strong enough to influence the dynamics of the system significantly. No wonder magnetic fields play an important role in almost every area of astrophysics. Formation of planetary and stellar objects, production of jets and outflows, synchrotron sources like radio galaxies and neutron stars, accretion disks, inter stellar medium (ISM), supernovae and gamma ray bursts (GRBs) are just a few examples.

From observations, we know that the magnetic fields are present quite ubiquitously in the universe. Small scale objects like planets and stars, at large scale tenuous gas in the inter stellar medium of galaxies and even more tenuous intracluster medium are all magnetized. The first extraterrestrial magnetic field were observed in sunspots by Hale 1908. Starting from 1949, microgauss strength magnetic fields have been observed in several galaxies coherent over galactic sizes $\simeq$ 10 - 100 kpc, weaker magnetic fields have been observed with coherence length scales up to cluster sizes, and there is evidence of supercluster scale magnetic fields also. Origin and the maintenance of magnetic fields coherent over such cosmological scales is still an unresolved issue in astrophysics.

How did the Universe get magnetized at the first place? Is magnetic fields in the universe a result of top-down process, ie. a weak uniform magnetic field formed during

very early universe and propagated to small scale objects as they collapsed, or bottom-up process like structure formation in the ΛCDM, in which it would have been created in small scale objects like stars and accretion disks first and then propagated to large scales through outflows and bursts. The two leading theories for the origin and the maintenance of the galactic magnetic fields representing the above two scenarios are the dynamo model (bottom-up) and the primordial magnetic field model (top-down). These two theories are quite different from each other in the sense of the initial conditions and what they predict about the galactic magnetic fields. The concept of primordial magnetic theory initially came as an attempt to understand the galactic/cosmic magnetic fields, as battery mechanisms to generate magnetic fields were unable to explain μG level of galactic magnetic fields. Dynamo theories came later.

According to primordial magnetic field theory the cosmic magnetic fields (magnetic fields with very large coherence length) were generated in the very early universe (possibly during inflation). These cosmic magnetic fields got amplified by flux freezing and got twisted around the galactic center, along with the process of galaxy formation and this is what we see as galactic magnetic fields. The magnetic diffusivity of galaxy was assumed to be very low and in this case there is no need of any mechanism to maintain the magnetic fields once it got created.

Later it was realized that, the magnetic field diffusivity could be very high inside a galaxy because of the turbulent nature of the galactic medium, and the magnetic field would quickly decay at all scales. Therefore the galactic magnetic field has to be maintained by continuous regeneration of magnetic field by fluid motion. And thus people started approaching the problem using dynamo theory.

1.2 Large Scale Magnetic Fields

While analyzing MHD problems in the astrophysical context the usual practice is to divide the total magnetic field into two components (known as two-scale theory first used by Steenback, Krause & Rädler (1966)), the uniform large scale component $\mathrm{B_u}$ and a random component $\mathrm{b_r}$ which is such as $\langle \mathbf{b_r} \rangle = 0$, the total field becomes $\mathbf{B} = \mathbf{B_u} + \mathbf{b}$ with $\langle \mathbf{B} \rangle = \mathbf{B_u}$ and $\langle \mathrm{B}^2 \rangle = \mathrm{B_u^2} + \langle \mathrm{b}^2 \rangle$. Among large scale magnetic fields, galactic magnetic fields have been studied in quite detail. Our own galaxy the Milky Way provides us with the spatial detail of galactic magnetic field, whereas large number of external galaxies give us the global field structure that is unattainable from the Milky Way. Though there are several observational tracers to probe the magnetic fields, they respond only to either the plane of the sky component $\mathrm{B}_\perp$ or the line of sight component $\mathrm{B}_\parallel$. The total

magnetic field in a galaxy can be estimated from the nonthermal radio emission, assuming equipartition between the magnetic field energy and kinetic energy of the relativistic particles. Intensity and polarization of observed synchrotron radiation, polarization of star light and polarization of infrared emission from the interstellar dust are the main probes of $\mathrm{B}_{\perp}$, Faraday rotation and Zeeman splitting are used to probe $\mathrm{B}_{\parallel}$. Based on the these observational tracers, magnetic fields have been mapped for several galaxies. The morphology and the symmetry features of the galactic magnetic fields constrain theory of its origin and evolution. In spiral galaxies the magnetic fields have been found to be mostly parallel to the galactic plane and field lines closely follow the optical spiral arms of the galaxy. There are cases when we do not see a well defined material spiral arms (flocculant and irregular galaxies) but we see a definite spiral magnetic field lines. The total magnetic field strength is generally highest at the position of optical spiral arms, whereas the highest regular fields are found in the interarm region of the spiral galaxy. The mean equipartition value of the total magnetic field is around 10 μG, the strength of the regular field is of the order of 1-5 μG in the interarm region. From the measurements of polarization of synchrotron radiation at high radio frequencies coming from external galaxies one can estimate the relative energies in uniform and random component of the magnetic field and it is found that the energy in uniform component is about two-thirds of that of random component, and it can go to as low as 5% in the regions of heavy star formation. There are feeble evidence for magnetic fields in elliptical galaxies also Greenfield, Roberts & Bruke (1985); Moss & Shukurov (1996), the total field strength is similar to that of spiral galaxies but there are positive detection of polarized synchrotron emission, indicating almost zero uniform component of the magnetic field.

Large scale magnetic fields in galaxies can be categorized into several types based on their symmetry properties of their structure. Figure 1.2 and 1.3 shows such various possible configurations of the large scale galactic magnetic fields. On the basis of symmetry around the galactic axis magnetic fields could be either axisymmetric spiral (ASS) or bisymmetric spiral (BSS). Along the plane perpendicular to galactic plane it can have configurations like quadrupole (symmetric) and dipole (antisymmetric). ASS and BSS configurations can be distinguished observationally, it has been found that many galaxies have superposition of different modes with the exceptions like M31 and IC342 which show clear ASS field and M81 with dominating BSS field. In M51 galaxy there is evidence of two different magnetic field configuration for disk and halo, a halo with an axisymmetric field configuration parallel to disk and a superposition of axisymmetric and bisymmetric with about equal weights in the disk (Berkhuijsen et al. 1997).

Detections of synchrotron radiation and Faraday rotation from clusters of galaxies pro-

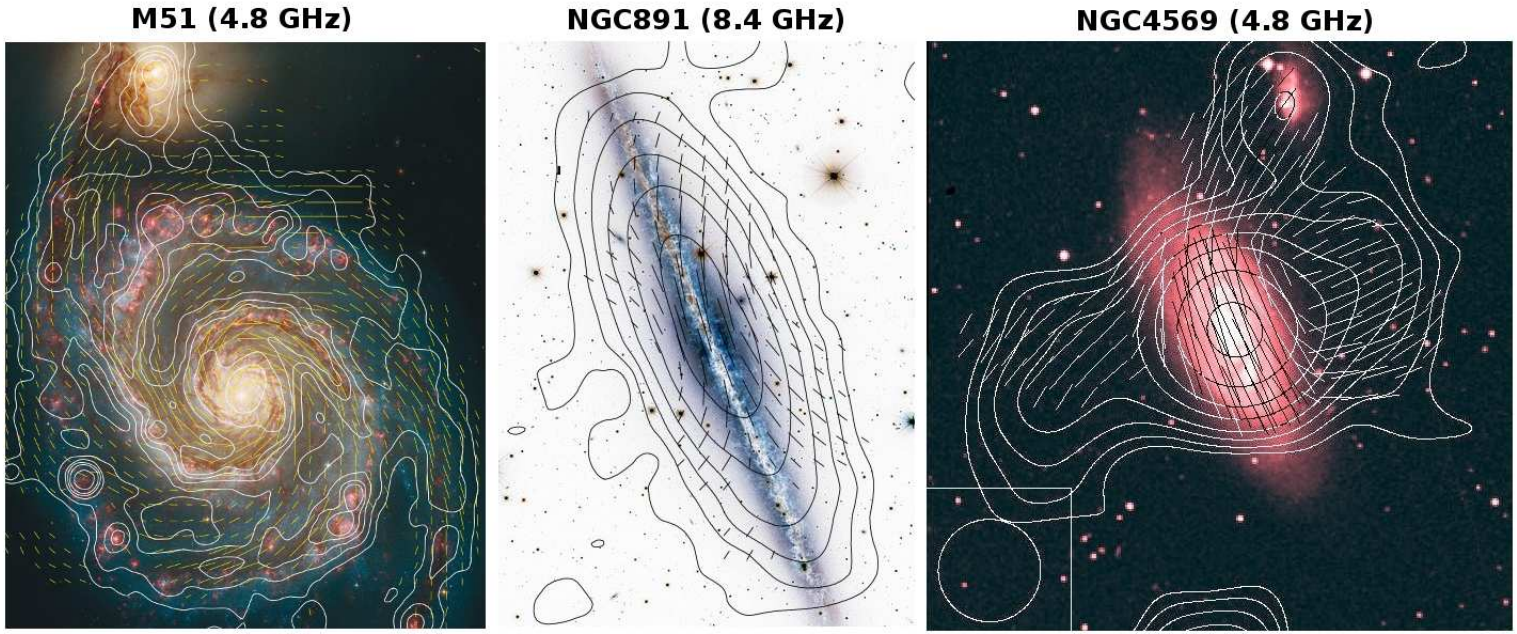

Figure 1.1: galactic magnetic fields of various galaxies overlaid on their optical images, the continuous lines are contours of radio intensity. Picture source: Max Planck Institute for Radio Astronomy ; http://www.mpifr-bonn. mpg.de/staff/rbeck/MKSP/pictures.html

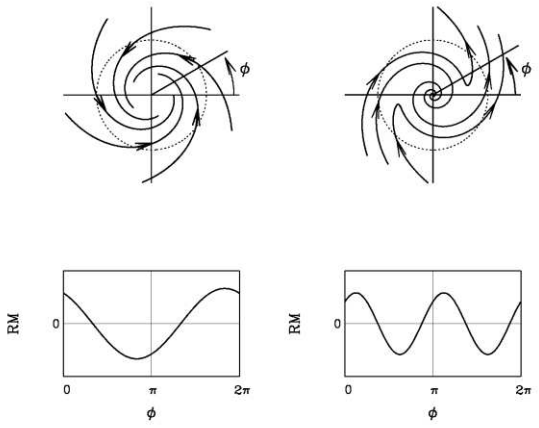

Figure 1.2: Axisymmetric (left side) and bisymmetric (right side) configurations of galactic magnetic fields. Picture source : Widrow (2002).

vide evidence for magnetic fields in the intracluster medium also. The polarization of synchrotron radiation coming from clusters is very low, indicating that the field is almost entirely random. The lower limits on the total field coming from these polarization studies are $B_t > 0.4\ \mu G$ and $B_t > 0.1\ \mu G$ (Rephaeli et al. (1994),Sreekumar, P. et al. (1996)). The coherent field over these scales have been estimated by excess mean RMs (above those of a control sample) of extragalactic radio sources located behind clusters of galaxies, the estimated value of the uniform (coherent) magnetic field over these scales by this method is about $B_u \approx 0.02\ \mu G$ (Kim et al. (1990),Kim et al. (1991). These magnetic fields in the cluster could have been ejected from the galaxies accompanied by the material ejecta of the radio jets or galactic winds. But measured strength of the magnetic field present in the intracluster medium is much larger than the field that would be obtained from the galactic ejecta only.

Even there are observations which suggests the existence of magnetic fields on supercluster scales Kim et al. (1989). Faraday rotation of quasars lying behind the high redshift galaxies show significant RM detection in their absorption line system. A radio interferometric study of a Lyα damped system in front of PKS1229-021 measured RMs that indicates existence of magnetic field of strength of a few microgauss at moderate redshifts ($\simeq$ 0.4)Kronberg et al. (1992). Athreya et al. (1998) did a multiband study of polarized radio emission coming from high redshift (z $\lesssim$ 2) radio galaxies and found significant RMs ($\gtrsim$ 1000) in most of the objects. RMs of this magnitude requires microgauss field coherent over several kpc.

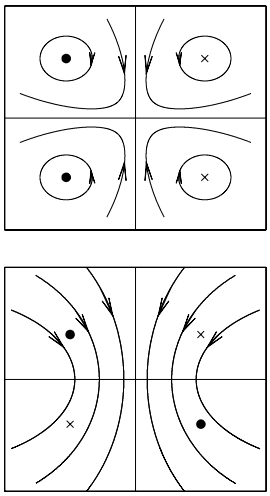

Figure 1.3: In the plane perpendicular to galactic plane the symmetric/quadrupole (top) and the antisymmetric/dipole (bottom) galactic magnetic field configurations. Picture source : Widrow (2002).

Though we still do not know whether cosmological magnetic fields are of primordial origin or not, there is evidence such as existence of magnetic fields over supercluster scales, in IGM and in early radio galaxies, which indicates that these magnetic fields are of primordial origin. A detection of sufficiently strong (nano Gauss strength) magnetic fields over large scales will support primordial origin theory. On the other hand even slightly weaker magnetic fields of primordial origin could be a good candidate for seed magnetic fields for the turbulent dynamo theories.

1.3 Origin Of Large Scale Magnetic Fields

There are two distinct possible ways to understand the existence of large scale (galactic scale and larger) magnetic fields in the universe. i) Sufficiently strong magnetic fields were already generated during the very early stages of the Universe ii) amplified version of already existing but comparatively weaker (seed) magnetic fields due to dynamo action. Again these seed magnetic fields could be of primordial origin or produced later by battery mechanism or it could be just the early stellar magnetic fields thrown out in the galactic medium during nova and supernova phase of the star. Similarly The extragalactic magnetic fields could be a result of thrown galactic magnetic fields by galactic winds/outflows/AGN activities.

It has been suggested that the primordial magnetic fields could have been generated during various early phases of the universe like the inflation, the electroweak phase transition, the quark-hadron phase transition, during the formation of the first objects or even during reionization Turner & Widrow (1988); Widrow (2002); Gnedin et al. (2000). As a matter of fact we do not have any observation which can confirm these theories, but still we can put theoretical limits on the strength of these primordial (cosmological) magnetic fields and probe it indirectly using some other cosmological observables. Several constraints of this kind have already been derived using Faraday rotation estimates of high redshift sources, estimates of anisotropy of the CMB caused by these cosmological magnetic fields, predictions of light elements abundance from big-bang nucleosynthesis (BBN) in the presence magnetic fields etc. For example based on 4-year Cosmic Background Explorer (COBE) data, Barrow (1997) suggested an upper limit on cosmological magnetic field which is $B \lesssim 5 \times 10^{-9} h_{75} \Omega^{1/2} G$ and coherent over scales larger than the present horizon size. Constraints from BBN suggests an upper limit of $B < 10^{-6}\, G$. These values are scaled to present epoch values, assuming the scaling relation as $B_t = a(t)^2 B_0$.

Other than primordial origin of magnetic fields there are battery mechanisms which can generate seed magnetic fields from zero magnetic field conditions. This process was first discovered by Biermann in 1950. The Biermann battery works on basis of relative motion of electrons and ions (since electrons are much lighter than their positively charged counterparts, the ions, and respond much more to a pressure gradient (force) in a medium) that give rise to a net electric field ($E_b = -\nabla p_e / e n_e$) in the medium, if this electric field has a curl it can give rise to magnetic field. Since $p_e = n_e k_B T$, the condition $\nabla \times E_b \neq 0$ indicates $\nabla n_e \times \nabla T \neq 0$ for this whole thing to happen, ie. the gradients ∇n_e and ∇T are not parallel to each other. Such scenario are not very rare in astrophysics the example could be the ionization fronts where the temperature gradient is normal to the front but the density gradient can have different direction as the ionization front is sweeping across the arbitrarily distributed density fluctuations. This mechanism can produce a seed magnetic field of strength of the order of $\sim 10^{-20}$.

Since the magnetic fields over larger scales than the galactic scales have not been observed in good details because of several observational limitations, the present day available detailed observations of galactic magnetic fields in our own Milky Way and other galaxies can provide a good probe to distinguish between the models. The salient features of the two models, the dynamo theory and the primordial theory are as given below

Dynamo theories : Magnetic field in a conducting medium can be amplified by the inductive effects associated with the motions of the medium, this process is generally referred to as dynamo. In the dynamo process the kinetic energy associated with the motions

in the medium is converted into magnetic energy. The medium inside galaxy or cluster is very turbulent and the dynamo action happening in these systems are commonly known as turbulent dynamo. Turbulent dynamos are conveniently divided into fluctuation (small scale) dynamo and the mean field (large scale) dynamo. Fluctuation dynamo produces magnetic fields that are correlated only over the scales which are comparable (or smaller) than the scales of energy carrying random/turbulent motions.

The fluctuation dynamo are generic to any random flow where magnetic Reynold's number R_m is greater than a critical value $R_{m,crit} \sim 30 - 100$, depending on the form of velocity correlation function. The field grows exponentially roughly on the eddy turn over time scale l_0/v_0, where v_0 is the typical variation in velocity over the scale l_0 with the magnetic field scale $l_B \sim l_0/R_m^{1/2}$. In the context of galaxy clusters turbulence are mainly be driven by the merging of subclusters and the typical values for the largest turbulent scales and the turbulent velocity would be $l_0 \sim 100\ kpc\ ;\ v_0 \sim 300\ kms^{-1}$, leading to a growth time $\tau_0 \sim l_0/v_0 \sim 3 \times 10^8\ yr$; thus for a cluster lifetime of a few Gyr, one could then have significant amplification by the fluctuation dynamo. And in the case of galactic interstellar turbulence driven by supernovae, if we take typical values to be $l_0 \sim 100\ pc, v_0 \sim 10\ kms^{-1}$ one gets $\tau_0 \sim 10^7\ yr$. Again the fluctuation dynamo would rapidly grow the magnetic field even for very young high redshift protogalaxies.

If the turbulence are helical the $\alpha\Omega$ mean field dynamo mechanism can play a role and produce magnetic fields at even larger scales (by inverse cascade of magnetic-energy/helicity). The interstellar medium is assumed to become turbulent, due to for example the effect of supernovae randomly going off in different regions. In a rotating, stratified (in density and pressure) medium like a disk galaxy, such turbulence becomes helical and thus $\alpha\Omega$ mean field dynamo can actually work in these kinds of system. In spiral galaxies large scale differential rotation (mean velocity) can stretch the radial field into azimuthal toroidal fields (Ω-effect), whereas small scale helical turbulence can convert the toroidal fields into poloidal fields (α-effect). In this also the magneto-fluid dynamics equations gives exponentially growth of magnetic fields as a solution for conditions which can be easily met in the spiral galaxies. The mean field grows typically on time-scales a few times the rotation time scales, of order 3-10 $\times 10^8$ yr. Unlike primordial origin theory this model can accommodate various shorts of galactic magnetic field configurations and can give explanations for them, This model also has gotten its own share of problems, validity of FOSA (first order smoothing assumption, on which theory relies) in the galactic medium is one of them. In the linear limit this theory is well worked out and works quite fine, but in the non-linear regime it becomes a very complex and complicated.

According to the simplest version of mean field dynamo theory, when the governing

equations are linear in B_u, the mean field B_u can grow exponentially in the low (but non-zero) resistivity limit. In the nonlinear regime when B_u becomes significant and its back reaction on the fluid motion becomes important, quenching of the magnetic field happens. It inhibits the dynamo action and the magnetic field gets saturated at some value. This happens when the magnetic field energy becomes of the order of the turbulent energy and thus B_u saturates at about its equipartition value. Early quenching of magnetic fields (α quenching problem) is one of the problems with this dynamo theory for galactic magnetic fields, though various theories have been already proposed and an active research is still going on to resolve these problems, because of complexity of the problem there are still some open questions to be answered.

Primordial origin theory : Just after the discovery of galactic magnetic fields Hoyle, F. (1958) came up with the idea of primordial magnetic fields to understand the existence of magnetic fields over galactic scales, as battery mechanisms can not produce such magnetic fields, dynamo theories were not known at that time. Later Piddington (1964, 1972), Howard & Kulsurd (1997) took forward this hypothesis. In this theory it is assumed that the large scale magnetic fields are of primordial origin and sufficiently strong magnetic field was already present before the formation of galaxies started and the present (large scale) galactic magnetic fields are just the primordial magnetic fields twisted by the differential rotation in the galaxy. This theory rely on low magnetic diffusivity of the galaxies and therefore there have not been any significant decay of the galactic magnetic fields. The primordial magnetic fields could have been generated during various early universe phase transitions. The exponential stretching of the vacuum fluctuations of the electromagnetic fields during inflation could produce magnetic fields coherent over very large scale. Other mechanisms like electroweak transition or QCD transition produce magnetic fields coherent over smaller scales and thus very tiny magnetic fields over galactic scales, unless helicity is also generated, in which case the inverse cascade of the energy to larger scales is possible. The problem with the inflationary model is that the electromagnetism is conformally coupled to gravity and therefore, in a spatially flat FLRW cosmology, the magnetic field generated during inflation will decay adiabatically ($B \sim 1/a(t)^2$, where a is the expansion factor), Turner & Widrow (1988) suggested that one need to break the conformal and gauge invariance of the electromagnetic action to get away with this effect. Various authors have attempted to find an effective and natural way to break conformal invariance and still research is going on in this field. In these models $B \sim 1/a(t)^\epsilon$ with typically $\epsilon \ll 1$ for getting a strong field. Since a is exponentially increasing during the inflation the predicted field strength is exponentially sensitive to any changes of the parameters of the model which affects the ϵ, and therefore these model of primordial magnetic

field generation can lead to a wide range of magnetic field strength based on the values of cosmological parameters used. The strongest field which can be generated by these mechanism is estimated to be around 10^{-9} G (redshifted to present epoch). A magnetic field of the strength $\sim 10^{-9}$ can also be sheared and amplified due to flux freezing, during the collapse to form a galaxy and lead to a microgauss field observed in several galaxies. The differential rotation wraps the field in a bisymmetric spiral, none of the field component reverses across the galactic mid plane, unless the field was initially nearly vertical in that case the field would be axisymmetric but with odd parity about the galactic mid plane.

Primordial magnetic field strength of a few nG coherent over Mpc scales could strongly influence several astrophysical processes which occurred during the early phases of the universe, and therefore signature of the primordial magnetic fields can be found in several cosmological observables like in CMBR temperature and polarization anisotropies have extensively been investigated. These fields have several implications in the process of early structure formation also. These effects of the primordial magnetic field will be discussed in detail in the following sections.

In summary, both the models have got their own share of difficulties in understanding of the origin of large scale magnetic fields, and explaining the observations, the dynamo theory of galactic magnetic field favours ASS configuration and even parity (quadrupole) structure along vertical B_{uz} direction, whereas primordial theory favours the BSS configuration with odd parity (dipole) structure along the vertical direction, a careful observation of these features in galactic magnetic fields can reveal which model is more close to reality. In observations we see most of the spiral galaxies have a mixture of ASS and BSS configuration of magnetic fields, though recent observation of quadrupole (even) symmetry of magnetic field in the Milky Way favours the dynamo model, since in the primordial theory it is difficult to sustain a quadrupole symmetric magnetic field which comes naturally as a favored solution in the dynamo theory. But again the existence of microgauss strength magnetic fields in disk galaxies at high redshift such as z $\approx$ 2 is a challenge for dynamo theory as they have very less time for amplification. A good understanding of magnetic field diffusion in the galaxies is also crucial for all these models and a better understanding of this process is needed to resolve the problem.

1.4 Modelling The Primordial Magnetic Fields

For the calculations the primordial magnetic field is assumed to be statistically homogeneous and isotropic Gaussian vector random process, in this case for this field the two

point correlation function in Fourier space can be written as,

$$\langle B_i(\mathbf{q})B_j^*(\mathbf{k})\rangle = \delta_D^3(\mathbf{q}-\mathbf{k})(\delta_{i,j} - q_i q_j/q^2)B^2(q) \tag{1.1}$$

where the first term in RHS assures the statistical isotropy and homogeneity, and the second term (known as transverse plane projector) is to assure that the field is divergence-less. The third term says that the magnetic field is assumed to follow a power law, $\mathbf{B}^2(k) = Ak^n$ for $k_{min} \leq k \leq k_{max}$. Where $A \simeq \pi^2(n+3)\langle B_0^2\rangle/k_{max}^{(n+3)}$, n is the spectral index. B_0 is given by following expression (Kim et al. (1996))

$$B_0^2 \equiv \langle B_i(\mathbf{q})B_j^*(\mathbf{k})\rangle = \frac{1}{\pi^2}\int_0^{k_c} dk\, k^2 B^2(k) \tag{1.2}$$

where k_c is the coherence length (smoothing scale, which is usually taken to be 1 Mpc). k_{min} is the scale which is set by the scales which crossed the horizon during inflation, if the number of e-folding during the inflation is very large $k_{min} \to 0$, in this thesis we will take $k_{min} = 0$ throughout. k_{max} is the scale at which damping of magnetic fields due to radiative viscosity (before recombination) becomes important, numerically this scale is given by (Sethi & Subramanian (2005))

$$k_{max} = 235 Mpc^{-1}\left(\frac{B_0}{10^{-9}\,G}\right)^{-1}\left(\frac{\Omega_m}{0.3}\right)\left(\frac{\Omega_b h^2}{0.02}\right)^{1/2}\left(\frac{h}{0.7}\right)^{1/4} \tag{1.3}$$

The energy density of the magnetic field is given by (Kahniashvili & Ratra, 2007)

$$\rho_B(\lambda) = \frac{B_\lambda^2 (k_D\lambda)^{n_B+3}}{8\pi\Gamma(n_B/2+5/2)}. \tag{1.4}$$

this Eqn tells us that the magnetic field energy goes as $k^{-(n_B+3)}$, and as $n_B \to -3$ the magnetic field energy spectrum becomes scale invariant. This case is actually favored by many primordial magnetic field origin theories such as (inflationary origin) and is ideal for a model of large scale primordial magnetic fields. In this thesis work we have mostly considered the spectral index n_B values close to -3.

1.5 Role Of Primordial Magnetic Fields In Early Structure Formation

1.5.1 Magnetic field induced density & velocity perturbations

In the linearized Newtonian theory, the magneto-hydrodynamic equations takes the following form in comoving coordinates,

$$\frac{d(a\mathbf{v}_b)}{dt} = -\nabla\phi + \frac{(\nabla\times\mathbf{B})\times\mathbf{B}}{4\pi\rho_b} \tag{1.5}$$

$$\nabla\cdot\mathbf{v}_b = -a\dot{\delta}_b \tag{1.6}$$

$$\nabla^2\phi = 4\pi G a^2(\rho_{DM}\delta_{DM} + \rho_b\delta_b) \tag{1.7}$$

$$\frac{\partial(a^2\mathbf{B})}{\partial t} = \frac{\nabla\times(\mathbf{v}_b\times a^2\mathbf{B})}{a} \tag{1.8}$$

$$\nabla\cdot\mathbf{B} = 0 \tag{1.9}$$

as our interest here is the scales over which perturbations are linear at present epoch ($k \lesssim 0.2$ h Mpc^{-1}),in equation (1.4) the pressure gradient term is neglected because it is important for length scales smaller than Jeans length ($> k \simeq 1\ Mpc^{-1}$). Again in equation (1.7) the resistivity term has been dropped assuming that the medium has infinite conductivity, further neglecting the right hand side (RHS) in equation (1.7) we get

$$\mathbf{B}(x,t)a^2 = constant \tag{1.10}$$

that means in the linear regime $\mathbf{B}$ simply redshifts as $(1+z)^2$.

Combining equations (1.4) and (1.5) gives,

$$\frac{\partial^2\delta_b}{\partial t^2} + 2\frac{\dot{a}}{a}\frac{\partial\delta_b}{\delta t} - 4\pi G(\rho_{DM}\delta_{DM} + \rho_b\delta_b) = \frac{\nabla\cdot[(\nabla\times\mathbf{B})\times\mathbf{B}]}{4\pi a^2\rho_b} \tag{1.11}$$

here the subscripts ‘b’ refers to baryonic and ‘DM’ refers to dark matter component. The above equation (eq 1.10) contains two source terms: dark matter + baryonic perturbations and the magnetic fields. The RHS in the equation (1.10) acts as an additional source term for density perturbations in the mhd fluid coming through the magnetic fields. If we drop the magnetic field terms in the above equations (eq 1.4-1.8 and 1.10) we get the fluid equations for the evolution of dark matter perturbations (eq 1.11).

$$\frac{\partial^2\delta_{DM}}{\partial t^2} = -2\frac{\dot{a}}{a}\frac{\partial\delta_{DM}}{\delta t} + 4\pi G(\rho_{DM}\delta_{DM} + \rho_b\delta_b) \tag{1.12}$$

The evolution dark matter component is not directly affected by the magnetic fields but does get affected indirectly through the baryonic component (eq 1.12).

$$\frac{\partial^2 \delta_m}{\partial t^2} = -2\frac{\dot{a}}{a}\frac{\partial \delta_m}{\delta t} + 4\pi G \rho_m \delta_m + \frac{\rho_b}{\rho_m} S(t,x) \tag{1.13}$$

where $\delta_m = (\rho_{DM}\delta_{DM} + \rho_b\delta_b)/\rho_m$ and $\rho_m = (\rho_{DM} + \rho_b)$. $S(t,x)$ is the source term from the magnetic fields (RHS of eq 1.7). The above equation can be easily solved using Green's function methods. Wasserman (1978) showed that the equation (1.12) admits a growing solution too, i.e., tangled magnetic fields can provide initial conditions for the growth of density perturbations. Furthermore the tangled magnetic fields give rise to both the divergence (compressional) and curl part of the velocity field (for details see Gopal & Sethi 2003).

1.5.2 Matter power spectrum of density field induced by primordial magnetic fields

The real space spatial density contrast and peculiar velocity component (induced by magnetic fields) along the line of sight can be given as (Wasserman 1978),

$$\delta(\mathbf{x}) = \nabla \cdot [\mathbf{B} \times (\nabla \times \mathbf{B})] \tag{1.14}$$

$$\mathbf{v}(\mathbf{x}) \cdot \hat{\mathbf{z}} = \nabla \cdot [\mathbf{B} \times (\nabla \times \mathbf{B})] \cdot \hat{\mathbf{z}} \tag{1.15}$$

Here $B \equiv B(\mathbf{x}, t_0)$, i.e., the value of magnetic field at the present epoch. In Fourier space the above expression becomes,

$$\delta(\mathbf{k}) = \int d^3k_1 [(\mathbf{k_1} \cdot \mathbf{B}(\mathbf{k} - \mathbf{k_1}))(\mathbf{k} \cdot \mathbf{B}(\mathbf{k_1})) - (\mathbf{k_1} \cdot \mathbf{k})(\mathbf{B}(\mathbf{k_1}) \cdot \mathbf{B}(\mathbf{k} - \mathbf{k_1}))] \tag{1.16}$$

$$\mathbf{v}(\mathbf{k}) = -i \int d^3k_1 [(\mathbf{B}(\mathbf{k_1}) \cdot \mathbf{B}(\mathbf{k} - \mathbf{k_1}))\mathbf{k_1} - (\mathbf{k_1} \cdot \mathbf{B}(\mathbf{k} - \mathbf{k_1}))\mathbf{B}(\mathbf{k_1})] \tag{1.17}$$

by choosing $\mathbf{k}$ to lie along the z-axis and $\hat{n}$ to lie in the $x - z$ plane, we have,

$$\int d^3k_1 = \int dk_1 k_1^2 \int d\mu \int d\phi \tag{1.18}$$

where $\mu \equiv cos\theta$ (θ is the angle between k_1 and the z-axis) and ϕ is the azimuthal angle. In the integral k_1 ranges from k_{min} to k_{max}, μ from -1 to +1 and ϕ from 0 to 2π. Since μ depends on k_1 ($\mu = \mathbf{k} \cdot \mathbf{k_1}/(kk_1)$), care needs to be taken while evaluating the above

integral, in fact the above integral can be computed by splitting it in three parts as following

$$\int d^3k_1 = \int_0^k dk_1 \int_{-1}^{+1} d\mu + \int_k^{k_{max}-k} dk_1 \int_{-1}^{+1} d\mu + \int_{k_{max}-k}^{k_{max}} dk_1 \int_{\mu_{max}}^{1} d\mu \qquad (1.19)$$

where $\mu_{max} = (k^2 + k_1^2 - k_{max}^2)/(2kk_1)$. Now $P(k)$ can be computed as $\langle \delta^2(\mathbf{k}) \rangle$, using equation (1.1) and simplifying we get the following expression for $P(k)$ (Gopal & Sethi (2003)),

$$P(k) = \int_{k_{min}}^{k_{max}} dk_1 \int_{-1}^{+1} d\mu \frac{B^2(k_1)B^2(|\mathbf{k}-\mathbf{k_1}|)}{|\mathbf{k}-\mathbf{k_1}|^2} \times [2k^5k_1^3\mu + k^4k_1^4(1-5\mu^2) + 2k^3k_1^5\mu^3] \qquad (1.20)$$

The above integral can be evaluated numerically. The plot of this integral for various values of magnetic field strength and spectral indices are given in the Figure (1.3) along with the standard ΛCDM inflationary matter power spectrum. In the plot the magnetic

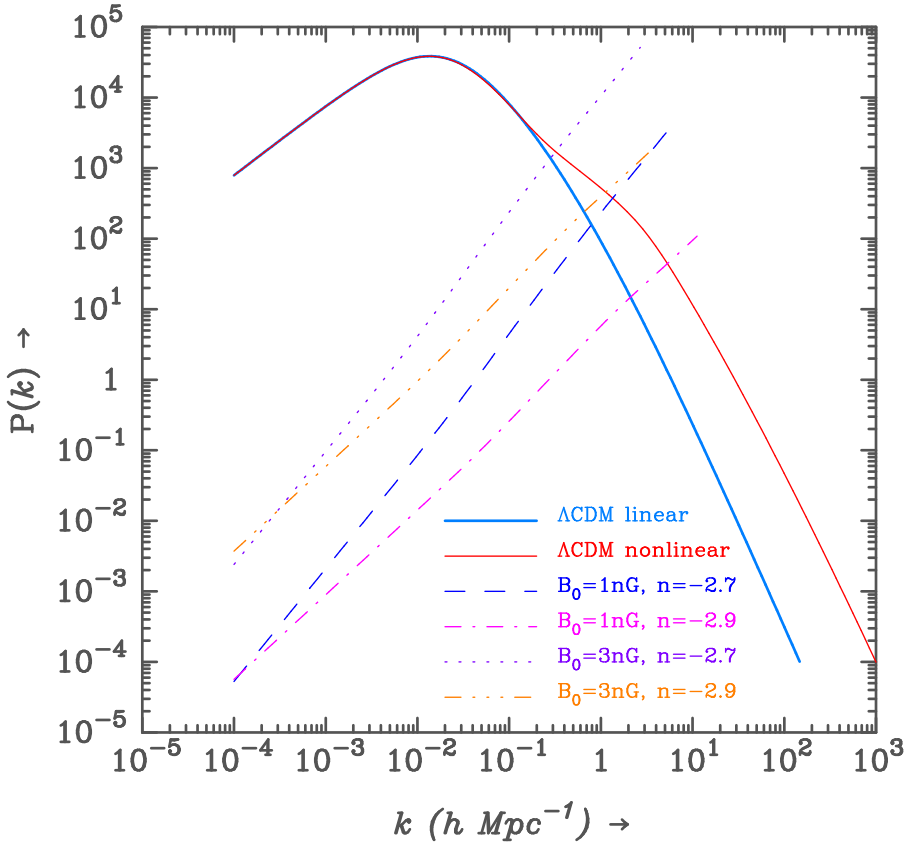

Figure 1.4: The Matter power spectrum is displayed for the magnetic and non magnetic cases. Magnetic field-induced matter power spectra are plotted for $k < k_{\rm B}$ in each case.

field induced matter power spectrum has been shown for the values of $k < k_{\rm B}$, where $k_{\rm B}$

is magnetic Jeans scale. In analogous to thermal Jeans scale $\lambda_{\rm J} = v_s(\pi/\rho G)^{1/2}$ this scale is given as $\lambda_{\rm B} = v_{\rm A}(\pi/\rho G)^{1/2}$ where $v_{\rm A}$ is Alfvén speed. Using the appropriate form of Alfvén speed $v_{\rm A}$ ($\equiv B/(4\pi\rho)^{1/2}$), we get the following formula to compute magnetic Jeans scale (Sethi & Subramanian (2005)),

$$k_{\rm J} \simeq 14.8\,{\rm Mpc}^{-1}\left(\frac{\Omega_m}{0.3}\right)^{-1}\left(\frac{h}{0.7}\right)\left(\frac{B_{\rm J}}{10^{-9}\,G}\right)^{-1} \tag{1.21}$$

where

$$B_{\rm J}(a) = B(k_{\rm J}, a)a^2(t) \quad and \quad B_{\rm J} = B_c(k_{\rm B}/k_c)^{\frac{n+3}{2}} \tag{1.22}$$

In the plot we can see that at smaller scales ($k > 0.1h{\rm Mpc}^{-1}$) there is appreciable enhancement in the matter power spectrum due to magnetic field generated perturbations, at these scales it is almost comparable to standard inflationary (λCDM) matter power spectrum, whereas at larger scales ($k << 0.1h{\rm Mpc}^{-1}$) it is almost negligible in comparison to inflationary matter power spectrum. Thus we see the existence of primordial magnetic fields can have implications in the matter distribution in the universe at smaller scales. Apart from this these primordial magnetic fields can have other implications also in early structure formation, for example decay of these fields via turbulence and ambipolar diffusion can heat the surrounding medium and this can affect several astrophysical processes including star formation etc., in the first chapter we will see how can this phenomenon have a role in understanding the early formation of super massive black holes.

1.6 This Thesis

The aim of this chapter was to set up the stage for the rest of the chapters which discuss my actual thesis work. In this chapter we learned that, there are some indications which suggests that there was some amount of magnetic field which existed during the primordial ages of the universe, and the existence of these primordial magnetic fields could influence the structure formation process in the universe. A quantitative knowledge of these effects can actually help us probing these primordial magnetic fields through various cosmological observables. The next chapter, **Chapter Two** of this thesis covers my first thesis project which was to study the possible role of primordial magnetic fields in understanding the puzzle posed by observations of very early (z = 6 - 8) but bright quasars ($M \simeq 10^{4-5}M_{\odot}$). The strength of the primordial magnetic fields play a key role in the analysis given in the chapter two. In the literature there are several bounds primordial magnetic field parameters (strength and coherence scale) have been proposed based on

various kinds of observations and theories but still we have very limited knowledge about them. Further chapters, **Chapter Three, Four** and **Five** discuss our work towards deriving constraints on primordial magnetic field strength coming from various cosmological observables. In the **Third Chapter** we discuss the large scale imprints of cosmological magnetic fields, such as, their effects on the formation of the first bound structures in the universe and the rotation of CMB polarization plane. As we saw in this chapter, the existence of primordial magnetic fields could produce extra matter perturbations over and above the inflationary matter perturbations, at very early stage of the universe. This would influence the matter distribution in the universe favorably at the scales which are smaller than ($k \sim 0.1\mathrm{Mpc}^{-1}$), these are the scales which are mainly probed by weak lensing and Lyα distribution. The **Fourth** and the **Fifth Chapter** is about the exercise of constraining the primordial magnetic field parameters using weak lensing shear analysis and the effective opacity of Lyα distribution along the line of sight. Finally the last chapter, **Chapter Six** is a brief discussion and conclusion about this whole thesis work.

2

Early Formation Of Supermassive Black Holes (SMBHs) : Role Of Primordial Magnetic Fields

2.1 Formation Of SMBHs At High Redshifts

With the advent of Sloan Digital Sky Survey (SDSS) and the other large area surveys discovery of very bright quasars with luminosity $\geqslant 10^{47}$ erg-s^{-1}) at high redshifts $z \gtrsim 6$ suggests that some supermassive object as massive as $10^9 M_\odot$ were already present when the universe was very young Fan (2006). Formation of such high mass objects at such an early stage of the universe poses a puzzle for astrophysics. Early population III stars of masses $\sim 100\ M_\odot$ are expected by the time of redshift $z \gtrsim 25$ (Abel et al., 2002; Bromm et al., 2002; Yoshida et al., 2008). Even if these stars leave behind similar mass black holes after they die out, the Eddington time for growing these seed black holes to the mass of $10^{8-9} M_\odot$ is of the order of the age of the universe. Thus we see that it is difficult to generate a SMBH of mass $10^{8-9} M_\odot$ from the given $10^2 M_\odot$ seed black holes unless considering a phase of super-Eddington accretion or using some very optimistic assumptions in hierarchical merger models (Haiman & Loeb, 2001; Yoo & Miralda-Escudé, 2004; Bromley et al., 2004; Shapiro, 2005; Volonteri & Rees, 2006; Li et al., 2007; Tanaka & Haiman, 2009).

In the models involving rapid (super-Eddingtopn) collapse the primordial gas rapidly gets accreted onto a pre-existing seed BH and collapses into a SMBH as massive as $10^{4-6} M_\odot$ (Oh & Haiman, 2002; Bromm & Loeb, 2003; Lodato & Natarajan, 2006; Spaans & Silk, 2006; Begelman et al., 2006; Volonteri et al., 2008; Wise et al., 2008; Regan & Haehnelt, 2009; Shang et al., 2010). These so called direct collapse models involve metal-free gas in relatively massive ($\gtrsim 10^8 M_\odot$) dark matter halos at redshift $z \gtrsim 10$, with virial temperature $T_{vir} \gtrsim 10^4 K$. The collapsing gas which collapse as it cools and sheds its angular momentum, must avoid fragmentation and collapse rapidly. These conditions are

very difficult to be satisfied simultaneously unless the gas remains warm i.e., at temperature $T_{vir} \sim 10^4$ K. An efficient formation of H_2 gas in such collapsing halos can cool the gas to the temperature of T $\sim$ 300 K (Shang et al., 2010), even if the fragmentation is avoided the inward flow of this cold gas is quite slow $\sim$ 2-3 km s^{-1} with a corresponding low accretion rate of $\sim 0.01\ M_\odot\ yr^{-1}$. We can get away with the H_2 cooling also in these models provided the gas is exposed to an intense UV flux J. The UV flux slows down the formation of H_2 by either directly photo-dissociating H_2 or photo-dissociating the intermediary H^-. To inhibit the formation of H_2 the photo-dissociation timescale, $t_{\rm diss} \propto J^{-1}$, has to be shorter than H_2 formation time scale, $t_{\rm form} \propto \rho^{-1}$. This leads to a critical UV flux density needed to inhibit the H_2 formation which is directly proportional to the density, $J^{\rm crit} \propto \rho$ for these halos the critical flux is high, $J \approx 10^2 - 10^5$ (Shang et al., 2010), at high redshifts only a small fraction of halos which are unusually close to UV bright sources may see this kind of flux, on the other hand, to avoid fragmentation the gas must remain metal/dust free (Omukai et al., 2008), which is not possible if the gas is nearby such luminous galaxies.

2.2 The Role Of Primordial Magnetic Fields

Magnetic heating can play an important role in keeping the collapsing gas warm. If we consider the existence of background primordial magnetic fields of strength (comoving) $\approx$ 1 nG (Widrow (2002) and references therein), it can be strongly amplified by flux-freezing inside the collapsing gas. This in turn will affect the H_2 formation and cooling. Sethi et al. (2008) have shown that 0.2 - 2 nG fields can significantly enhance the H_2 fraction during the early stages of the collapse, later Schleicher et al. (2009) found similar results, and emphasized that the magnetic heating from 0.1 - 1 nG fields can result in significantly high temperatures in halos with high densities $n \gtrsim 10^8$ cm^{-3}, which can be achieved during later stages of the collapse.

This work is an extension of Sethi et al. (2008) & Schleicher et al. (2009) with higher particle density in the collapsing halo and the higher magnetic field. The main result of this work is that, there exist a critical density $n_{crit} \approx 10^3$ cm^{-3} above which H_2 cooling is inefficient, and the temperature stays near $\sim 10^4$ K, even as the gas collapse further, for $B < B_{\rm crit}$, though H_2 cooling is delayed, the gas eventually cools down below $\sim$ 1000 K. Though the critical magnetic field value is higher than the existing upper limits on primordial magnetic field strength, it can be realized in the rare $\gtrsim 2-3\sigma$ regions of the spatially fluctuating B field. The abundance of the halos located in these high magnetic field regions is sufficient to explain the number of quasars observed at $z \approx 6$ in the SDSS

observations.

2.3 Chemistry And The Thermo-dynamical Evolution Of Collapsing Primordial Gas

2.3.1 Formation of molecular hydrogen

In the context of formation of the first objects in the universe, H_2 has an important role as a coolant. Elements heavier than Lithium were first formed inside during stellar evolution and supernova events, and hence when the first structure were being formed there was no better coolant than H_2 molecule for temperatures below $\lesssim 10000$ K. In the context of primordial universe when there were no dust grains, the formation of molecular hydrogen progresses through two channels with either H^- or $H_2{}^+$ in the intermediate stage. In the first process an electron attaches to a neutral hydrogen atom radiatively to form H^-,

$$H + e^- \xrightarrow{k_9} H^- + \gamma \tag{2.1}$$

which in turn form H_2 molecule by the reaction:

$$H^- + H \xrightarrow{k_{10}} H_2 + e^- \tag{2.2}$$

At the same time H^- ion can also be destroyed by energetic CMB photons, or used up in some non H_2 productive reactions, following are some of the important reactions of such kind which we have taken into account (k's are the corresponding reaction rates (Shang et al., 2010; Sethi et al., 2008)),

$$H^- + \gamma_{\rm cmb} \xrightarrow{k_\gamma} H + e^- \tag{2.3}$$
$$H^- + H^+ \xrightarrow{k_{13}} H_2^+ + e^- \tag{2.4}$$
$$H^- + e^- \xrightarrow{k_{19}} H + 2e^- \tag{2.5}$$
$$H^- + H \xrightarrow{k_{20}} 2H + e^- \tag{2.6}$$
$$H^- + H^+ \xrightarrow{k_{21}} 2H \tag{2.7}$$

The alternative channel through the formation of $H_2{}^+$ occurs when a proton acts as a catalyst:

$$H + H^+ \leftrightarrow H_2^+ + \gamma, \qquad H_2^+ + H \rightarrow H_2 + H^+ \tag{2.8}$$

There is also a third channel through the formation of HeH^+. Recently, Hirata & Padmanabhan have shown that the H^- channel dominates the production of the H_2 molecule, with only ~ 1 per cent contribution from the $H_2{}^+$ channel, and ~ 0.004 per cent from the HeH^+ channel. Therefore in this work H^- channel has been used in the calculations. The net rate of formation of H_2 through the H^- channel is given by:

$$k_m = \frac{k_9 k_{10} x_{HI} n_b}{k_{10} x_{HI} n_b + k_\gamma + (k_{13} + k_{21}) x_p n_b + k_{19} x_e n_b + k_{20} x_{HI} n_b}\,. \tag{2.9}$$

The notation of the reaction rates follows the appendix of Shang et al. (2010), except the k_γ which is the rate of destruction of H^- by CMB photons (eq. 8 in Sethi et al. (2008)). The net destruction rate of H_2, $k_{\rm des}$, is:

$$k_{\rm des} = k_{15} x_{HI} + k_{17} x_p + k_{18} x_e. \tag{2.10}$$

rate of formation of molecular hydrogen is then given by,

$$\frac{dx_{\rm H_2}}{dt} = k_m n_b x_e (1 - x_e - 2x_{\rm H_2}) - k_{\rm des} n_b x_{\rm H_2} \tag{2.11}$$

where symbols have there usual meaning.

2.3.2 Density evolution of the collapsing halo

The density from the equation of motion of a bound shell collapsing under gravity (for details see e.g. Peebles 1980; Padmanabhan 1993):

$$\ddot{r} = -\frac{GM}{r^2} \tag{2.12}$$

(ignoring the effect of cosmological constant at high redshift). The parametric solutions of this equation are given by

$$r = 2r_{vir}[(1 - cos\theta)/2] \tag{2.13}$$

$$t = t_c[(\theta - sin\theta)/2\pi] \tag{2.14}$$

Here, t_c is the age of the universe at the collapse redshift z_{vir} and $r_{vir} = r_{max}/2 = \frac{1}{2}[(2GMt_c^2)/\pi^2]^{1/3}$ is the radius at virialization. The collapse of the cold dark matter (cdm) part of the halo halts at the point of virialization and the overdensity of the region at this

point of time is given by ($\sim 18\pi^2$ in the spherical top-hat model of gravitational collapse in the cosmological settings of Einstein d'Sitter universe. In this case, the gas density first decreases due to universal expansion, and then slowly increases prior to the collapse redshift to reach an overdensity of $18\pi^2$ at z_{vir}. The temperature reached by the gas after virialization depends on the mass of the object, M, through the virial condition (Sethi et al., 2008):

$$T_{vir} \simeq 800\ K\ \left(\frac{M}{10^6\ M_\odot}\right)^{2/3} \left(\frac{1+z}{20}\right) \left(\frac{\Omega_m}{0.3}\right)^{1/3} \left(\frac{h}{0.7}\right)^{2/3} \left(\frac{\mu}{1.22}\right) \tag{2.15}$$

Even though the dark matter part of halo stops collapsing, the gas part still continues to collapse as it cools, to follow the evolution of the gas to higher densities beyond the stage of virialization, we have followed a prescription given the paper Birnboim & Dekel (2003).

Under this prescription we follow a spherical shell of gas as it collapse down inside the fixed dark matter halo using energy conservation arguments. We have taken the dark matter profile as of a fixed isothermal sphere, and it is assumed that the shells do not cross each other as they contract. The total mass inside a shell at radius r, which originally (at z_{vir}) containing a total mass M_{vir} is,

$$M(r) = f_b M_{vir} + (1+f_b) M_{vir} \frac{r}{r_{vir}} \tag{2.16}$$

where f_b is the baryonic fraction, gravitational potential at r can be given by,

$$\phi(r) = -\frac{GM(r)}{r} - (1-f_b)\frac{GM_{vir}}{r_{vir}}\ \ln\left(\frac{r_{vir}}{r}\right) \tag{2.17}$$

now we can calculate the evolution of the shell in time in the step of dt by increasing r to $r + udt$, where u is the velocity of the shell at radius r and then recalculating the velocity of the shell $u(r+dr)$ using the energy conservation,

$$\frac{1}{2}u^2 + \phi(r) = \frac{1}{2}v_{vir}^2 + \phi(r_{vir}) = \text{constant} \tag{2.18}$$

v_{vir} is the velocity of the shell at virialization, and is related to M_{vir} and r_{vir} by $v_{vir}^2 = GM_{vir}/r_{vir}$, using this method we have followed the infalling gas to the densities up to 10^8 cm^{-3}.

2.3.3 Thermal evolution of the collapsing gas

2.3.3.1 Magnetic heating

The dissipation of primordial magnetic field due to ambipolar diffusion and the decaying turbulence in the post recombination era can substantially change the ionization fraction and the temperature of the gas even before the halo starts collapsing (Sethi & Subramanian, 2005; Schleicher et al., 2009).

The magnetic field energy dissipation due to ambipolar diffusion can be expressed as (see e.g. Cowling (1956); Shu (1992); Sethi & Subramanian (2005))

$$\left(\frac{dE_B}{dt}\right)_{\rm ambi} = \frac{7\rho_n f(t)}{48\pi^2\gamma\rho_b^2\rho_i}\int dk_1 \int dk_2 M(k_1)M(k_2)k_1^2k_2^4. \tag{2.19}$$

All quantities in eq. (2.19) are expressed at redshift $z = 0$. The time–dependence of the decay rate is given by $f(t) = (1+z)^4$ during the pre-collapse stage, and $f(t) \propto \rho^{-4/3}$ during the collapse phase. Here, ρ_n, ρ_b and ρ_i correspond to the neutral, total and ionized mass density respectively; $\gamma = \langle w\sigma_{in}\rangle/(m_n + m_i)$ (Shu, 1992), where w is the ion-neutral relative velocity and σ_{in} is the cross-section for the collision between ions and neutrals. For $w \lesssim 10$ km s^{-1}, which is relevant for this analysis, $\langle w\sigma_{in}\rangle \simeq 3\times10^{-9}$ cm^3 s^{-1} is independent of the relative velocity of ions and neutrals. The tangled magnetic field is assumed to be statistically homogeneous and isotropic and Gaussian with a power spectrum: $M(k) = Ak^n$ with a large-k cut-off at $k = k_{\rm max} \simeq 235(1\,{\rm nG}/B_0)\,({\rm comoving})\ {\rm Mpc}^{-1}$; $k_{\rm max}$ is determined by the effects of damping by radiative viscosity during the pre-recombination era (for more details see section 1.4). B_0, referred to as the magnetic field strength, is defined as the r.m.s. value at $k = 1\,{\rm Mpc}^{-1}$. The normalization A can be determined by smoothing the magnetic field over a given scale k_G. Magnetic field power spectrum is assumed to be nearly scale invariant with $n \simeq 3$ for this study. Many theoretical analyses show that these are the only power spectra compatible with current observations (e.g. Sethi & Subramanian (2005), and references therein). For obtaining numerical results, $n = -2.9$ has been used. Unless specified otherwise, the time–evolution of the magnetic field is assumed to be given by flux-freezing, which implies a power–law dependence $B \propto \rho^\alpha$ on the gas density with $\alpha = 2/3$. In practice, this scaling may be less steep; below we will explore how our results change for different values of α.

Though magnetic field energy can also be dissipated by generating decaying magnetohydrodynamic (MHD) turbulence, we found that the ambipolar diffusion always domi-

nates for our case The evolution of magnetic field energy density can be written as

$$\frac{dE_{\rm B}}{dt} = \frac{4}{3}\frac{\dot{\rho}}{\rho} - \left(\frac{dE_{\rm B}}{dt}\right)_{\rm turb} - \left(\frac{dE_{\rm B}}{dt}\right)_{\rm ambi} \tag{2.20}$$

The first term on the right-hand side takes into account the change in the magnetic field energy due to adiabatic expansion (in the early stages of the evolution of a halo) and compression (during the halo collapse). The heating L_{heat} can be expressed as,

$$L_{heat} = \left(\frac{dE_{\rm B}}{dt}\right)_{\rm turb} + \left(\frac{dE_{\rm B}}{dt}\right)_{\rm ambi} \tag{2.21}$$

2.3.3.2 Other cooling (heating) processes

The cooling (heating) processes that dominate in primordial gas in the density and temperature range we consider for this problem, are: (a) Compton cooling (heating) k_{iC} (eq. 15 in SBK08), (b) atomic H cooling (eq. 16 in SBK08), and (c) $\rm H_2$ molecular cooling (Galli & Palla 1998) and (d) the adiabatic cooling (heating) due to expansion (collapse) of the system. In the following section,

$$L_{\rm cool} \equiv \text{atomic H cooling} + \text{molecular } \rm H_2 \text{ cooling} \tag{2.22}$$

2.3.3.3 Evolution of density (n), temperature (T) and other related quantities

Following Sethi et al. (2008), the evolution of the ionization fraction (x_e), magnetic field energy density (E_B), temperature (T), and $\rm H_2$ molecule fraction ($x_{\rm H_2}$) are described by the equations

$$\begin{aligned}
\dot{x}_e &= \left[\beta_e(1-x_e)\exp\left(-h\nu_\alpha/(k_B T_{\rm cbr})\right) - \alpha_e n_b x_e^2\right] C + \\
&\quad + \gamma_e n_b (1-x_e) x_e && (2.23)\\
\frac{dE_B}{dt} &= \frac{4}{3}\frac{\dot{\rho}}{\rho} - \left(\frac{dE_B}{dt}\right)_{\rm turb} - \left(\frac{dE_B}{dt}\right)_{\rm ambi} && (2.24)\\
\frac{dT}{dt} &= \frac{2}{3}\frac{\dot{n_b}}{n_b}T + k_{iC}x_e(T_{\rm cbr}-T) + \frac{2}{3n_b k_B}(L_{\rm heat} - L_{\rm cool})\,, && (2.25)\\
\frac{dx_{\rm H_2}}{dt} &= k_m n_b x_e (1 - x_e - 2x_{\rm H_2}) - k_{\rm des} n_b x_{\rm H_2}\,. && (2.26)
\end{aligned}$$

The symbols here have their usual meaning. Eq. 2.24 and 2.26 are just the Eq. 2.20 and 2.11 described in the previous subsections, Eq. 2.25 is for the temperature evolution of the collapsing gas, in which the first term correspond to adiabatic cooling (or heating), second term is accounting for inverse Compton cooling (heating), $L_{\rm cool}$, $L_{\rm heat}$ are the other

heating and cooling (volume) rates, described in the previous sections. Eq. 2.23 describes the evolution of the ionized fraction, the first two terms are the terms for the recombination of the primordial plasma (for details and notation see Peebles 1968, 1993), the third term on the right-hand side of the equation corresponds to the collisional ionization (for details see Sethi et al. (2008)).

2.4 Results

In Figure 2.1, 2.2, and 2.3 the evolution of the temperature, the H_2 fraction (n_{H2}/n_H), and the ionized fraction for a single halo from $z \simeq 800$ (corresponding to the initial number density $n \simeq 100\,\mathrm{cm}^{-3}$ on the left of Figures 2.1, 2.2, and 2.3), down to a maximum density of $n \simeq 10^6\,\mathrm{cm}^{-3}$ in the collapsed halo. The evolution on these figures is monotonically to the right: the x–axis shows the density decreasing to the right (until the turnaround redshift), and then increasing again as the halo collapses.

These figures show an interplay between several physical effects. First, the magnetic field decay directly increases the temperature. This increases the electron fraction (due to more rapid collisional ionization), the larger electron fraction in turn tends to increase the molecular hydrogen fraction, but at the same time high temperature increases the collisional destruction rate of molecular hydrogen. Thus the molecular hydrogen cooling rate depends on the temperature directly. As the temperature reaches $\gtrsim 8,000$K, atomic cooling dominates, which, again, is governed by the ionized fraction. A higher magnetic field strength generally results in more rapid heating, and therefore a higher temperature. This, in turn results in higher ionized fractions, higher H_2 fraction but controlled by its destruction again due to high temperature. In the collapsing stage when HI cooling is not efficient because of low temperature, molecular hydrogen becomes the dominant coolant, and thus play an important role during the collapsing phase of the halo.

Figures 2.4 and 2.5 show the variation of various kind of heating and cooling functions as the halo collapse for magnetic field strength $B_0 = 1$ nG and 4 nG respectively. In both the Figures we see that during the collapse phase, adiabatic heating or Compton cooling rates are much lower than the magnetic heating, H_2 cooling or HI cooling, and therefore they do not play an important role in this whole process. For $B_0 = 1$ nG case, (Figure 2.4) we see that the atomic HI cooling becomes unimportant soon after the start of the collapse phase, as the magnetic heating is not sufficient to keep the temperature above 8000 K, as a consequence temperature goes down below 8000 K and atomic cooling rate decreases sharply. But H_2 cooling quickly becomes more important, dominating the magnetic heating for a short period of time when the density is around 0.1 - 0.2 cm^{-3}, resulting in a

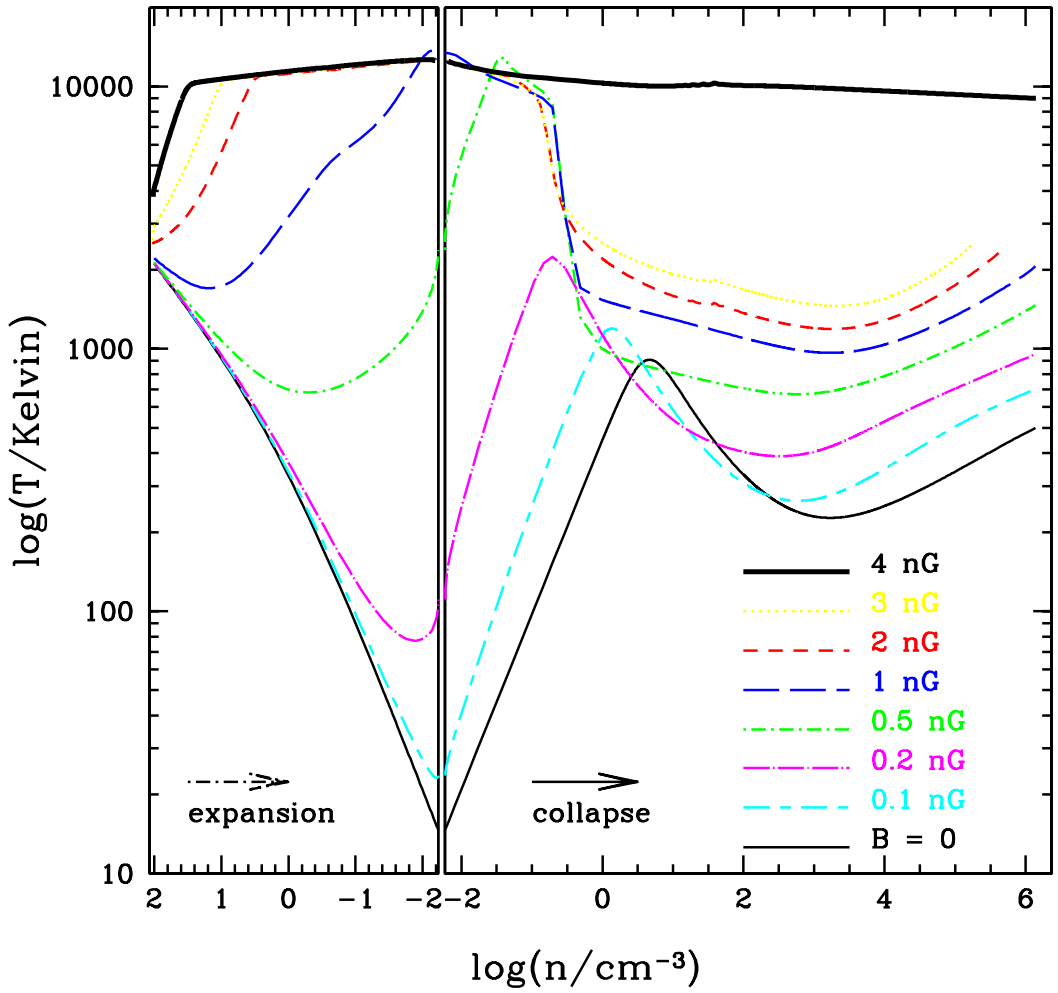

Figure 2.1: The temperature evolution of a patch of the intergalactic medium is shown as it initially expands and then turns around and collapses to high density. The different curves correspond to different values of the assumed primordial magnetic field, as labeled. The gas evolves from the left to the right on this figure. The left panel shows the expanding phase, starting from an initial density of $\approx 100\ \mathrm{cm}^{-3}$ (corresponding to the mean density at redshift $z \simeq 800$) and ending at the turnaround just below $n = 10^{-2}\ \mathrm{cm}^{-3}$. The right panel follows the subsequent temperature evolution in the collapsing phase.

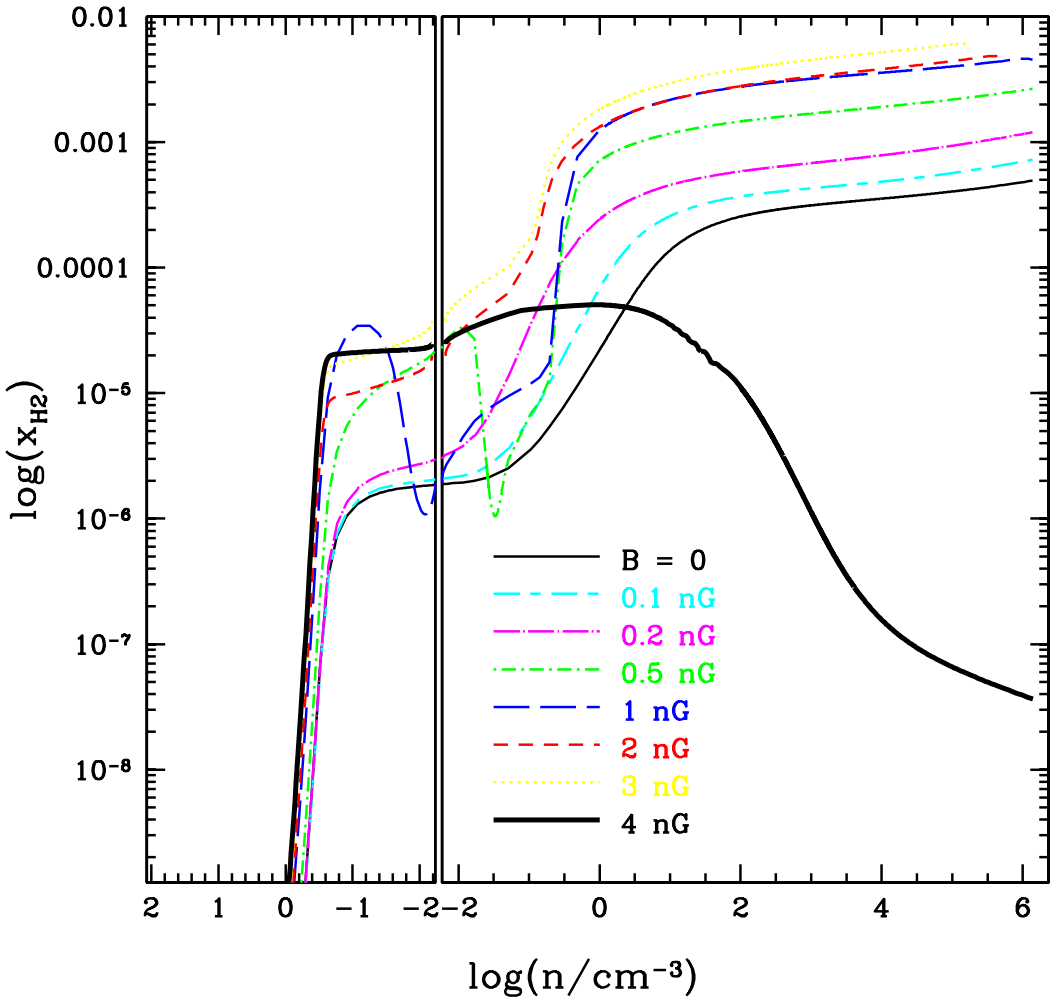

Figure 2.2: The evolution of the H_2 fraction in the same gas clouds shown in Figure 2.1.

rapid drop in temperature (see Fig. 2.1). As the halo collapses further, the gas begins to recombine and ionized fraction decreases (see Fig. 2.3) whereas magnetic heating increases due to increase in ambipolar diffusion, as a result magnetic heating catches up with H_2 cooling, resulting in a nearly constant temperature, this occurs only when the collapse has proceeded beyond a critical density $n \approx 10^3 \mathrm{cm}^{-3}$.

For $B_0 = 4$ nG (Figure 2.5) magnetic heating is sufficient enough to keep the temperature high (above 10000 K) and atomic HI cooling remains important, and the magnetic field roughly balances the atomic HI cooling during the whole collapse stage, resulting in a nearly constant temperature $T \approx 10^4$ K throughout. The high temperature gives rise to higher ionization fraction and therefore helps H_2 formation but at the same time the high temperature causes increase in H_2 destruction rate and as a net result because of high magnetic heating H_2 cannot form fast enough to ever become an important coolant. The halo remains at a temperature $\simeq 10^4$ K up to the critical density. By experimenting with several

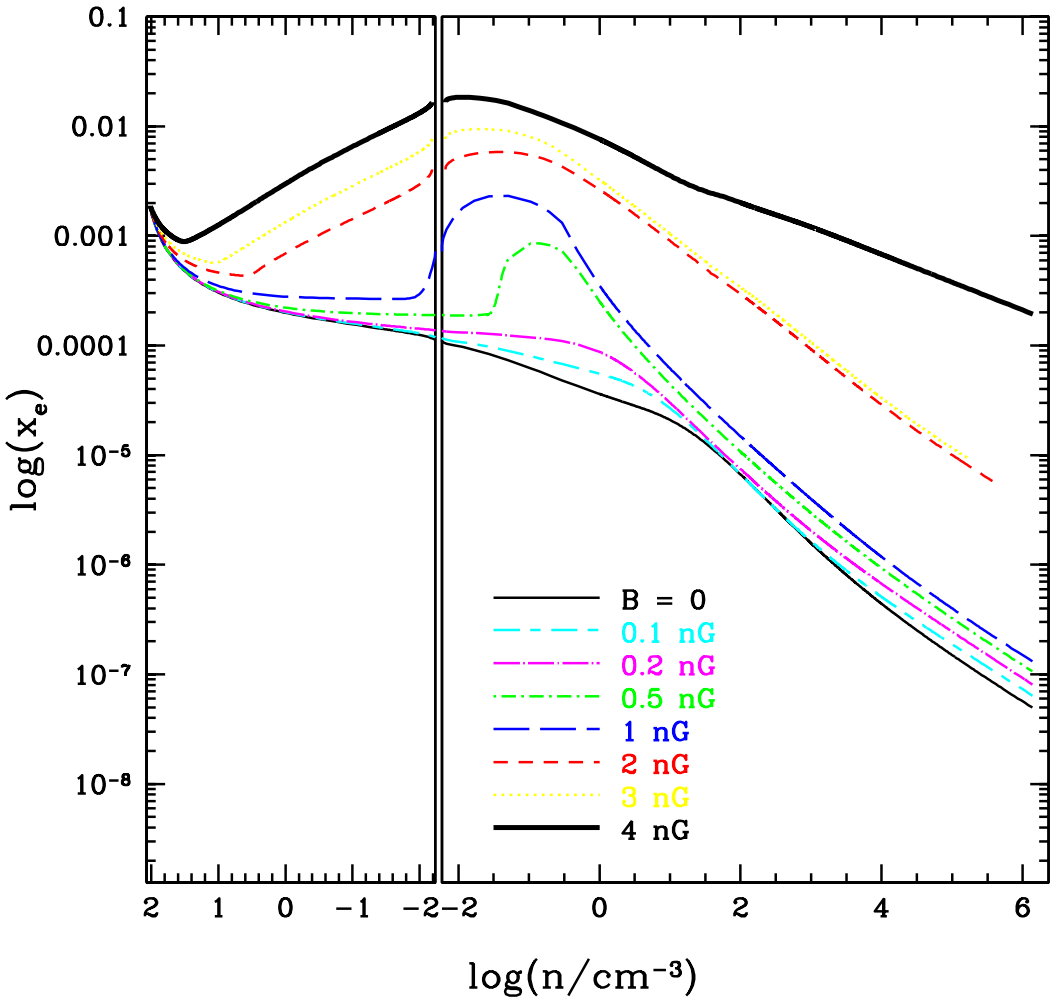

Figure 2.3: The evolution of the ionized fraction in the same gas clouds shown in Figure 2.1.

intermediate values of the magnetic field, we have found that this clear–cut bifurcation in the thermal evolution occurs at a critical magnetic field strength of $B_{\rm crit} = 3.6\,{\rm nG}$.

To check the robustness of our results against the collapse history of the halo, we changed altered the density (obtained using the prescription of Birnboim and Dekel) by an order of magnitude. We found that the apart from weaker/stronger or delayed/advanced H_2 cooling the other qualitative features like the bifurcation of the behavior around the magnetic field strength $B_{\rm crit} = 3.6\,{\rm nG}$ were unchanged. Apart from this another concern about this analysis could be the assumption of flux–freezing. Schleicher et al. (2009) note the possibility of the breakdown of this approximation in a collapsing halo. If the field is not sufficiently tangled, collapse can occur with little dissipation in the direction of the field lines; the magnetic field might grow less rapidly than our adopted $\rho^{2/3}$. Our computations in the range $\alpha \simeq 0.55$–0.6 show that the critical magnetic field required to prevent the halo from cooling increases to $B_0 \simeq 5$–$7\,{\rm nG}$.

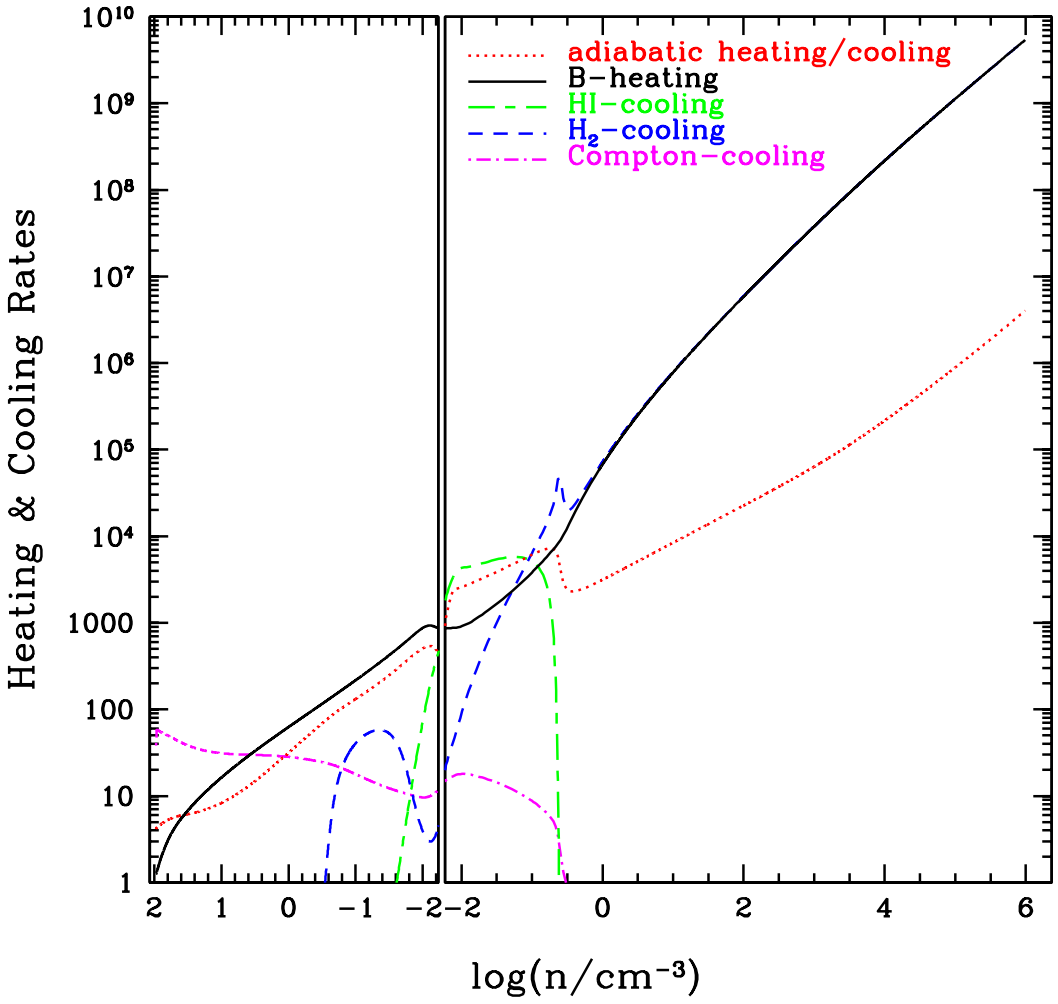

Figure 2.4: The heating and cooling rates are shown for various processes as labeled, for $B = 1$ nG. The rates are in the units $dt/dz = H_0^{-1}\Omega_m^{-1/2}(1+z)^{-5/2}$.

2.5 The Mass Of The Central Object

The expected mass of the central object scales approximately as $M \propto t_{\rm acc}^{-1} \propto c_s^3 \propto T^{3/2}$ (Bondi accretion; see, e.g., Shang et al. 2010). This implies that a stellar mass of $\sim 200 {\rm M}_\odot$, expected for $T = 300$K, can increase to $\approx 4 \times 10^4$ M$_\odot$ when H_2–cooling is inefficient and $T \approx 10^4$K (in their three–dimensional simulations, Shang et al. find a somewhat still steeper scaling). A small fraction of halos at $z = 10 - 15$, which contain pristine, metal–free gas when they collapse, and which reside in regions of an unusually high initial seed magnetic field, may produce a SMBH with a mass of up to $\sim 10^{4-5}$ M$_\odot$. The time available between $z = 6$ and $z = 10 - 15$ is $\approx (4 - 6) \times 10^8$ yrs, allowing for a further growth in mass by a factor of $\approx (2 \times 10^4) - (3 \times 10^6)$ at the e–folding time of 4×10^7 yr, (corresponding to Eddington–limited growth at the radiative efficiency 10%).

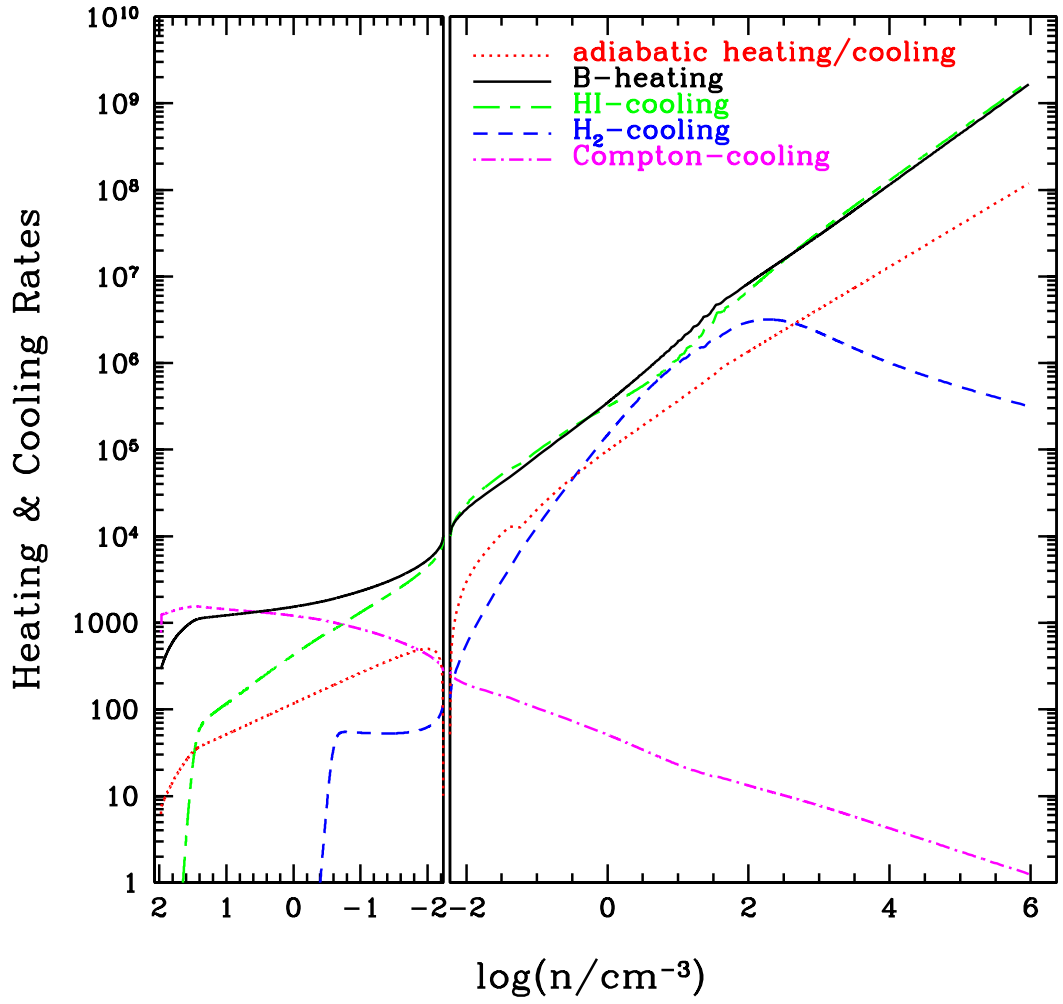

Figure 2.5: Same as Figure 2.4, but for $B = 4$ nG.

Hence, the 10^{4-5} $M_\odot$ BHs, produced through the primordial magnetic field, can indeed grow into the $\gtrsim 10^9$ $M_\odot$ SMBHs by $z = 6$.

The abundance of halos in the PMF–induced structure formation case drops very sharply for masses above the magnetic Jeans mass (e.g. SS05), and for simplicity, we conservatively drop this contribution in our analysis. In the usual ΛCDM model, using the fitting formula for the halo mass function from Jenkins et al. (2001), and the current best fit cosmological parameters from Komatsu et al. (2009), we find that the abundance of all $M > 3 \times 10^{10}$ $M_\odot$ halos at $z = 10$ is $\approx 5 \times 10^{-5}$ (comoving) Mpc^{-3}. At the somewhat higher redshift of $z = 15$, the abundance of halos above the same mass drops sharply to $\approx 3 \times 10^{-8}$ Mpc^{-3}.

The space density of $\gtrsim 10^9$ $M_\odot$ SMBHs, inferred from the observed abundance of bright $z \approx 6$ quasars, is $\sim \epsilon_{\rm Q}^{-1}$ (comoving) Gpc^{-3}. Here $\epsilon_{\rm Q}$ denotes the duty cycle, defined as the fraction of the Hubble time that $z = 6$ supermassive black holes are observable as

luminous quasars. Assuming a quasar lifetime of ~ 50 Myr (e.g. Martini 2004), we have $\epsilon_{\rm Q} \sim 0.05$, and the space density of $z = 6$ SMBHs is ~ 20 Gpc^{-3}. Therefore, at redshift $z = 10$, a fraction as low as $f \sim (20\ {\rm Gpc}^{-3})/(5 \times 10^{-5}\ {\rm Mpc}^{-3}) = 3 \times 10^{-3}$ of the whole population of $M \gtrsim 3 \times 10^{10}\ {\rm M}_{\odot}$ halos is sufficient to account for the presence of these rare $z \approx 6$ SMBHs. Such a small fraction would correspond to $\sim 2.8\sigma$ upward fluctuations of a Gaussian random PMF.

2.6 Discussion

In this work we have investigated the role of primordial magnetic fields in the formation of SMBHs at high redshifts. Calculations showed that the direct gas collapse in the early dark matter halos, aided by heating from the dissipation of a primordial magnetic field can lead to the formation of high mass objects which in turn can grow into a SMBH by the redshifts of 6-8. This model avoids many of the odd assumptions required in earlier models (such as an extremely high UV flux and the absence of H_2 and of other molecules and metals). But at the same time this model requires a large primordial magnetic field, and relies on metal-free primordial gas. From this analysis, in general, it seems that any other heating mechanism, which could compete with atomic HI cooling in the collapsing halo, down to a density of $n \sim 10^3\ {\rm cm}^{-3}$, would produce similar effect as the magnetic field produced here.

3

Primordial Magnetic Field Limits From Cosmological Data

3.1 Introduction

In the previous chapter we saw that, presence of magnetic fields can play an important role in the formation of early collapsed halos . If the magnetic field strength around the collapsing halo is strong enough ($B_{crit} = 3.6$ nG), it can drastically change the course of thermal and dynamical evolution of the halo, and as a result more massive stars can form and consequently it can lead to formation of early supermassive black holes. The abundance of such objects will depend on the value of primordial magnetic field at those high red shifts, which is still not a well probed quantity. This chapter is about the study of limits on primordial magnetic field coming from various cosmological observables. The aim of this work was to investigate the limits on primordial magnetic fields coming from the observational constraint on the Farady rotation of CMB polarization plane and the Large Scale Structures (LSS) in the universe.

A quadrupole anisotropy in the temperature inhomogeneity can lead to polarization of CMB photons. This quadrupole anisotropy could arise from the following 3 types of perturbations,

① Scalar (due to density fluctuations)

② Vector (due to vorticity)

③ Tensor (due to gravity waves)

To study the polarization pattern in the CMB, the CMB polarization can be decomposed into two components:

① Curl free component : E-mode or gradient-mode

② Grad free component : B-mode or curl-mode

the E-mode may arise due to both the scalar and the tensor perturbations (the contribution from vector perturbations is expected to be negligible), but the B-mode could arise due to only vector or tensor perturbations. In fact a cosmological magnetic field also can source a B-mode in CMB polarization and CMB B-polarization measurement can be a crucial test to limit the primordial magnetic field strength. In this analysis we are not going to take this into account.

Presence of magnetic field during recombination causes a rotation in CMB polarization plane due to Faraday effect. The same field could cause additional density perturbations and thus affect the structure formation scenario and the LSS statistics (Section 1.5).

3.2 Modeling The Primordial Magnetic Fields (Concept of $\mathbf{B}_{\rm eff}$)

Assuming primordial magnetic field as a stochastic Gaussian magnetic field it can be fully described by its two-point correlation function . For simplicity we consider here the case of the non-helical magnetic field, in this case the two-point correlation function in wavenumber space can be written as (Section 1.4, equation 1.1)

$$\langle B_i^\star(\mathbf{k}) B_j(\mathbf{k}')\rangle = (2\pi)^3 \delta^{(3)}(\mathbf{k}-\mathbf{k}') P_{ij}(\hat{\mathbf{k}}) P_B(k). \tag{3.1}$$

Here i and j are spatial indices, $i,j \in (1,2,3)$, $\hat{k}_i = k_i/k$ a unit wave vector, $P_{ij}(\hat{\mathbf{k}}) = \delta_{ij} - \hat{k}_i\hat{k}_j$ the transverse plane projector, $\delta^{(3)}(\mathbf{k}-\mathbf{k}')$ the Dirac delta function, and $P_B(k)$ is the power spectrum of the magnetic field.

We define the smoothed magnetic field B_λ through the mean-square magnetic field (Mack et al., 2002)

$$B_\lambda{}^2 = \langle \mathbf{B}(\mathbf{x}) \cdot \mathbf{B}(\mathbf{x})\rangle|_\lambda, \tag{3.2}$$

where the smoothing is done on a comoving length λ with a Gaussian smoothing kernel function $\propto \exp[-x^2/\lambda^2]$. Corresponding to the smoothing length λ is the smoothing wavenumber $k_\lambda = 2\pi/\lambda$. The power spectrum $P_B(k)$ is assumed to be a simple power law on large scales, $k < k_D$ (where k_D is the cutoff wavenumber),

$$P_B(k) = P_{B0} k^{n_B} = \frac{2\pi^2 \lambda^3 B_\lambda^2}{\Gamma(n_B/2+3/2)} (\lambda k)^{n_B}, \tag{3.3}$$

and assumed to vanish on small scales where $k > k_D$.

The energy density of the magnetic field is given by (Kahniashvili & Ratra, 2007)

$$\rho_B(\lambda) = \frac{B_\lambda^2 (k_D \lambda)^{n_B+3}}{8\pi\Gamma(n_B/2+5/2)}. \tag{3.4}$$

For this work we define an effective magnetic field $B_{\rm eff}$ such that $\rho_B = B_{\rm eff}^2/(8\pi)$. For the scale-invariant spectrum ($n_B = -3$; (Ratra, 1992)) we get $B_{\rm eff} = B_\lambda$ for all values of λ. The scale-invariant case is the only case where the values of the effective and smoothed fields coincide.

The cut-off scale k_D ($\equiv k_{max}$ Section 1.4, equation 1.3) is determined by the Alfvén wave damping scale $k_D^{-1} \sim v_A L_S$ where v_A is the Alfvén velocity and L_S the Silk damping scale (Jedamzik et al., 1998). This description is more appropriate when we are dealing with an homogeneous magnetic field and the Alfvén waves are the fluctuations $\mathbf{B}_1(\mathbf{x})$ with respect to a background homogeneous magnetic field $\mathbf{B}_0$ ($|\mathbf{B}_1| \ll |\mathbf{B_0}|$). In the case of the stochastic magnetic field we generalize the Alfvén velocity definition, see Ref. Mack et al. (2002), by referring to the analogy between the effective magnetic field and the homogeneous magnetic field. Assuming that the Alfvén velocity is determined by $B_{\rm eff}$, a simple computation gives the expression of k_D in terms of $B_{\rm eff}$ (Kahniashvili et al., 2011):

$$\frac{k_D}{1{\rm Mpc}^{-1}} = 1.4\sqrt{\frac{(2\pi)^{n_B+3}h}{\Gamma(n_B/2+5/2)}}\left(\frac{10^{-7}{\rm G}}{B_{\rm eff}}\right). \tag{3.5}$$

Here h is the Hubble constant in units of 100 km s^{-1} Mpc^{-1}. The BBN limit on the effective magnetic field strength, $B_{\rm eff} \leq 8.4\times10^{-7}$ G (Kahniashvili et al., 2011), gives an upper limit on the cut-off wavenumber k_D,

$$k_D^{\rm BBN} \geq 0.17 h^{1/2} \frac{(2\pi)^{(n_B+3)/2}}{\Gamma^{1/2}(n_B/2+5/2)}\,{\rm Mpc}^{-1}. \tag{3.6}$$

In the case of an extremely large magnetic field it is possible to have $\lambda_D > 1$ Mpc. At this point it would seem unreasonable (unjustified) to consider a smoothing scale $\lambda = 1$ Mpc as is conventionally done.

3.3 CMB Polarization Plane Rotation

The presence of (primordial) magnetic field during recombination causes a rotation of the CMB polarization plane through the Faraday effect (Kosowsky & Loeb, 1996). The rms rotation angle $\alpha_{\rm rms} = (\langle\alpha^2\rangle)^{1/2}$ induced by a stochastic magnetic field with smoothed

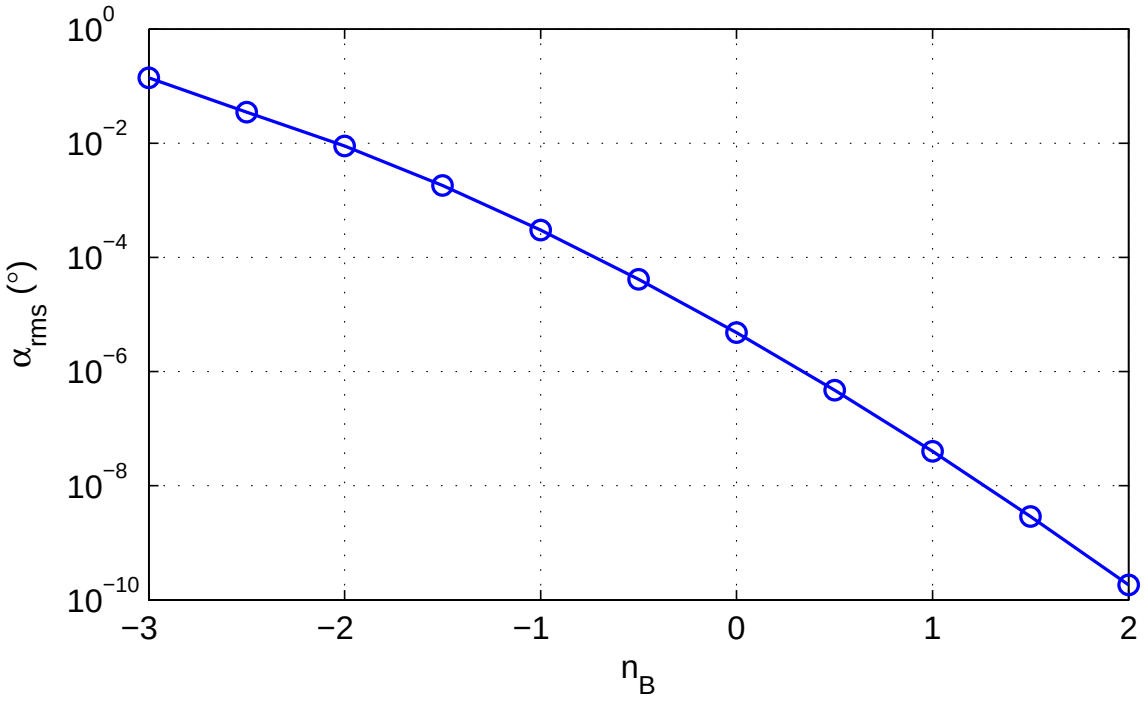

Figure 3.1: Rms rotation angle $\alpha_{\rm rms}$ as a function of spectral index n_B for the case when $B_{\rm eff} = 1\,{\rm nG}$ and $\nu_0 = 100\,{\rm GHz}$. Circles correspond to the computed values.

amplitude B_λ and spectral index n_B is given by

$$\langle \alpha^2 \rangle = \sum_l \frac{2l+1}{4\pi} C_l^\alpha, \tag{3.7}$$

where the rotation multipole power spectrum C_l^α is (Kosowsky et al., 2005)

$$\begin{aligned} C_l^\alpha \;\simeq\; & \frac{9l(l+1)}{(4\pi)^3 q^2 \nu_0^4} \frac{B_\lambda^2}{\Gamma\left(n_B/2+3/2\right)} \\ & \times \left(\frac{\lambda}{\eta_0}\right)^{n_B+3} \int_0^{x_S} dx\, x^{n_B} j_l^2(x). \end{aligned} \tag{3.8}$$

Here η_0 is the conformal time today, ν_0 is the CMB photon frequency, $q^2 = 1/137$ is the squared elementary charge in cgs units, $j_l(x)$ is a Bessel function with argument $x = k\eta_0$, and $x_S = k_S\eta_0$ where $k_S = 2\ {\rm Mpc}^{-1}$ is the Silk damping scale. In the case of an extreme magnetic field which just satisfies the BBN bound, k_D might become less than the Silk damping scale. In this case the upper limit in the integral above must be replaced by $x_D = k_D\eta_0$.

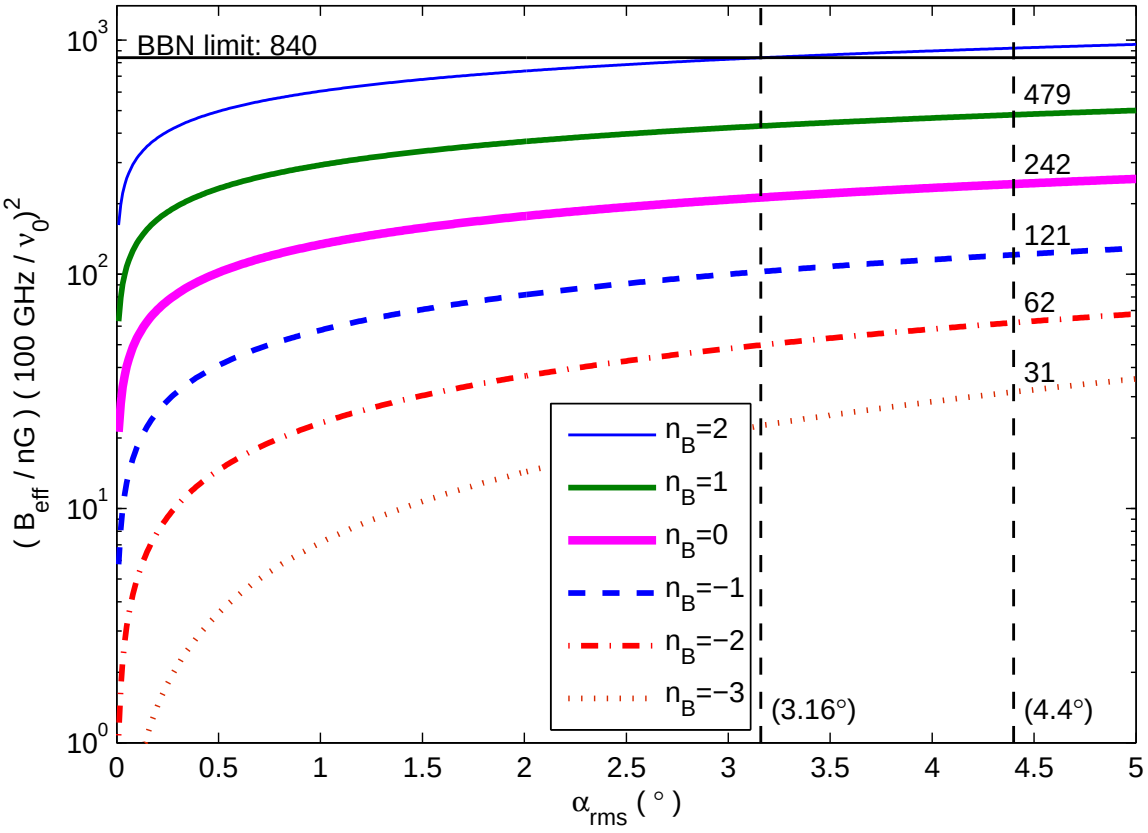

Figure 3.2: Effective magnetic field limits set by the measurement of the rotation angle $\alpha_{\rm rms}$ for different spectral index ($n_B = -3, -2, -1, 0, 1, 2$, from bottom to top). The horizontal solid line shows the upper limit set by BBN. Vertical dashed lines correspond to the angles $\alpha_{\rm rms} = 3.16^\circ$ that is set by the BBN limit on the effective magnetic field with spectral index $n_B = 2$ and $\alpha_{\rm rms} = 4.4^\circ$ set by the WMAP 7-year data. The numerical values of the effective magnetic field constraints (in nG at 100 GHz) from the $\alpha_{\rm rms} = 4.4^\circ$ limit are shown on the graph for each spectral index value.

In terms of $B_{\rm eff}$, Eq. (3.8) can be rewritten in the following form,

$$C_l^\alpha \simeq 1.6\times10^{-4}\frac{l(l+1)}{(k_D\eta_0)^{n_B+3}}\left(\frac{B_{\rm eff}}{1\,{\rm nG}}\right)^2\left(\frac{100\,{\rm GHz}}{\nu_0}\right)^4 \times\frac{n_B+3}{2}\int_0^{x_S} dx\, x^{n_B} j_l^2(x), \tag{3.9}$$

and, as a result,

$$\alpha_{\rm rms} \simeq 0.14^\circ\left(\frac{B_{\rm eff}}{1\,{\rm nG}}\right)\left(\frac{100\,{\rm GHz}}{\nu_0}\right)^2\frac{\sqrt{n_B+3}}{(k_D\eta_0)^{(n_B+3)/2}} \times\left[\sum_{l=0}^{\infty}(2l+1)l(l+1)\int_0^{x_S} dx\, x^{n_B} j_l^2(x)\right]^{1/2}. \tag{3.10}$$

It is of interest to compare Eq. (3.10) with the corresponding result, Eq. (2) of Ref. (Kosowsky & Loeb, 1996), derived for a homogeneous magnetic field and at frequency $\nu_0 = 30$ GHz,

$$\alpha_{\rm rms} \simeq 1.6^\circ \left(\frac{B_0}{1\,{\rm nG}}\right) \left(\frac{30\,{\rm GHz}}{\nu_0}\right)^2 \tag{3.11}$$

Both expressions agree for $n_B \to -3$ after accounting for $\sum_l (2l+1) j_l^2(x) = 1$ and the fact that Bessel functions peak at $x \sim l$ for given l (see Appendix A).

Figure 3.1 shows the rms rotation angle $\alpha_{\rm rms}$, Eq. (3.10), as a function of the spectral index n_B when the effective magnetic field is normalized to be 10^{-9} G. The WMAP 7-year data limits the rms rotation angle to be less then 4.4° at 95% C. L. (Komatsu et al., 2011). This allows us to limit the effective magnetic field as shown in Fig. 3.2.

3.4 Large Scale Structures

A primordial tangled magnetic field can also induce the formation of structures in the Universe. In particular, these fields can play an important role in the formation of first structures (see, e.g. Refs. Wasserman (1978); Kim et al. (1996); Subramanian & Barrow (1998); Gopal & Sethi (2005); Sethi & Subramanian (2005); Sethi et al. (2008); Yamazaki et al. (2008); Sethi, Haiman, Pandey (2010)).

The magnetic-field-induced matter power spectrum $P(k)$ is $\propto k^4$ for $n_B > -1.5$ and $\propto k^{2n_B+7}$ for $n_B \leq -1.5$ (Kim et al., 1996; Gopal & Sethi, 2005). The cut-off scale of the power spectrum is determined by the larger of the magnetic Jeans' wavenumber $k_{\rm J}$ and the thermal Jeans' wavenumber $k_{\rm therm}$ (for a detailed discussion, see, e.g. Ref. Sethi et al. (2008)). Here the magnetic Jeans' wavenumber is (see, e.g. Ref. Kim et al. (1996))

$$k_J \simeq (230^{(n_B+3)/2} \times 13.8)^{2/(n_B+5)} \left(\frac{1\,{\rm nG}}{B_{\rm eff}}\right) {\rm Mpc}^{-1}. \tag{3.12}$$

Unlike the ΛCDM matter power spectrum, the magnetic-field-induced matter power spectrum increases at small scales and can exceed the ΛCDM matter one at small scales (for a comparison of these two spectra, see, e.g. Fig. 3 of Ref. Gopal & Sethi (2005)). And, therefore, one of the more important contributions of the additional power induced by magnetic fields is to the formation of the first structures in the Universe (e.g. Refs. Sethi & Subramanian (2005); Sethi, Haiman, Pandey (2010); Yamazaki et al. (2008) and references therein).

In Fig. 3.3 we show the linear mass dispersion $\sigma(M)$ for matter power spectra induced by a primordial magnetic field with $B_{\rm eff} = 6\,{\rm nG}$ at $z = 10$ for different values of n_B.

Notable features of Fig. 3.3 are: (a) the mass dispersion on small scales is larger for a larger value of n_B; and, (b) for $n_B \geq -1.5$, the mass dispersion drops more sharply at larger scales than for $n_B \leq -1.5$. We focus here on the mass dispersion on the smallest scales, as these scales are more relevant for the formation of the first structures in the Universe. These first structures were responsible for the reionization of the Universe at $z \simeq 10$. To obtain meaningful constraints on $B_{\rm eff}$ from the formation of first structures, we need to know how the curves shown in Fig. 3.3 vary as $B_{\rm eff}$ is changed and as the Universe evolves.

The mass dispersion $\sigma(M, z)$ evolves with the time dependence of the growing mode of the linear density perturbations sourced by the primordial magnetic field (Kim et al., 1996; Gopal & Sethi, 2005). The growing mode is $\propto a(t)$, the scale factor, at high redshifts, the same as in the "standard" ΛCDM case without a magnetic field. To account for this evolution the curves corresponding to σ in Fig. 3.3 must be scaled by roughly a factor of $\simeq 11/(1+z)$ for redshifts $z \gg 1$.

It can be shown that the value of σ at the smallest scales ($M \simeq 10^6\,{\rm M}_\odot$) is invariant under a change in $B_{\rm eff}$ if the cut-off scale is determined by $k_{\rm J}$: an increase/decrease in the value of $B_{\rm eff}$ is compensated by a decrease/increase in the value of $k_{\rm J}$. However, if $B_{\rm eff}$ is decreased to a value at which $k_{\rm therm} \leq k_{\rm J}$, then the value of σ decreases with a decrease in $B_{\rm eff}$, as the cut-off scale becomes independent of the value of $B_{\rm eff}$.

It has been shown that the dissipation of magnetic fields in the post-recombination era can substantially alter the thermal and ionization history of the universe (Yamazaki et al., 2008; Sethi & Subramanian, 2005; Sethi et al., 2008). In particular, this dissipation raises the matter temperature and therefore the Jeans' scale in the IGM. For $B_{\rm eff} \geq 1\,{\rm nG}$ the matter temperature rises to $\simeq 10^4\,{\rm K}$ as early as $z \geq 100$, (Sethi & Subramanian, 2005), resulting in a steep rise in the Jeans' scale as compared to the usual case. The Jeans' wave number corresponding to this temperature is $k_{\rm therm} \simeq 10\,{\rm Mpc}^{-1}$ (see, e.g. Fig. 4 of Ref. Sethi et al. (2008)).

WMAP results show that the Universe reionized at $z \simeq 10$. This reionization was caused by the non-linear collapse of the first structures, followed by star formation and the emission of UV photons from the collapsed halos. For a virialized structure in the spherical collapse model, the linear mass dispersion $\sigma \simeq 1.7$. This implies that the value of σ at the scales of interest at $z \simeq 10$ is not expected to be much higher than 1.7. Consider the $n_B = 2$ model in Fig. 3.3; the value of mass dispersion at the smallest scales is $\simeq 100$, which means that the first structures formed at $z \simeq 650$ in this case (the redshift of the collapse of first structures is $\simeq 6.5\sigma_{\rm max}$, where $\sigma_{\rm max}$ is the maximum value of σ at $z \simeq 10$), which can certainly be ruled out by the WMAP data on CMB anisotropies. A similar

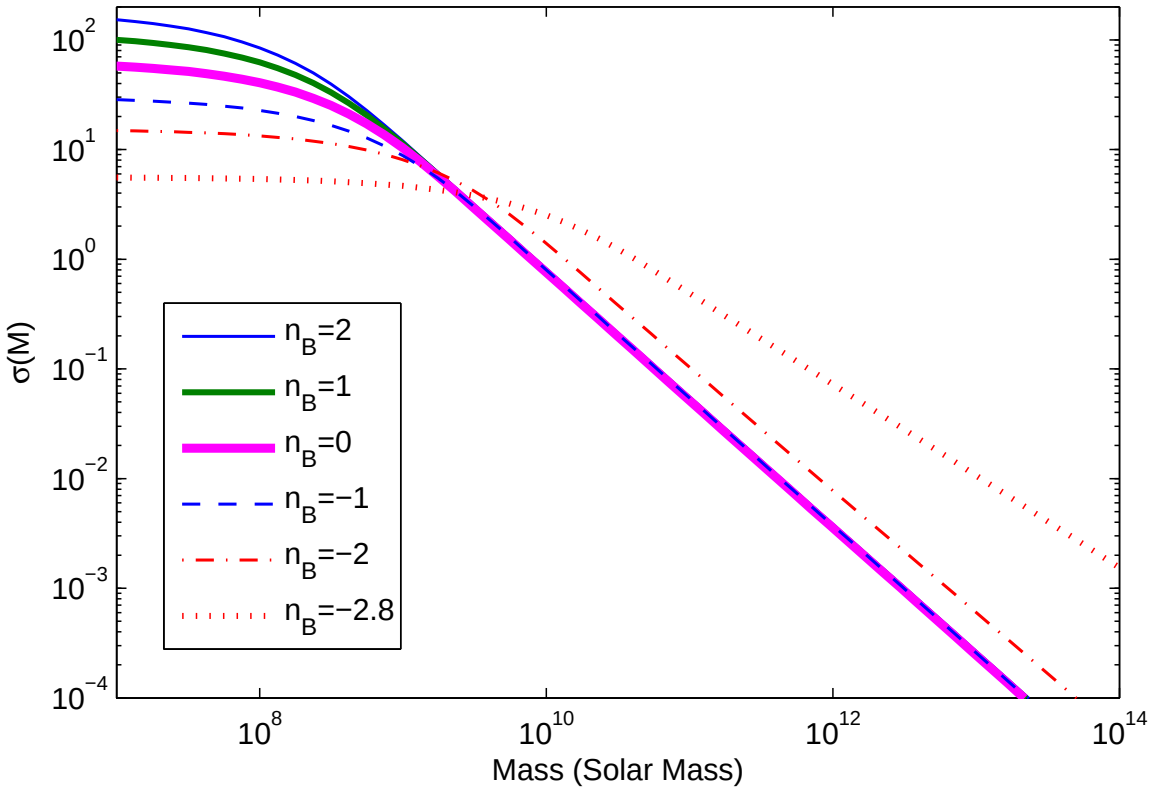

Figure 3.3: The mass dispersion at $z = 10$ for $B_{\rm eff} = 6\,{\rm nG}$ as a function of magnetic field power spectral index n_B. From top to bottom (at the left hand side of the plot), the curves correspond to $n_B = 2, 1, 0, -1, -2, -2.8$.

arguments can be used to rule out almost all the models shown in Fig. 3.3. Only the nearly scale-invariant models with $n_B \simeq -3$ do not put strong constraints on the strength of the magnetic field. As argued above, the value of mass dispersion at the smallest scales to collapse is nearly independent of the magnetic field strength unless $B_{\rm eff}$ decreases to a value such that $k_{\rm J} = k_{\rm therm}$. In this case, the value of σ decreases below those shown in Fig. 3.3. We have explored a wide range of $B_{\rm eff}$ for the range of spectral index shown in Fig. 3.3. We find that the range of acceptable values is 1–3 nG. In Fig. 3.4 we show the $B_{\rm eff}$ corresponding to $k_{\rm J} = k_{\rm therm}$. Notwithstanding various complications discussed above, this figure gives a rough sense of the acceptable range of $B_{\rm eff}$ over the entire range of n_B.

In the foregoing, we neglect the impact of the ΛCDM model on the process of reionization. As the density fields induced by the ΛCDM model and the magnetic field are uncorrelated, the matter power spectra owing to these two physical phenomena would add in quadrature. The smallest structures to collapse at $z \simeq 10$ in the WMAP-normalized ΛCDM model are 2.5σ fluctuations of the density field as opposed to the magnetic field case where 1σ collapse is possible (Fig. 3.3). This means the number of collapsed halos is

more abundant in the latter case. Therefore, depending on the star-formation history, if the magnetic-field-induced halo collapse made an important contribution to the reionization process, the far rarer halos from ΛCDM would have made a negligible impact (for further details and references see Ref. (Sethi, Haiman, Pandey , 2010)).

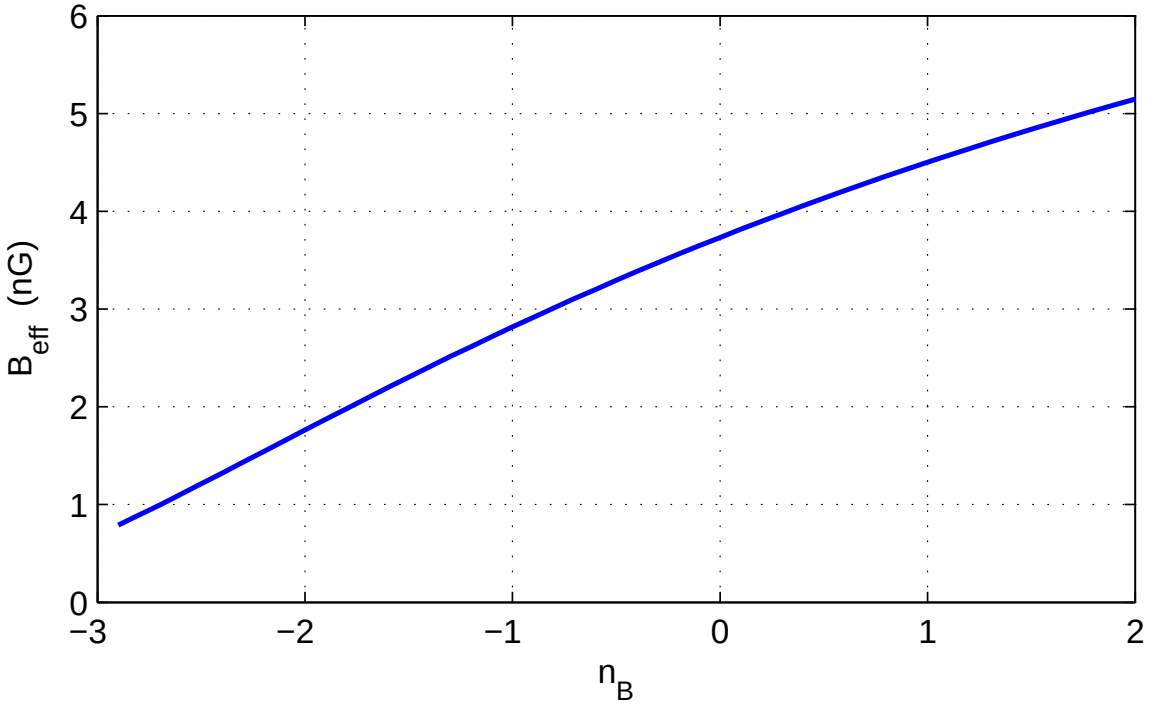

Figure 3.4: Constraint on the magnetic field strength $B_{\rm eff}$ as a function of the power spectral index n_B.

3.5 Discussion

In this work we study the large-scale imprints of a cosmological magnetic field, such as the rotation of the CMB polarization plane and formation of the first bound structures. We derive the corresponding limits on a primordial magnetic field energy density, expressed as limits on the effective value of the magnetic field, $B_{\rm eff}$. These limits are identical to limits on the smoothed magnetic field B_λ (smoothed over a length scale λ that is conventionally taken to be 1 Mpc) only in the case of the scale-invariant magnetic field (when $n_B = -3$). For a steep magnetic field with spectral index $n_B = 2$ the difference between $B_{\lambda=1\ \rm Mpc}$ and $B_{\rm eff}$ is enormous (greater than 10^{15}). We show that using the smoothed magnetic field can result in some confusion; e.g. an extremely small smoothed magnetic field on large scales does not mean that this field cannot leave observable traces on cosmological scales.

An intergalactic magnetic field of effective value larger than 1-10 nG (with, depending on magnetic spectral index, corresponding values of $B_{\lambda=1\ \mathrm{Mpc}}$ in the range $10^{-8} - 10^{-26}$ G) is ruled out by cosmological data. These limits of 1-10 nG are consistent with recent observational bounds on the intergalactic magnetic field (Neronov & Vovk, 2010; Tavecchio et al., 2010; Ando & Kusenko, 2010) if the field was generated in the early Universe with spectral shape $n_B \leq 1$. This favors the inflationary magnetogenesis scenario.

Appendix: Evaluating the right hand side of Eq. (3.10) when $n_B \to -3$

The $\sqrt{n_B+3}$ factor in the numerator of the right hand side of Eq. (3.10) is compensated by a corresponding $1/\sqrt{n_B+3}$ from the Bessel function integral when the spectral index $n_B \to -3$ and so the expression for $\alpha_{\rm rms}$ remains finite in this limit. To establish this we use properties of the Bessel function. Recall that $j_l^2(x)$ peaks at $x \sim l$, as shown in Fig. 3.5. This allows us to replace the factor $l(l+1)j_l^2(x)$ by $x^2 j_l^2(x)$ (the accuracy of this approximation is of order 15-20$\%$). The next step is to perform the sum over l. It is obvious that there is cut-off multipole number l_C that corresponds to the cut-off wavenumber, $l_C \sim \min(x_D, x_S)$. Now $j_l^2(x)$ satisfies

$$\sum_{l=0}^{\infty}(2l+1)j_l^2(x) = 1, \tag{3.13}$$

while we are interested in computing $\sum_{l=0}^{l_C}(2l+1)j_l^2(x)$. The Silk damping scale cutoff multipole number is $l_S \simeq 16000$, Kosowsky et al. (2005). Figure 3.6 shows that the sum to l_S converges to 1.

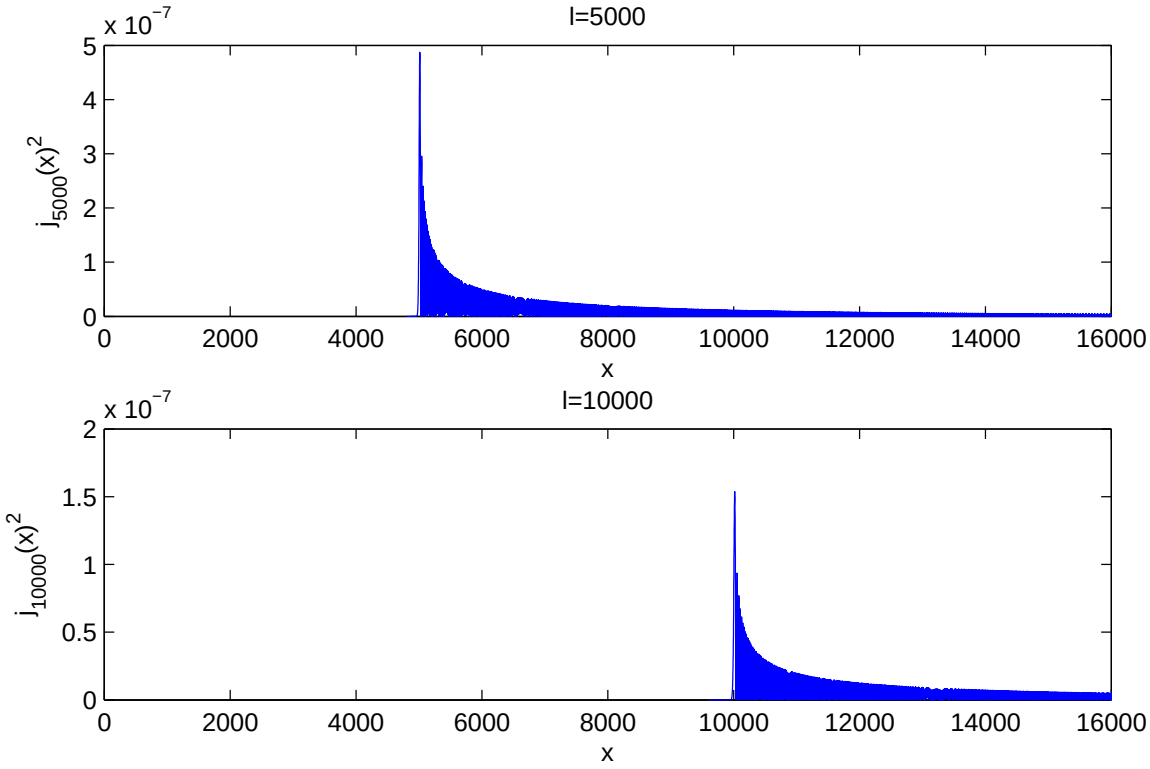

Figure 3.5: The squared spherical Bessel functions $j_l^2(x)$ for $l = 5000$ (top) and $l = 10000$ (bottom). Clearly $j_l^2(x)$ peaks at $x \approx l$.

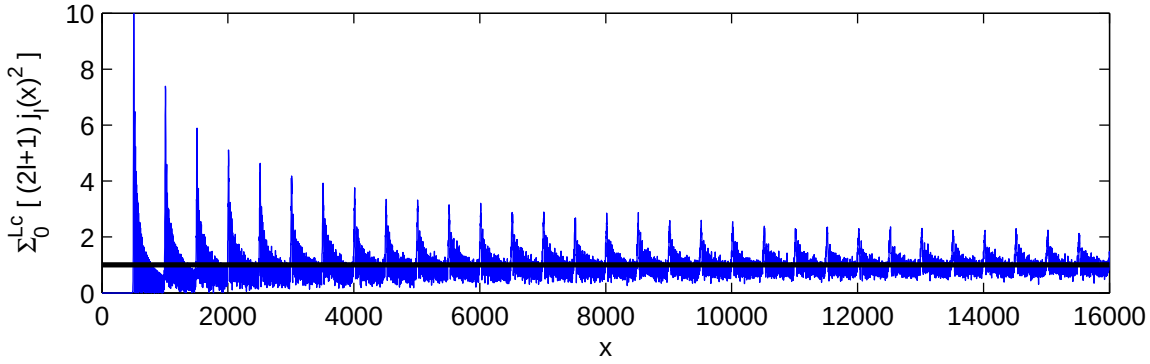

Figure 3.6: The sum of the squared spherical Bessel function $\sum_{l=0}^{l_C}(2l+1)j_l^2(x)$ for $l_C = x_S \simeq 16000$. The sum converges to 1 (horizontal solid line).

4 Probing Primordial Magnetic Fields Using Weak Lensing

4.1 Introduction

In recent years, weak gravitational lensing has proved to be one of best probes of the matter power spectrum of the universe. In particular, this method can reliably estimate the matter power spectrum at small scales which are not directly accessible to other methods e.g. galaxy surveys (for details and further references see e.g. Munshi et al. (2008); Hoekstra & Jain (2008); Refregier (2003); Bartelmann & Schneider (2001)) (Figure 4.1). These are the scale which are affected by the existence of primordial magnetic fields (see Figures 1.4 or 4.4) and thus a careful analysis of the cosmological observables which probe these small scale density distribution in the Universe such as weak lensing shear and Lyα distribution can actually provide information about primordial magnetic fields also.

In this work we attempt to constrain primordial magnetic fields within the framework of the two-point shear correlation function induced by gravitational lensing, including the contribution of matter perturbations induced by these magnetic fields. We compare our results with the CFHTLS (Canada-France-Hawaii Telescope Legacy Survey) Wide data (Fu et al., 2008).

4.2 Weak Lensing & Cosmic Shear

4.2.1 Gravitational lensing in general

From Einstein's general theory of relativity we know that light rays passing close to a massive object are bent by the object's gravitational field. The bending of light rays because of the intervening massive object give rise to the phenomenon which is known as

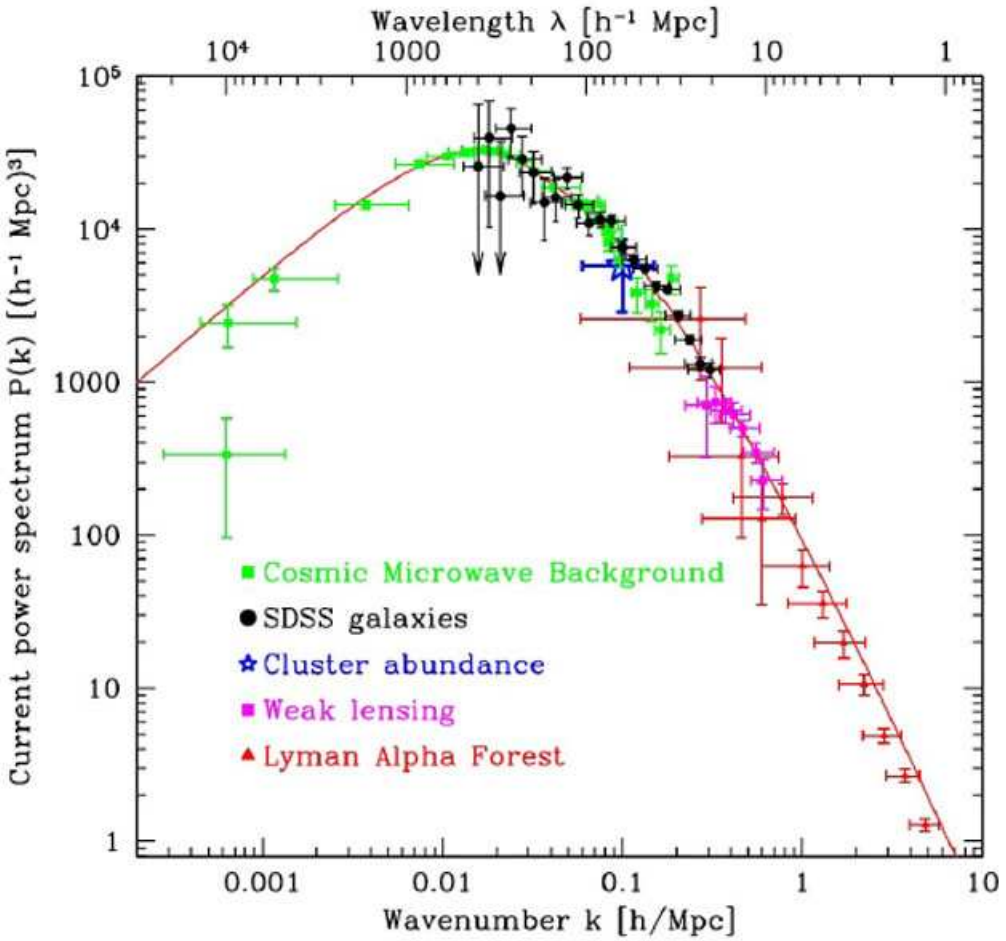

Figure 4.1: Inflationary matter power spectrum, showing the various probe of matter distribution in the Universe at different scales. Picture source: Tegmark, M. et al. 2004. PhRvD, 69, (10), 103501.

gravitational lensing, as the massive object behaves like a lens between the source object and the observer. Gravitational lensing often creates multiple and deformed (in a shape of arc) images of the background objects. One of the great advantage of gravitational lensing is that it allows us to estimate the mass of the lensing object in quite a direct way. Gravitational lensing can occur on various scales, from planets and stars to cluster and super cluster scales. In the case of lensing objects being planets and stars, the lensing effect is called microlensing, which turned out to be a great help in finding faint objects of the mass range of planets and stars which are difficult to be observed otherwise. The gravitational lensing of background objects by intervening large clusters facilitates a direct probe of the total (baryonic + dark matter) mass of the cluster. The other two main types of gravitational lensing are strong and weak lensing of background galaxies by intervening cluster or a massive galaxy. In the case of strong gravitational lensing, as a result of short distance

between source and the lensing object, the produced distortion in the source image can be easily seen in the form of large arcs, rings or the multiple images. Whereas in the case of weak lensing the distortion in the image of an individual background source is too small to be detected, it can only be detected by analyzing a large number of background sources to find coherent distortion in their images in the form of preferred stretching in the direction perpendicular to the direction to the center of the lens.

4.2.2 Weak lensing theory & cosmic shear

As photons travel from a background galaxy to the observer, they get deflected by mass fluctuations along the line of sight (Figure 4.2). Summing up the deflections arising from all potential gradients between the observer and the source gives the total shift on the sky (Figure 4.3):

$$\delta\boldsymbol{\theta} = \boldsymbol{\theta}_I - \boldsymbol{\theta}_s = \frac{2}{c^2}\int_0^{\chi_s} \mathrm{d}\chi\, \frac{\mathcal{D}(\chi_s - \chi)}{\mathcal{D}(\chi_s)}\, \nabla_\perp \Phi(\chi), \tag{4.1}$$

where Φ is the gravitational potential, χ is the comoving distance along the light ray and

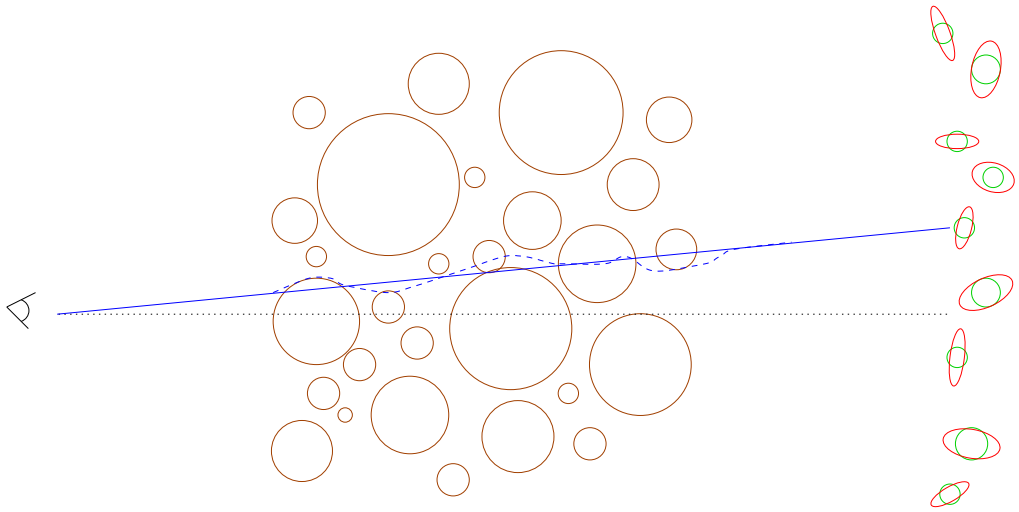

Figure 4.2: A light ray trajectory coming from a distant galaxy to the observer are deflected by intervening large scale structure (*center*). Picture source: Refregier (2003).

$\mathcal{D}(\chi)$ is the comoving angular diameter distance; for spatially flat (K=0) universe $\mathcal{D}(\chi)$ is numerically equal to the χ and the expression for χ in the flat universe is as given below,

$$\chi(z) = \frac{c}{H_0}\int_0^z (\Omega_m(1+z)^3 + \Omega_\Lambda)^{-1/2} dz \tag{4.2}$$

In equation 4.1, $\boldsymbol{\theta}_s$ is the intrinsic position of the source on the sky and $\boldsymbol{\theta}_I$ is the observed position (Figure 4.3). However, generally we do not know the true position of the source

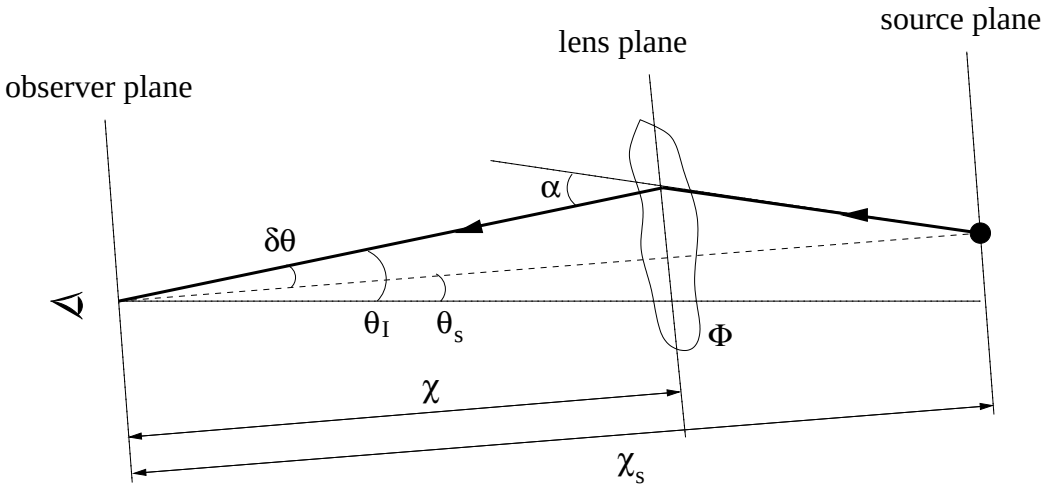

Figure 4.3: Deflection of light rays coming from a distant source by a gravitational potential fluctuation ϕ. Picture source: Munshi et al. (2008)

but only the position of the observed image. Thus the observable quantities are not the displacements $\delta\boldsymbol{\theta}$ themselves but the distortions induced by these deflections. They are given at lowest order (the weak lensing approximation) by the symmetric-shear (or distortion) matrix Ψ_{ij} (Munshi et al. (2008) and the references therein) which is defined as:

$$\Psi_{ij} = \frac{\partial \delta\theta_i}{\partial \theta_{sj}} = \frac{2}{c^2}\int_0^{\chi_s} \mathrm{d}\chi\, \frac{\mathcal{D}(\chi)\mathcal{D}(\chi_s-\chi)}{\mathcal{D}(\chi_s)}\, \nabla_i\nabla_j\Phi(\chi) \tag{4.3}$$

The above (matrix) can be conveniently written in terms of two quantities called convergence κ and the shear $\gamma = \gamma_1 + \mathrm{i}\,\gamma_2$, as following,

$$\Psi_{ij} \equiv \frac{\partial(\delta\theta_i)}{\partial\theta_j} \equiv \begin{pmatrix} \kappa+\gamma_1 & \gamma_2 \\ \gamma_2 & \kappa-\gamma_1 \end{pmatrix}, \tag{4.4}$$

From the above equation the convergence κ and the shear components γ_1,γ_2, can be written at linear order in terms of the shear tensors:

$$\kappa = \frac{\Psi_{11}+\Psi_{22}}{2},\ \ \gamma = \gamma_1 + \mathrm{i}\gamma_2 \ \text{ with } \ \gamma_1 = \frac{\Psi_{11}-\Psi_{22}}{2},\ \ \gamma_2 = \Psi_{12} \tag{4.5}$$

At linear order the convergence gives the magnification of the source and the shear describes the area preserving distortion of amplitude given by $|\gamma|$ and the direction given by its phase. Using equations 4.3 and 4.4 one can derive expression for convergence κ and the shear γ easily. In the weak lensing limit, small angle (few arc minutes) approximation, the convergence κ turns out to be nothing but the projected density field on the sky.

The cosmic shear power spectrum $P_k(\ell)$ is defined as the lensing convergence (κ)

power spectrum as a function of multipole moment ℓ (or inverse angular scale θ) P_κ, and is a measure of the projection of matter power spectrum P_δ on the sky plane,

$$\langle\kappa(\boldsymbol{\ell})\kappa^*(\boldsymbol{\ell})\rangle = (2\pi)^2\delta_D(\boldsymbol{\ell}-\boldsymbol{\ell'})P_\kappa(\ell) \tag{4.6}$$

From equation 4.5, $\kappa(\ell)$ and $\gamma(\ell)$ can be written as (Munshi et al., 2008),

$$\kappa(\boldsymbol{\ell}) = -\frac{1}{2}(\ell_x^2+\ell_y^2)\phi(\boldsymbol{\ell}) \tag{4.7}$$

$$\gamma(\boldsymbol{\ell}) = -\frac{1}{2}(\ell_x+\mathrm{i}\ell_y)^2\phi(\boldsymbol{\ell}) = \frac{\ell_x^2-\ell_y^2+2\mathrm{i}\ell_x\ell_y}{\ell_x^2+\ell_y^2}\kappa(\boldsymbol{\ell}) = \mathrm{e}^{\mathrm{i}2\beta}\kappa(\boldsymbol{\ell}) \tag{4.8}$$

where ϕ is called lensing potential defined as $\Psi_{ij} = \phi_{,ij}$, β is the polar angle of $\boldsymbol{\ell}$; $\tan\beta = \ell_y/\ell_x$, and $\boldsymbol{\ell} = (\ell_x, \ell_y)$. From the above it is obvious that $P_\kappa(\ell) = P_\gamma(\ell)$. Putting the value of $\phi(\boldsymbol{\ell})$ in terms of density contrast $\delta(\mathbf{k}, z)$ (using Poission's equation $\nabla^2\Phi = (3/2)\Omega_m H_0^2(1+z)\delta$, $\Psi_{ij} = \phi_{,ij}$ and Eq. 4.3) in the above equation and using Limber's approximation $k^2 \simeq k_\perp^2$ (here $\mathbf{k} = (k_\parallel, \mathbf{k}_\perp^{x,y})$ with $\mathbf{k}_\perp^{x,y} = \boldsymbol{\ell}/\mathcal{D}$) one can get the expression for κ and γ in terms of δ, further using the obtained expression for the convergence $\kappa(\boldsymbol{\ell})$ in equation 4.6 one can easily get the following relation for the cosmic shear power spectrum, which essentially relates the 3d matter power spectrum $P_\delta(\mathbf{k}, z)$ to the shear power spectrum $P_\gamma(\ell)$ $(= P_\kappa(\ell))$ and commonly known as Limber's equation,

$$\begin{aligned} P_\gamma(\ell) &= \frac{9}{4}\Omega_m^2\left(\frac{H_0}{c}\right)^4\int_0^{\chi_{lim}}\frac{d\chi}{a^2(\chi)}P_\delta\left(\frac{\ell}{\mathcal{D}(\chi)};\chi\right) \\ &\quad\times\left[\int_\chi^{\chi_{lim}}d\chi' n(\chi')\frac{\mathcal{D}(\chi'-\chi)}{\mathcal{D}(\chi')}\right]^2 \end{aligned} \tag{4.9}$$

where χ_{lim} is the limiting comoving distance of the survey; n(z) is the redshift distribution of the sources and ℓ is the modulus of a two dimensional wave vector perpendicular to the line of sight. P_δ is the matter power spectrum.

The correlation function $\xi(\theta)$ of the complex shear γ can be computed as,

$$\begin{aligned} \langle\gamma\gamma^*\rangle_\theta = \int\frac{d^2\ell}{(2\pi)^2}P_\gamma(\ell)\,e^{i\boldsymbol{\ell}.\boldsymbol{\theta}} &= \int\frac{\ell d\ell}{(2\pi)^2}P_\gamma(\ell)e^{i\ell\theta\cos\varphi}d\varphi \\ &= \int\frac{d\ell}{2\pi}\ell P_\gamma(\ell)J_0(\ell\theta). \end{aligned} \tag{4.10}$$

The cosmological shear field induced by density perturbations is a curl-free quantity and is donated as an E-type field. One can decompose the observed shear signal into E

(non-rotational) and B (rotational) components. Detection of non-zero B-modes indicates a non-gravitational contribution to the shear field, which might be caused by systematic contamination to the lensing signal. [1]

These decomposed shear correlation functions can be expressed as:

$$\xi_{E,B}(\theta) = \frac{\xi_{+}(\theta) \pm \xi'(\theta)}{2} \tag{4.11}$$

where ξ' is given by

$$\xi'(\theta) = \xi_{-}(\theta) + \int_{\theta}^{\infty} \frac{d\vartheta}{\vartheta} \xi_{-}(\vartheta) \left(4 - 12\left(\frac{\theta}{\vartheta}\right)^2\right) \tag{4.12}$$

ξ_{+} and ξ_{-} are two-point shear correlation functions which are related to the matter power spectrum according to the following relation,

$$\xi_{\pm}(\theta) = \frac{1}{2\pi} \int_{0}^{\infty} d\ell\ \ell P_{\gamma}(\ell) J_{0,4}(\ell\theta) \tag{4.13}$$

θ is the angular separation between the galaxy pairs, and $J_{0,4}$ are Bessel functions of the first kind.

4.3 Shear Power Spectrum From Tangled Magnetic Field Power Spectrum

We have used the magnetic field induced matter power spectrum P_{δ} (equation 1.19) to compute the shear power spectrum $P_{\gamma}(\ell)$ which in turn is used to calculate ξ_{+}, ξ_{-}, ξ_{E} and ξ_{B} using Eqs (4.11), (4.12) & (4.13). We have used the same source redshift distribution as in Fu et al. (2008):

$$n(z) = A\frac{z^a + z^{ab}}{z^b + c};\ \ A = \left(\int_0^{z_{max}} \frac{z^a + z^{ab}}{z^b + c} dz\right)^{-1} \tag{4.14}$$

where z_{max} = 6. Values of the parameters a, b, c & A we have taken from the same paper Fu et al. (2008). Values of these parameters as quoted in the paper are as, a = 0.612 $\pm$ 0.043 ; b = 8.125 $\pm$ 0.871 ; c = 0.620 $\pm$ 0.065 & A = 1.555. To evaluate the integral (4.9)

[1] The presence of primordial magnetic fields will also generate the B-modes of the shear power spectrum. Both the vector and tensor modes generated by magnetic fields could sources these modes. Vector modes are likely to play a more dominant role at angular scales of interest in this work.

we changed the variable from χ to z using (4.2).

$$P_\gamma(\ell) = \frac{9}{4}\Omega_m^2 \left(\frac{H_0}{c}\right)^4 \int_0^{z_{lim}} \frac{dz}{a^2(z)} P_\delta(k,z) \times \left[\int_z^{z_{lim}} dz'\, n(z')\, \frac{\chi(z'-z)}{\chi(z')}\right]^2 \quad (4.15)$$

where $k = \ell/\chi(z)$. Again P_δ (k,z) can be written as,

$$P_\delta(k,z) = P_\delta(k) \times D^2(z) \quad (4.16)$$

where D(z) is growth factor, which as noted above is the same as for the flat ΛCDM mode and is given by Peebles (1993):

$$D(z) = \frac{5\Omega_m}{2}[\Omega_m(1+z)^3 + \Omega_\Lambda]^{1/2} \int_z^\infty \frac{1+z}{(\Omega_m(1+z)^3+\Omega_\Lambda)^{3/2}}\, dz \quad (4.17)$$

We took z_{lim} = 2.5 for our calculations as in Fu et al. (2008).

For comparison, we also compute all the relevant quantities for the linear and non-linear ΛCDM models. For ΛCDM linear power spectrum we used $P(k,z) = AkT^2(k)D^2(z)$, where the transfer function $T(k)$ is given by Bond & Efstathiou (1984). For nonlinear ΛCDM we followed prescription given in Peacock & Dodds (1996). For all the calculations we have used flat (k=0) ΛCDM universe with Ω_m = 0.24, Ω_b = 0.044, h = 0.73 and σ_8 = 0.77.

4.4 Results

In Figure 4.4 we show the tangled magnetic field induced matter power spectra for a range of spectral index n and magnetic field strengths, B_0 at $z = 0$. The matter power spectra are plotted for $k < k_J$; a sharp cut-off below this scale is assumed for our computation. For comparison, we have also displayed the linear and non-linear ΛCDM matter power spectra (the non-linear power spectrum is obtained following the method introduced by Peacock & Dodds (1996)). The figure shows that the magnetic field induced matter power spectra can dominate over the ΛCDM case at small scales. Possible implications of this excess have already been studied for early formation of structures, reionization, and the HI signal from the epoch of reionization (Sethi & Subramanian, 2005; Tashiro & Sugiyama, 2006; Schliecher, Banerjee, Klessen , 2009; Sethi & Subramanian, 2009; Sethi, Haiman, Pandey

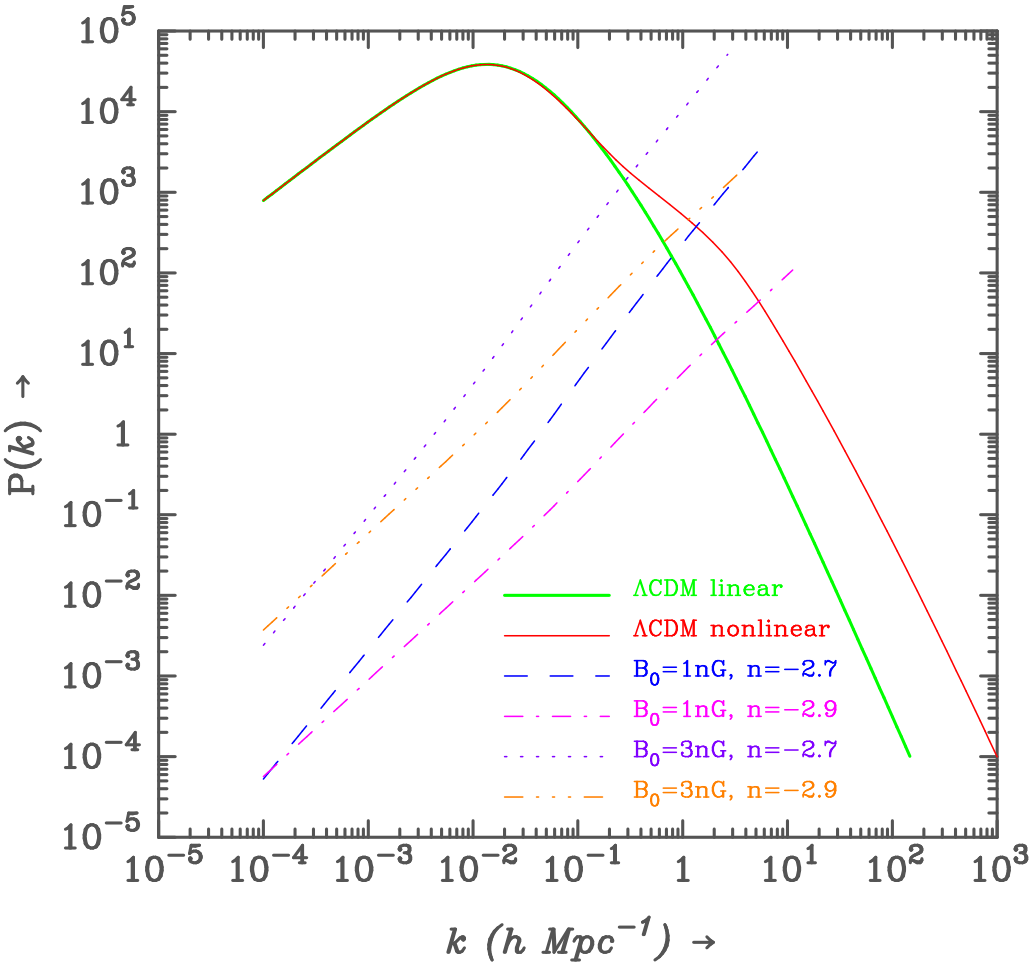

Figure 4.4: The Matter power spectrum is displayed for the magnetic and non magnetic cases. Magnetic field-induced matter power spectra are plotted for $k < k_{\rm J}$ in each case.

, 2010). Here we explore the observational signatures of this excess in the weak lensing data.

In Figure 4.5 we show the shear power spectra for magnetic and non-magnetic cases. The green and red curves present the shear power spectrum for ΛCDM linear and nonlinear matter power spectra, respectively. The blue curve shows the shear power spectrum for the tangled magnetic field power spectrum ($B_{\rm eff}$ = 3.0 nG and n = -2.9). In this figure we can see the impact of additional power in the tangled magnetic field-induced matter power spectrum as an enhancement in the shear power spectrum on angular scales $\simeq 1'$.

The peak of the matter power spectra of both the ΛCDM model and the magnetic-field induced matter power spectra are also seen in the shear power spectra. The ratio of angular scales at the peak of the two cases correspond to the ratio of these peaks of the matter power spectra: $k_{\rm eq}/k_J$. In the ΛCDM model the power at small scales falls as k^{-3}, while k_J imposes a sharp cut-off in the magnetic case. In both the cases, there is power at

angular scales smaller than the peak of the matter power spectra. But the sharp cut-off in the matter power spectrum at $k > k_J$ results in a steeper drop in shear power spectra as compared to the ΛCDM case. This cut-off ensures that the magnetic field-induced effects dominate the shear power spectrum for only a small range of angular scales.

In Figure 4.6, the two-point shear correlation functions ξ_E and ξ_B are shown for magnetic and non-magnetic cases. As noted in the previous section, we use the parameters of the paper of Fu et al. (2008) for all our computation, which allows us to directly compare our results with their data, shown in Figure 4.7.

For detailed comparison with the data of Fu et al. (2008), we performed a χ^2 including the effect of both the ΛCDM (non-linear model with the best fit parameters as obtained by Fu et al. (2008)) and the magnetic field induced signal. We fitted the sum of these two signals ($(\xi_E)_B$ + $(\xi_E)_{\Lambda CDM}$) against the CFHTLS data to obtain limits on the magnetic field strength B_0 and the spectral index n. As seen in Figure 4.6, the magnetic field induced signal dominates the data for only a small range of angular scales below a few arc-minutes. However, this can put stringent constraints on the magnetic field model. Our best fit values are $B_0 = 1.5\,\mathrm{nG}$ and $n = -2.96$. In Figure 4.7, we show the allowed contours of these parameters for a range of $\Delta\chi^2 = \chi_i^2 - \chi_{min}^2$. It should be noted that $B_0 = 0$ is an acceptable fit to the data because we fix the best fit parameters obtained by Fu et al. (2008).

4.5 Discussion

Primordial magnetic fields leave their signatures in a host of observables in the universe. Their impacts on CMBR temperature and polarization anisotropies have been extensively studied. Yamazaki et al. (2010) compute the allowed region in the $\{B_0, n\}$ plane by comparing the predictions of primordial magnetic field models with existing CMBR observations. Other constraints come from early formation of structures, Faraday rotation of CMBR polarization (e.g. Kahniashvili et al., 2010) and reionization in the presence of magnetic fields Schleicher & Miniati (2011).

In addition to the upper bounds on the magnetic field strength obtained by these observables, recent results suggests that there might be a lower bound of $\simeq 10^{-15}\,\mathrm{G}$ on the magnetic field strength (e.g. Dolag (2010); Neronov & Vovk (2010); Tavecchio et al. (2010); Taylor et al. (2011)). This would suggest that the magnetic field lies in the range $10^{-15} < B_0 <$ a few $10^{-9}\,\mathrm{G}$. This range is still too large for a precise determination of the magnetic field strength.

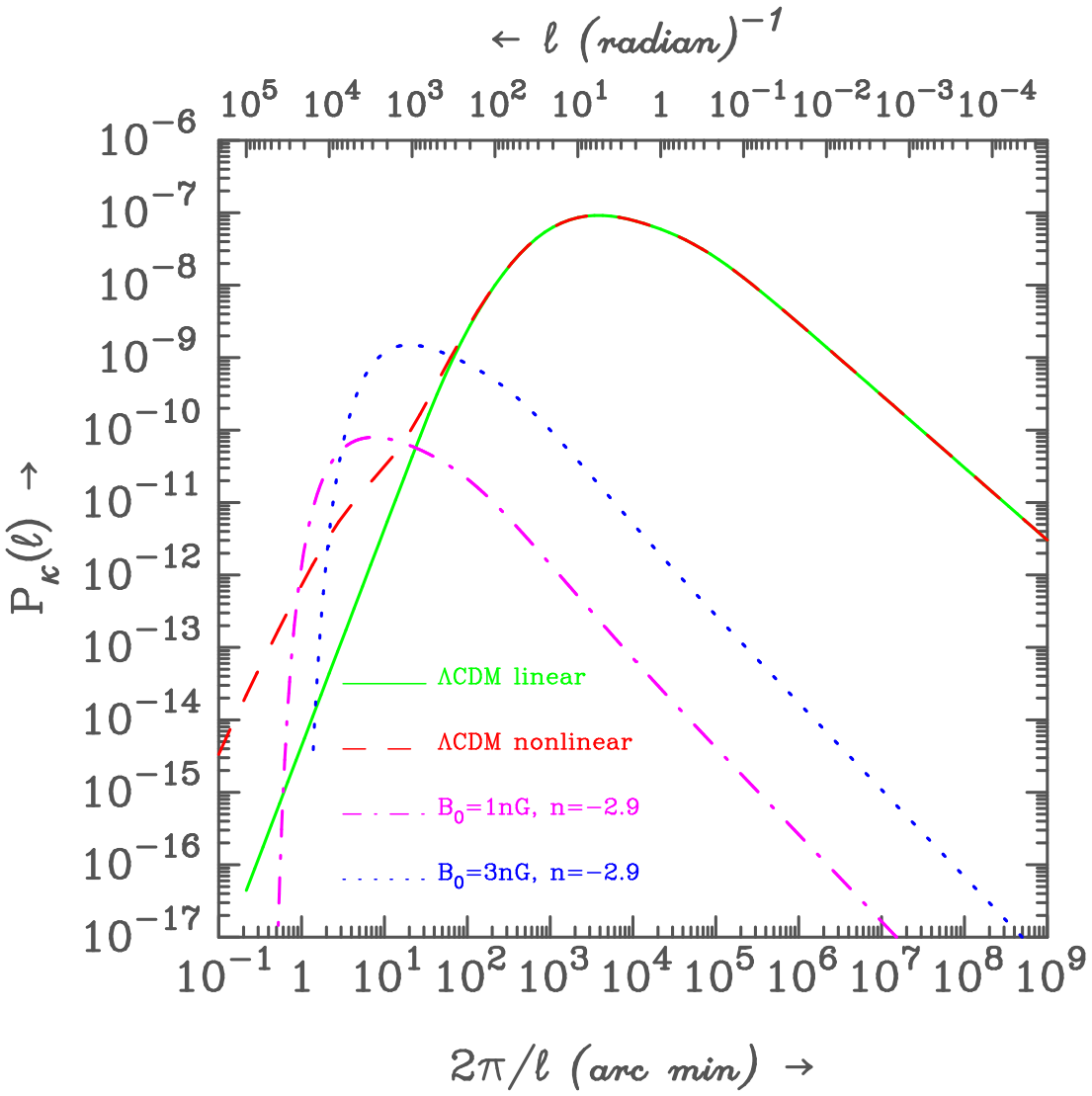

Figure 4.5: Shear power spectra for the magnetic and the ΛCDM models.

How do our constraints (Figure 4.7) compare with the existing bounds on primordial magnetic fields? CMBR constraints (e.g. Figure 1 of Yamazaki et al. (2010)) are stronger than our constraints for $n < -2.95$. For the entire range of spectral index above this value, we obtain stronger upper limits on B_0. Our limits are comparable to bounds obtained from the formation of early structures, which also arise from excess power in the magnetic field-induced matter power spectrum (e.g. Kahniashvili et al. (2010)).

Can primordial magnetic fields be detected in the Weak lensing data? As seen in Figure 4.6, detection of excess power in the measurement of ξ_E over what is expected for the ΛCDM model, constrained well from other observations, could be interpreted as contribution from primordial magnetic fields.

The present data is noisy at the scales at which magnetic fields begin to make signif-

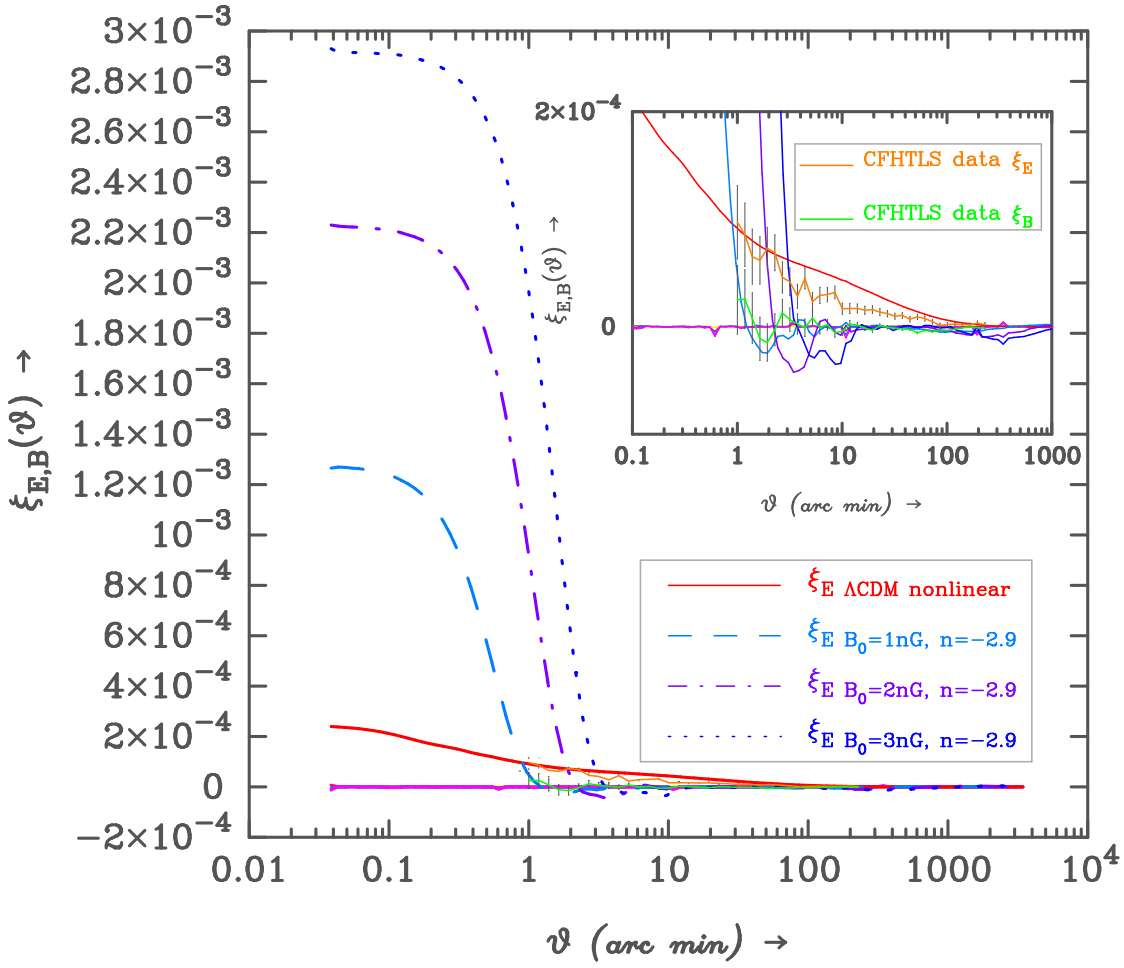

Figure 4.6: Decomposed 2-point shear correlation functions $\xi_{E,B}$ for magnetic and non magnetic cases along with CFHTLS data. The inset magnifies the relevant curves and data points for a smaller range of ordinate values. The solid (magenta) curves correspond to ξ_B.

icant contribution, at least partly owing to errors inherent in ground based measurements of shear, e.g. correction for point spread function, etc (e.g. Figure 5 of (Schrabback et al., 2010); a brief look at this figure might suggest that their measurements would already put stronger constraints on magnetic field strength than presented here). Future, proposed space missions such as SNAP are likely to greatly improve the errors on these measurements. A comparison of Figure 4 of the white paper on weak lensing with SNAP (Albert et al. , 2005) with the Figure 4.6 of this paper suggests that SNAP would easily be able to probe sub-nano Gauss magnetic fields.

The magnetic field signal could be degenerate with the overall normalization of the ΛCDM model as measured by σ_8 ; WMAP 7-year data give $\sigma_8 = 0.801 \pm 0.030$ ((Larson et al., 2011)). WMAP results are in reasonable agreement with the value of σ_8 as inferred by the weak lensing data. This error is not sufficient to mimic the much larger signal

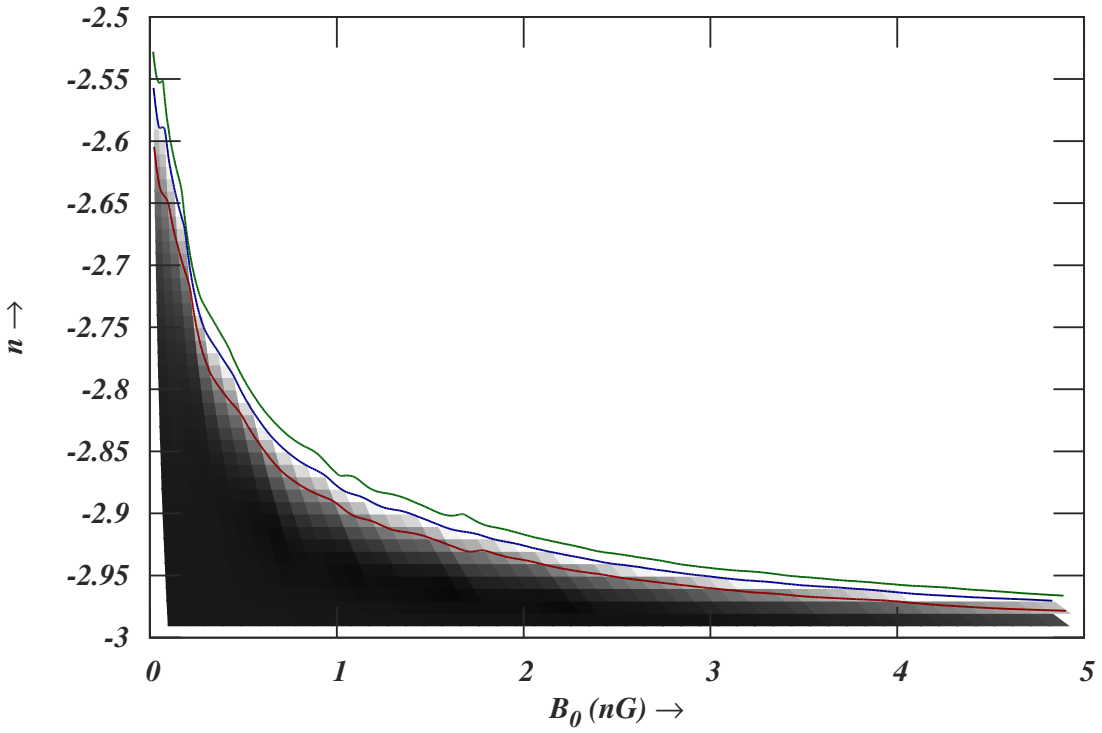

Figure 4.7: The figure shows the allowed region in the (B_0,n) plane, based on the analysis of ($(\xi_E)_B$ + $(\xi_E)_{\Lambda\mathrm{CDM}}$) against the CFHTLS data Fu et al. (2008). The shaded area is the 1-σ allowed region. The three curves (from top to bottom) are contours at 5σ, 3σ and 1σ level.

from magnetic field strengths considered in this work (e.g. Figure 4 of(Schrabback et al., 2010)). However, a more careful analysis will be needed to distinguish the error in σ_8 from the sub-nano Gauss magnetic fields.

One uncertainty in our analysis is that the magnetic Jeans scale, unlike the thermal Jeans scale which is well defined in linear perturbation theory, is obtained within an approximation in which the back-reaction of the magnetic field on the matter is not exactly captured (e.g. Kim et al., 1996; Sethi & Subramanian, 2005). Even though our results capture qualitatively the impact of such a scale, there could be more power on sub-Jeans scale which is lost owing to our approximation of the sharp k-cut off. In this analysis the cut-off scale used is the larger of the magnetic Jeans length and the thermal Jeans length. Magnetic field dissipation can raise the temperature of the medium to $\simeq 10^4\,\mathrm{K}$, thereby raising thermal Jeans length of the medium (Figure 4 of Sethi et al. (2008) for a compar-

ison between the two scales for different magnetic field strengths). For $B_0 \gtrsim 10^{-9}\,\mathrm{G}$, the magnetic Jeans scale is the larger of the two scales, as the maximum temperature of the medium reached owing to this process doesn't exceed $10^4\,\mathrm{K}$. In the more general case also this would be true as photoionization of the medium by other sources, e.g. the sources which could have cause reionization of the universe at $z \simeq 10$, also results in comparable temperatures. For magnetic field strengths smaller than considered in the work, the cut-off scale is likely to be determined by thermal Jeans scale, caused by the photoionization of the medium by sources other than the magnetic field dissipation. Our approximation allows us to identify important length and angular scales for our study (Figure 4.5 and 4.6). However, further work along these lines could extend our analysis by taking into account the physical effects of sub-magnetic Jeans scales.

The analysis of Lyman-α forest in the redshift range $2 \lesssim z \lesssim 4$ is another powerful probe of the matter power spectrum of at small scales (e.g. Croft et al., 2002). Primordial magnetic field can alter this interpretation in many ways: (a) more small scale power owing to magnetic field induced matter power spectrum (Figure 4.4), (b) dissipation of magnetic field can change the thermal state of Lyman-α clouds (Sethi, Haiman, Pandey , 2010; Sethi & Subramanian, 2005, e.g.), (c) magnetic Jeans length can reduce the power at the smallest probable scale. In the next chapter we will look into and discuss some of these effects in detail.

5

Probing Primordial Magnetic Fields Using Lyα Clouds

5.1 Introduction

In the past 10 years, cosmological weak lensing and the study of Lyα clouds in the redshift range $2 \lesssim z \lesssim 5$ have emerged as reliable methods to precisely determine the matter power spectrum on scales below $10\,h^{-1}\mathrm{Mpc}$ (Figure 4.1). In particular, these methods can estimate the matter power spectrum at small scales which are not directly accessible to other methods e.g. galaxy surveys (for details and further references see e.g. Munshi et al. (2008); Hoekstra & Jain (2008); Croft et al. (1998, 1999, 2002)). Since these are the scales which are highly affected by the existence of primordial magnetic fields (see Figures 1.4 or 5.3), a careful analysis of these cosmological variables can actually probe the existence of these magnetic fields.

In this work we attempt to constrain primordial magnetic fields within the framework of the distribution of Lyα clouds in the intergalactic medium (IGM) in the redshift range $2 \lesssim z \lesssim 5$. These clouds have been shown to originate in the mildly non-linear density regions of the IGM (Cen & Ostriker (1994)). This has allowed development of detailed semi-analytic methods to understand the observed properties of these clouds (e.g. Bi et al., 1995; Hui et al., 1997; Choudhury et al., 2001a,b). Adopting a semi-analytic approach, we simulate density fluctuation along the line-of-sight, including the contribution of matter perturbations induced by these magnetic fields. We compute effective Lyα opacity of the IGM for this computed Lyα cloud distribution and compare our results with the existing data (e.g. Faucher-Giguère et al., 2008).

In the previous analysis, the density perturbations induced by magnetic fields are assumed to be uncorrelated to the density field generated by the usual ΛCDM model. Re-

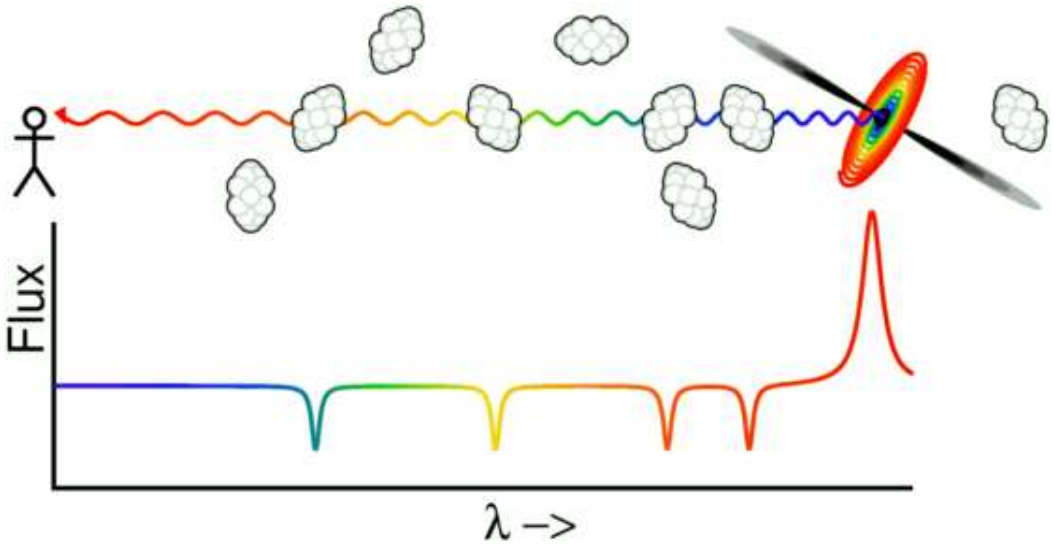

Figure 5.1: Formation of Lyα lines in quasar spectra; Picture source: Professor Edward L. Wright's webpage.[1]

cently, Caldwell & Motta (2011) showed that if the conformal invariance of electromagnetism is broken during the inflation and thus produced the primordial magnetic fields, these magnetic fields may be correlated with the primordial density perturbations. In our analysis we have made a separate case for such fields.

The PMF induced matter perturbations grow in the post recombination era by gravitational instability. The matter power spectrum of these perturbations is given by: $P(k) \propto k^{2n+7}$, for $n < -1.5$, the range of spectral index we consider here (Wasserman, 1978; Kim et al., 1996; Gopal & Sethi, 2003).

Magnetic field induced matter perturbations can only grow for scales above the magnetic field Jeans length: $k_{\rm J} \simeq 15 \times (10^{-9}\,{\rm G}/{\rm B_{eff}})$ (e.g. Kim et al., 1996; Kahniashvili et al., 2010). The dissipation of tangled magnetic field in the post-recombination era also results in an increase in the thermal Jeans length (Sethi & Subramanian, 2005; Sethi et al., 2008). For most of the range of magnetic field strengths and the physical setting (Lyα clouds at a temperature of $\simeq 10^4\,{\rm K}$) considered here, the scale corresponding to $k_{\rm J}$ generally are comparable to or smaller than the thermal Jeans length.

For our computation, we need to know the time evolution of the matter power spectrum induced by tangled magnetic fields. It can be shown that the dominant growing mode in this case has the same time dependence as the ΛCDM model (see e.g. Gopal & Sethi (2003) and references therein)

[1] http://www.astro.ucla.edu/∼wright/Lyman-alpha-forest.html

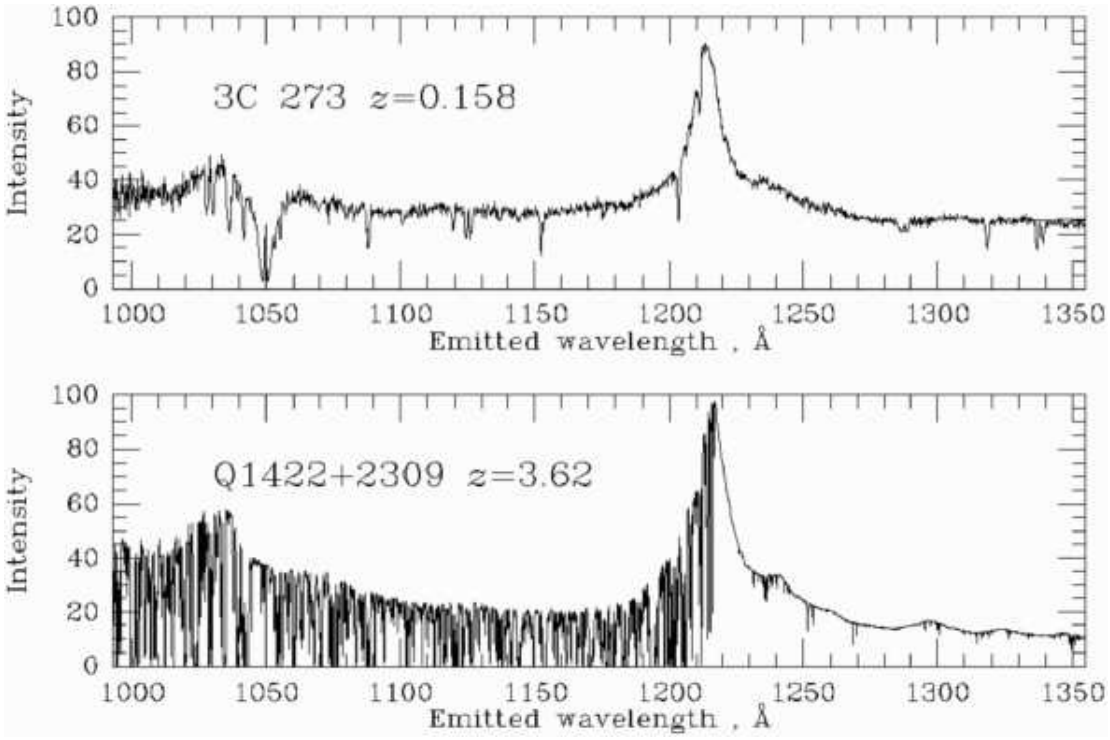

Figure 5.2: Two actual quasar spectra. One is the nearby quasar 3C273 while the other is a large redshift object; Picture source: Professor Edward L. Wright's webpage.[1]

5.2 Lyα Clouds

Lyα clouds are cosmological objects of smaller overdensities of around a few to a few hundred. These are much smaller in size and mass than that of a typical galaxy, and can be seen only by the absorption line they produce in the Lyα radiation coming from luminous high redshift quasars. These absorption lines can be seen in the spectrum of a quasar towards the blue or shorter wavelength side of the quasar emission (Lyα) line (Figure 5.1). In the spectrum of a high redshift quasar these line appear as a very finely spaced forest of lines and thus called Lyα forest (Figure 5.2). By Studying these Lyα forest in the spectrum of redshift quasars we can learn about the density fluctuation in the Universe on the smallest scales. Due to the background ionizing uv radiation coming from the surrounding QSO and star-forming galaxies, they are highly ionized gas clouds with the neutral fraction of Hydrogen of the order of 10^{-5}. Following are some of typical values related to Lyα clouds:

Table 5.1: Typical values of some physical properties of Lyα clouds

#	**Physical Property**	**Value**
1	Physical Size	100 kpc
2	Number Density	2.5×10^{-5} cm^{-3}
3	Column Density	10^{14} cm^{-2}
4	Neutral Fraction	$\approx 10^{-4}$
5	Temperature	$\gtrsim 10^5 K$

5.3 The Simulation: Density Fluctuation Along The Line-Of-Sight: Distribution Of Lyα Clouds

We describe a brief outline of the numerical simulation in this section. Hydrodynamical simulations have shown that Lyα clouds are mildly non-linear ($\delta \lesssim 10$) regions of the IGM at high redshifts. This allows one to analytically derive important observables from the Lyα clouds semi-analytically, in terms of a few parameters denoting the ionization, thermal, and dynamical state of the clouds.

Here we have closely followed the semi-analytic prescription given in Bi & Davidson (1997). In this paper we have considered two cases of primordial magnetic field induced matter perturbations : (1) pure ΛCDM matter perturbations and primordial magnetic field (PMF) induced matter perturbations are uncorrelated (2) those two are correlated. In both cases we compute two separate line-of-sight density (and velocity) fields each corresponding to a single kind of matter perturbations. In the former case, these fields are drawn from different realizations and in the latter the fields are generated from the same realization. We add these two density (and velocity) fields to get the final density (and velocity) fields in the IGM. To simulate line-of-sight IGM density and velocity fields for a given three-dimensional matter power spectrum (inflationary/PMF induced), first we calculate the corresponding three-dimensional baryon power spectrum, which corresponds to the original power spectrum smoothed over the scales below the larger of the thermal or Magnetic Jeans scale x_b

$$P_{\rm B}^{(3)}(k,z) = \frac{P_{\rm DM}^{(3)}(k,z)}{[1 + x_b^2(z)k^2]} \tag{5.1}$$

where

$$x_b(z) = \frac{1}{H_0}\left[\frac{2\gamma k_{\rm B} T_{\rm m}(z)}{3\mu m_p \Omega_{\rm m}(1+z)}\right]^{1/2} \tag{5.2}$$

then we compute one-dimensional baryon (density, velocity and density-velocity) power

spectra, which will be used in the further computation. We note here that the relevant scale of smoothing for the range of magnetic field values and the IGM temperatures we consider is thermal Jeans scale and not the magnetic Jeans scale. The one-dimensional power spectra can be computed using the following relations

$$P_{\rm B}^{(1)}(k,z) = \frac{1}{2\pi}\int_{|k|}^{\infty} dk' k' P_{\rm B}^{(3)}(k,z) \tag{5.3}$$

$$P_{\rm v}^{(1)}(k,z) = \dot{a}^2(z)k^2\frac{1}{2\pi}\int_{|k|}^{\infty} \frac{dk'}{k'^3} P_{\rm B}^{(3)}(k,z) \tag{5.4}$$

$$P_{\rm Bv}^{(1)}(k,z) = i\dot{a}(z)k\frac{1}{2\pi}\int_{|k|}^{\infty} \frac{dk'}{k'} P_{\rm B}^{(3)}(k,z) \tag{5.5}$$

where a is the scale factor.

The density ($\delta_0(k,z)$) and velocity ($v(k,z)$) fields in one dimension are two correlated Gaussian random fields (the correlation is given by the density-velocity power spectrum), we use the inverse Gram-Schmidt procedure to simulate them in terms of two independent Gaussian random fields $w(k)$ and $u(k)$ of power spectra respectively $P_{\rm w}(k)$ and $P_{\rm u}(k)$

$$\delta_0(k,z) = D(z)[u(k) + w(k)] \tag{5.6}$$

$$v(k,z) = F(z)i\dot{a}k\beta(k,z)w(k,z) \tag{5.7}$$

where $D(z)$ and $F(z)$ are the linear density and velocity growth factors. Functions $\beta(k)$, $P_{\rm w}(k)$ and $P_{\rm u}(k)$ are function of $P_{\rm B}^{(3)}(k)$,

$$\beta(k,z) = \int_{|k|}^{\infty} \frac{P_{\rm B}^{(3)}/k'^3 dk'}{P_{\rm B}^{(3)}/k' dk'} \tag{5.8}$$

$$P_{\rm w}(k) = \frac{1}{\beta(k)}\int_{|k|}^{\infty} \frac{P_{\rm B}^{(3)}(k')}{k'} dk' \tag{5.9}$$

$$P_{\rm u}(k) = \frac{1}{2\pi}\int_{|k|}^{\infty} P_{\rm B}^{(3)}(k')k'dk' - P_{\rm w}(k) \tag{5.10}$$

We compute $\delta_0(k,z)$ and $v(k,z)$ for both kinds of perturbations separately, the corresponding $\delta_{\rm B}(x,z)$ and $v(x,z)$ is computed by using Fourier transforms. And then we add the contribution from both the kinds together ($\delta_{\rm B}(x,z) = \delta_{\rm B}^{\rm infl}(x,z) + \delta_{\rm B}^{\rm pmf}(x,z)$ and $v(x,z) = v^{\rm infl}(x,z) + v^{\rm pmf}(x,z)$) to get the final combined line-of-sight density and velocity fields. To compute one-dimensional density field for the PMF-induced perturbations

we use the three-dimensional matter power spectrum (e.g. Gopal & Sethi, 2003); for inflationary perturbations we use the standard ΛCDM power spectrum.

For our computations we have generated the density and velocity fields for 25 redshift bins between the redshifts 0 to 5. In each bin we have 2^{14} points resolving the Jeans scale by at least a factor of 4. The cutoff scale (Jeans scale, x_b) is the larger of the thermal Jeans length and the magnetic Jeans length.

To take into account the non-linearity of density perturbations in the IGM we use lognormal distribution of the IGM density field Bi & Davidson (1997), thus the number density of baryons in IGM is taken to be,

$$n_{\rm B}(x,z) = Ae^{\delta_{\rm B}(x,z)} \tag{5.11}$$

Here A is a constant which can be determined using the following relation:

$$\langle n_{\rm B}(x,z)\rangle \equiv n_0(z) = A\langle e^{\delta_B(x,z)}\rangle \tag{5.12}$$

since $\delta_{\rm B}(x,z)$ is a Gaussian random variable,

$$\left\langle e^{\delta_{\rm B}(x,z)}\right\rangle = e^{\langle\delta_{\rm B}^2(x,z)\rangle} \tag{5.13}$$

thus

$$n_{\rm B}(x,z) = n_0(z)e^{(\delta_{\rm B}(x,z)-\langle\delta_{\rm B}^2(x,z)\rangle)} \tag{5.14}$$

where $n_0(z)$ is the background baryon number density given by,

$$n_0(z) = \frac{\Omega_{\rm B}\rho_c}{\mu_{\rm B}m_p}(1+z)^3 \tag{5.15}$$

5.4 Calculation Of Lyα Opacity

The optical depth τ is given by

$$\tau(\nu) = \int n_{\rm HI}(t)\sigma_a\left(\frac{\nu}{a}\right)dt \tag{5.16}$$

where $n_{\rm HI}$ is number density of neutral hydrogen in the IGM, ν is the observed frequency, which is related to redshift z by $z \equiv (\nu_a/\nu) - 1$, ν_a is the Lyα frequency at rest. The

absorption cross section σ_a is given by,

$$\sigma_a = \frac{I_a}{b\sqrt{\pi}} V\left(\alpha, \frac{\nu-\nu_a}{b\nu_a} + \frac{v}{b}\right) \tag{5.17}$$

where parameter $b = (2kT/m_p)^{1/2}$ is the velocity dispersion and $v(x)$ is the peculiar velocity field, $\alpha \equiv 2\pi e^2 \nu_a / 3 m_e c^3 b = 4.8548 \times 10^{-8}/b$, $I_\alpha = 4.45 \times 10^{-18} \mathrm{cm}^{-2}$ and V is the Voigt function.

The number density of neutral hydrogen, n_{HI} can be computed by solving ionization equilibrium equation,

$$n_{\rm HI}(x,z) = \frac{\alpha[T(x,z)] n_{\rm B}(x,z)}{\alpha[T(x,z)] + \Gamma_{ci}[T(x,z)] + J(z)/[\mu_e n_{\rm B}(x,z)]} \tag{5.18}$$

where $T(x,z)$ is given by $T(x,z) = T_0(z)[n_{\rm B}(x,z)/n_0(z)]^{\gamma-1}$ where $T_0(z)$ is the temperature of the IGM at the mean density and γ is the polytropic index for the IGM; γ captures the dynamical state of the IGM gas which gives rise to the observed Lyα absorption. These parameters are likely to take values in the ranges 4000 $\lesssim T_0 \lesssim$ 15,000 K and 1.3 $\lesssim \gamma \lesssim$ 1.6 (Hui & Gnedin, 1997). $\alpha(T)$, $\Gamma_{ci}(T)$ and $J(z)$ are recombination rate, collisional ionization rate and photo ionization rates in the IGM. For temperature $T \simeq 10^4$ K, the combination of these effects yields (Croft et al.1998),

$$\tau(z) \propto n_{\rm B}^2 T^{-0.7} = A(n_{\rm B}/n_0)^{2-0.7(\gamma-1)},$$

$$A = 0.946 \left(\frac{1+z}{4}\right)^6 \left(\frac{\Omega_{\rm B} h^2}{0.0125}\right)^2 \left(\frac{T_0}{10^4 \mathrm{K}}\right)^{-0.7} \left(\frac{J}{10^{12} \mathrm{s}^{-1}}\right)^{-1} \left[\frac{H(z)}{H_0}\right]^{-1} \tag{5.19}$$

To compare with the data we have computed effective optical depth which is the observable quantity in the form of decrease in observed flux ($F \propto e^{-\tau}$) and is given by,

$$\tau_{\rm eff}(z) = -\log\left[\langle \exp(-\tau) \rangle\right] \tag{5.20}$$

The data which we have used for comparison with simulation results has been obtained using high resolution spectral observations such as the High resolution Echelle Spectrometer (HIRES), the Echelle Spectrograph and Imager (ESI), and MIKE having FWHM in the range of 6–$44\,\mathrm{km\,s^{-1}}$ (Faucher-Giguère et al. (2008)), which resolve the Jeans scales over the redshifts we are considering. Since we are also resolving Jeans scale in our simulation, we can directly compare our theoretical results with these data without taking into account the scale dependence of $\tau_{\rm eff}$ in our analysis.

The mean opacity $\langle\tau\rangle$ and the effective opacity are computed by averaging over all the realizations of τ for a given redshift bin.

We have used flat (k=0) ΛCDM universe with $\Omega_{\rm m}$ = 0.24, $\Omega_{\rm b}$ = 0.044, h = 0.73 and σ_8 = 0.77.

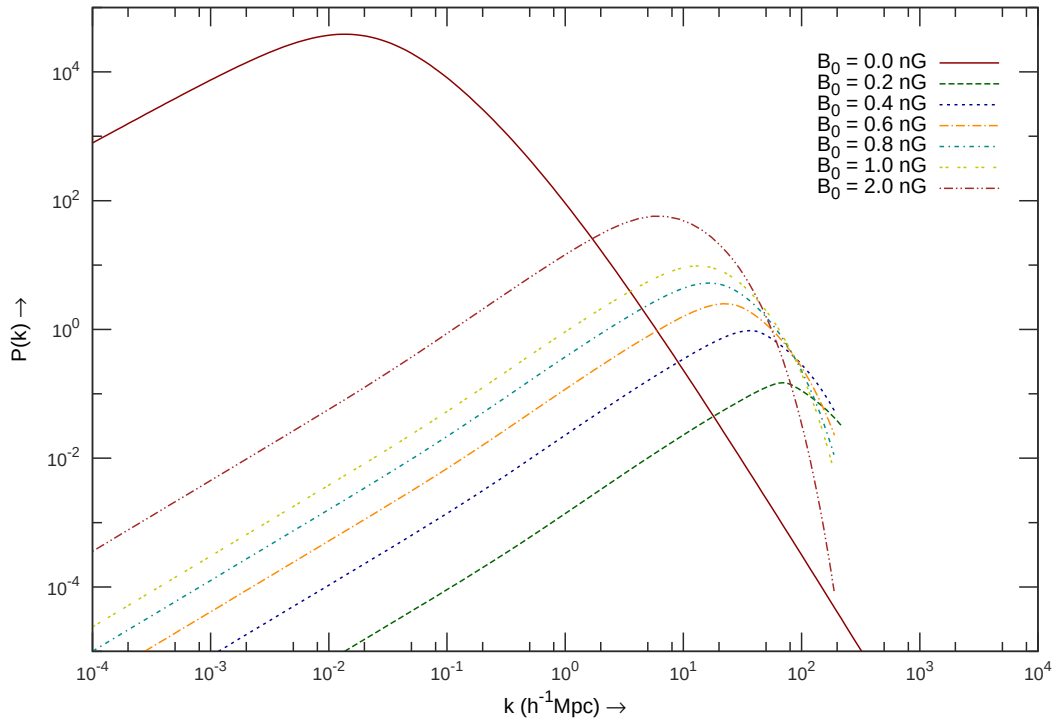

Figure 5.3: The matter power spectrum for magnetic case, with added exponential cutoff and then smoothed around magnetic Jeans length $k_{\rm J}$, is displayed for various values of magnetic field strength B_0. Spectral index n is -2.95 for each case. Along with that the red curve is matter power spectrum for pure ΛCDM non-magnetic case.

5.5 Results

In Figure 5.3 we show the matter power spectra at the present epoch for magnetic case, along with the pure ΛCDM (non-magnetic) matter power spectrum, which has been used in our calculations, here an exponential cut-off around k magnetic Jeans scale is assumed. This figure shows that the magnetic field induced matter power spectra can dominate over the pure ΛCDM case at small scales ($k \geq 1\, h\mathrm{Mpc}^{-1}$). The effect of this excess has already been studied in the context of early structure formation, reionization, and weak-lensing signals (Sethi & Subramanian (2005, 2009), Pandey & Sethi (2012)) As an extension to that body of work we explore the effect of this excess on Lyα effective opacity in this

paper.

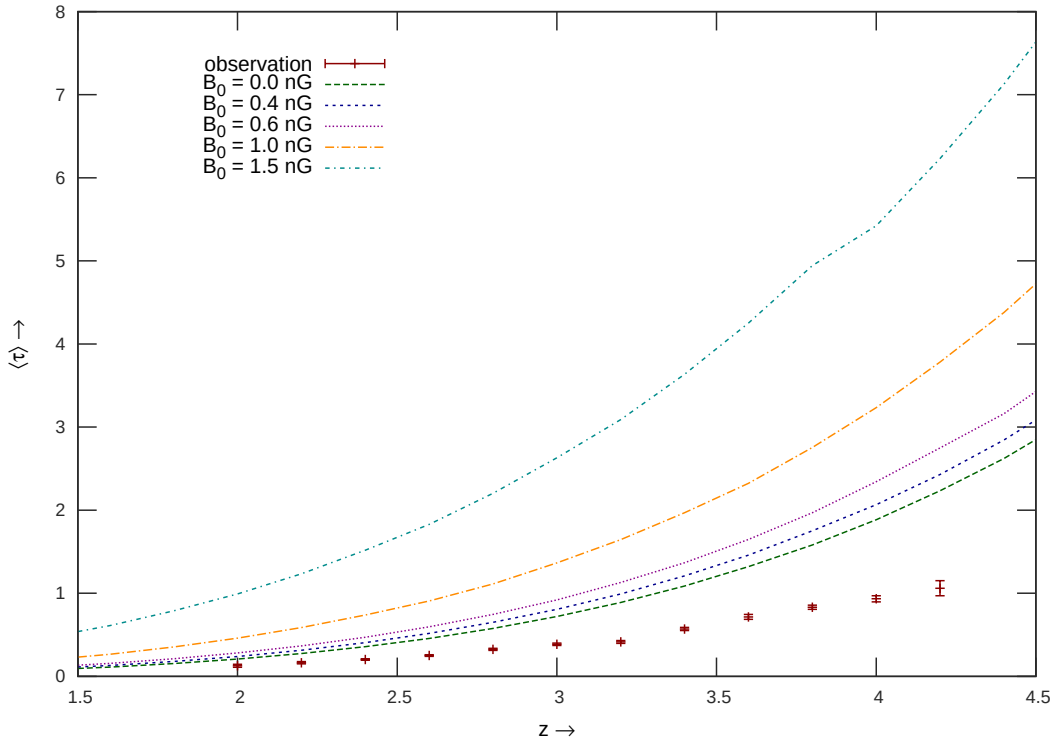

Figure 5.4: Evolution of $\langle\tau\rangle$ for the uncorrelated $\delta_{\rm infl}$ and $\delta_{\rm pmf}$ case.

In Figure 5.4 we show the variation of Lyα opacity $\langle\tau\rangle$ with redshift for various values of magnetic field strengths. The red dots with y-errorbars are the observed values of Lyα opacity $\tau_{\rm eff}$ (Faucher-Giguère et al. (2008)). It should be pointed out that the inclusion of peculiar velocities in the computation of τ (Equation (5.17)) makes a negligible difference to the value of either average or effective opacity.

Figure 5.4 corresponds to the case when matter perturbations induced by primordial magnetic fields and the inflationary matter perturbations are not correlated. The average opacity $\langle\tau\rangle$ is not an observable quantity.The aim of Figure 5.4 is to demonstrate that the inclusion of PMF matter perturbations enhances the average opacity of the IGM.

In Figure 5.5 we show the variation of $\tau_{\rm eff}$ with redshift for various values of magnetic field strength along with the observed evolution of $\tau_{\rm eff}$. This plot is for the case when matter perturbations induced by primordial magnetic field and the inflationary matter perturbations are not correlated. Comparing this figure with Figure 5.4 we see that the slope of redshift evolution of $\tau_{\rm eff}$ is far smaller than for average opacity. This difference is owing to the fact that for HI column densities $N_{\rm HI} \gtrsim 10^{14}\,{\rm cm}^{-2}$, the optical depth exceeds one. For column densities larger than this saturation value, the optical depth increases only as logarithm of the column density and therefore these clouds get a smaller weight in the

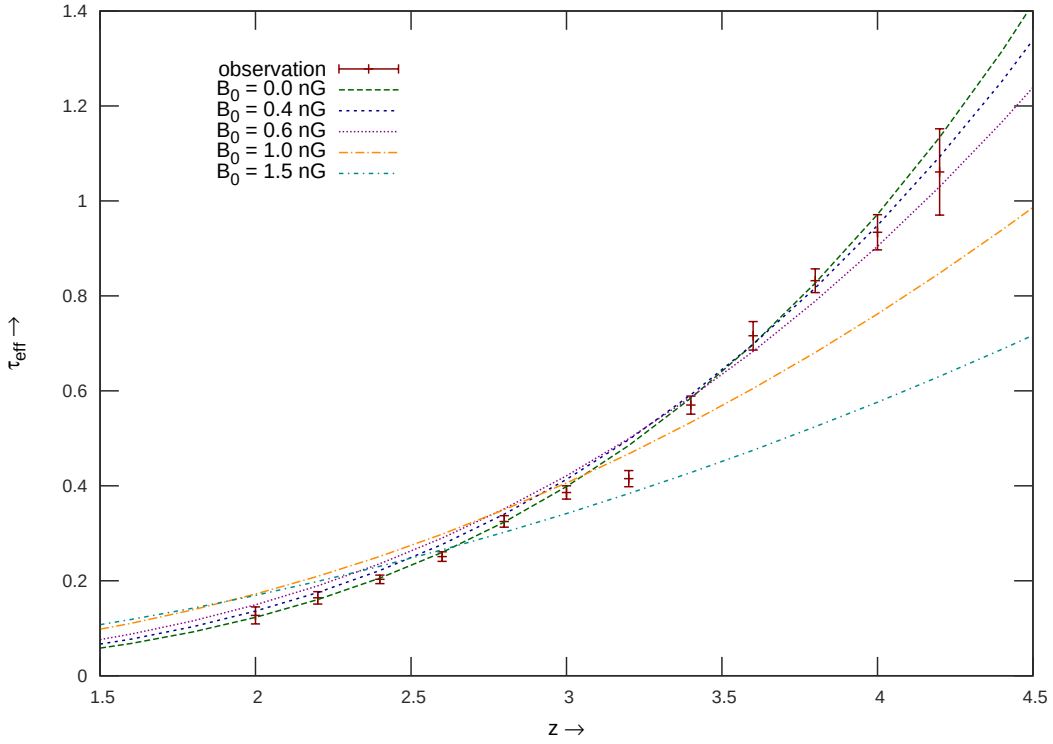

Figure 5.5: Evolution of $\tau_{\rm eff}$ for the uncorrelated $\delta_{\rm infl}$ and $\delta_{\rm pmf}$ case.

computation of $\tau_{\rm eff}$. As the average opacity of the IGM increases sharply with increasing redshift (Equation (5.19)), this effect is more enhanced at higher redshifts.

A comparison between Figures 5.4 and 5.5 shows that an increase in $\langle\tau\rangle$ doesn't necessarily lead to an increase in $\tau_{\rm eff}$. In Figure 5.5 it is seen that $\tau_{\rm eff}$ is greater than the usual ΛCDM case for $z \lesssim 3$ but falls below the predictions of this model for larger redshifts.

We can understand this behavior by the following set of arguments. The change in the effective optical depth $d\tau_{\rm eff} \propto \sum_i \exp(-\tau_i) d\tau_i$, where τ_i refers to optical depths of individual clouds. On the other hand, $d\langle\tau\rangle \propto \sum_i d\tau_i$. As seen in Figure 5.4, the inclusion of PMF density perturbations increase $\langle\tau\rangle$ or $\sum_i d\tau_i > 0$, but $\sum_i \exp(-\tau_i) d\tau_i$ could be negative if $d\tau_i$ is negative wherever τ_i is smallest. To elaborate this point, In Figure 5.8 we have plotted the distribution of optical depths τ_is for the 1.5 nG case ($z = 4$), against the $d\tau_i = \tau_i\ (2\ nG) - \tau_i\ (0\ nG); (z = 4)$. It is clear from this figure that τ_i values are small when $d\tau_i$ is more negative, or this can make $\sum_i \exp(-\tau_i) d\tau_i$ negative, and thus it explains the decrease of $\tau_{\rm eff}$ even when there is increase in $\langle\tau\rangle$ with increasing magnetic field values. It should be pointed out that this behavior of $\tau_{\rm eff}$ cannot be mimicked by a change in J, γ (Equation (5.19)) or by a scaling of the power spectrum by changing the value of σ_8.

The Figures 5.6 and 5.7 are for the same analysis as Figures 5.4 and 5.5 respectively,

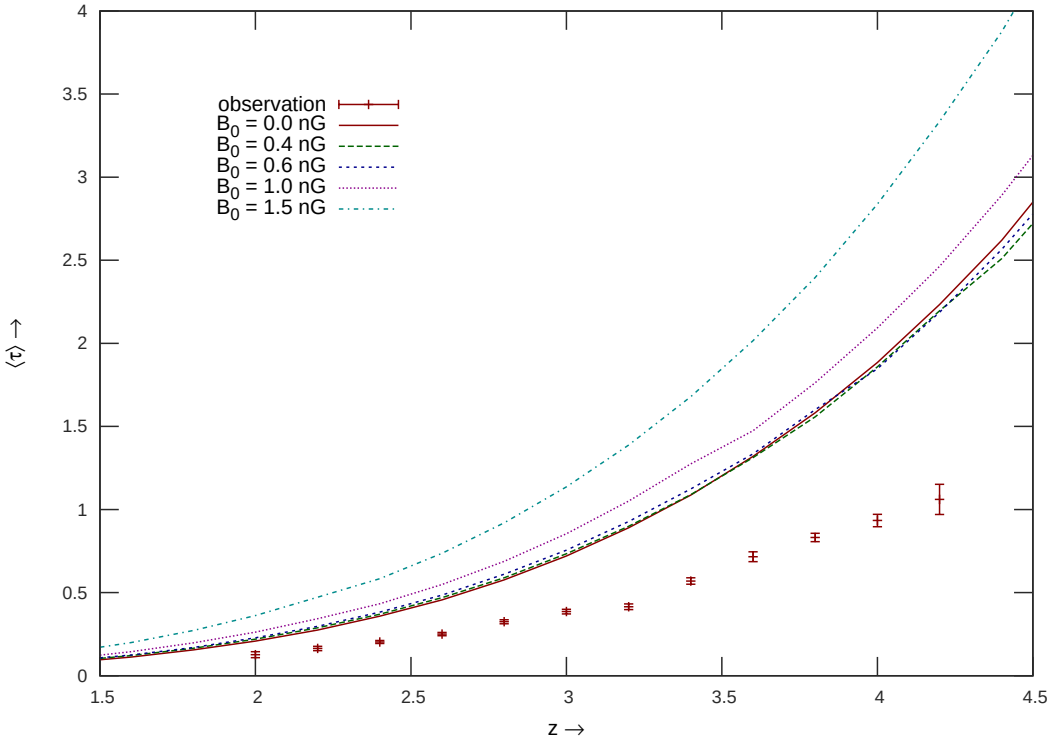

Figure 5.6: Evolution of $\langle\tau\rangle$ for the correlated $\delta_{\rm infl}$ and $\delta_{\rm pmf}$ case.

but for the case when induced matter perturbations and inflationary matter perturbations are correlated. In Figure 5.6 the values of $\langle\tau\rangle$ are smaller in comparison to the corresponding values in the case of uncorrelated matter perturbations.

For detailed comparison with observations we performed the likelihood analysis for the $\tau_{\rm eff}$ against the Faucher-Giguère et al. (2008) data as a function of four parameters, J ((1.4 to 2.0)10^{-12}), γ (1.4 to 2.0), B_0 ((0.1 to 2.0) nG), and n (-2.80 to -2.99). To compute the posterior probability for magnetic field parameters, we marginalized the likelihood function over the parameters J and γ. Figure 5.9 shows the results of this analysis for the uncorrelated case. The curves from top to bottom are the contours for 5σ, 3σ and 1σ levels for a range of $\Delta\chi^2 = \chi^2_{\rm i} - \chi^2_{\rm min}$. We see that in this case for $n = -2.90$ the allowed values (by 5σ) of magnetic field are $B_0 <$ 0.6-0.7 nG, and for $n = -2.95$ is $B_0 < 1.3\,{\rm nG}$.

In Figure 5.10, we compare this result with our previous analysis with the weak-lensing data Pandey & Sethi (2012) and the present analysis with the correlated case: the lower triplet (red green and blue), solid and dashed corresponds to the uncorrelated and the correlated cases respectively of the present analysis, whereas the upper triplet (dotted) correspond to our previous analysis with the weak-lensing data. It is clearly seen from Figure 5.10 that the constraints arising from the correlated case are not very different from the uncorrelated case. Or the Lyα clouds do not provide an appropriate physical setting

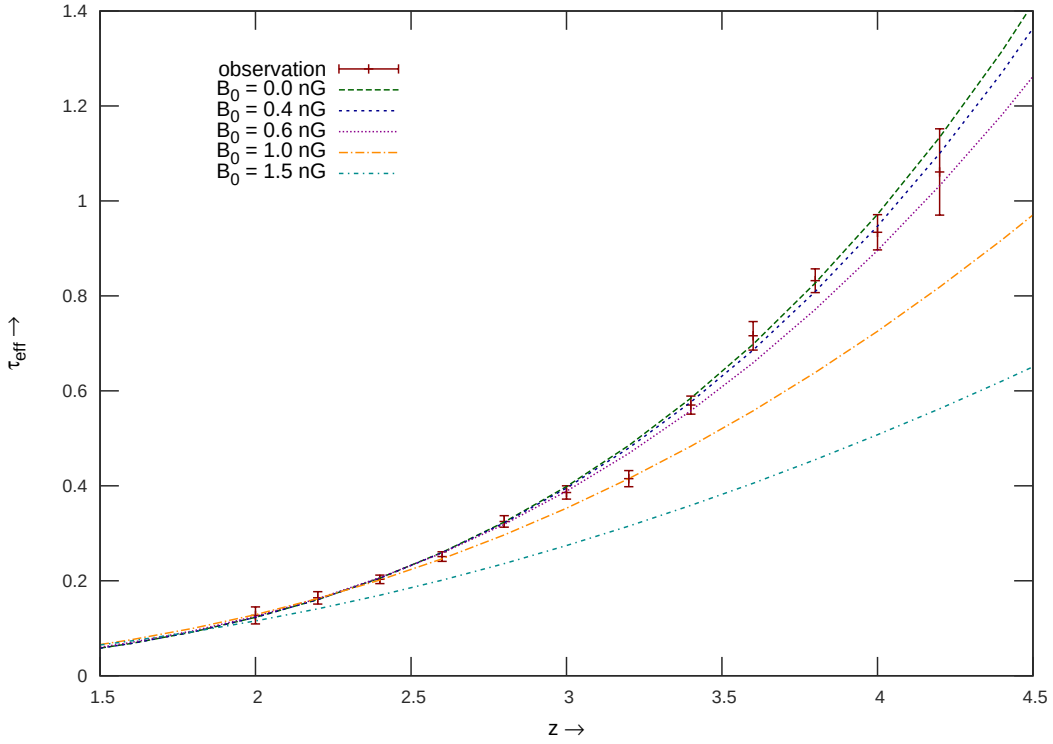

Figure 5.7: Evolution of $\tau_{\rm eff}$ for the correlated $\delta_{\rm infl}$ and $\delta_{\rm pmf}$ case.

for distinguishing between these two cases. From Figure 5.10 it also follows that our present constraints are considerably stronger that our previous analysis with the cosmological weak-lensing data.

5.6 Discussion

Primordial tangled magnetic fields leave their signatures on cosmological observables for a large range of scales from sub-Mpc to $10^4\,\mathrm{Mpc}$. CMBR temperature and polarization anisotropies provide probes for the magnetic fields for scales $\gtrsim 10\,\mathrm{Mpc}$ (e.g. Kahniashvili et al., 2010). Recently, Yamazaki et al. (2010) computed the allowed region in the $\{B_0, n\}$ plane by comparing the predictions of primordial magnetic field models with existing CMBR observations. Constraints on smaller scale come from early formation of structures induced by PMF. The observables that impact these scales include early reionization, HI signal from the epoch of reionization (Sethi & Subramanian (2009, 2005), Schleicher & Miniati (2011)), cosmological weak gravitation lensing (Pandey & Sethi (2012)), etc. Other constraints on large scale cosmological magnetic fields arise from rotation measure (RM) of high redshift polarized radio sources (e.g. Kolatt, 1998; Sethi, 2003; Blasi et al., 1999); RM of radio sources will be one of the methods employed by radio interferometers

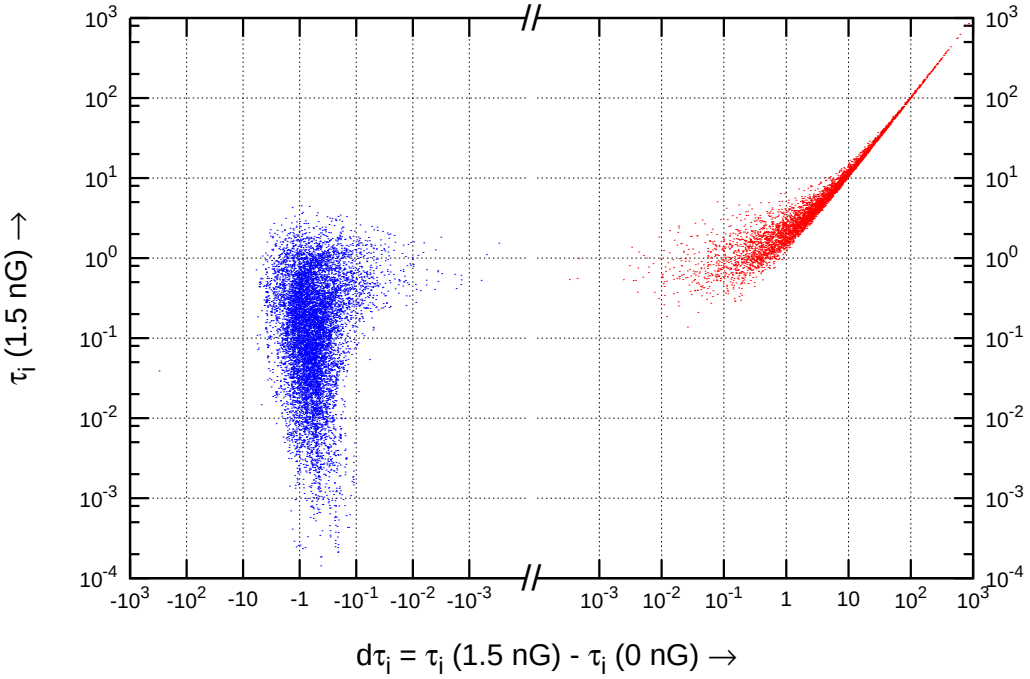

Figure 5.8: Distribution of τ_i $(1.5\ \mathrm{nG})$ vs $d\tau_i$ $(= \tau_i\ (1.5\ \mathrm{nG}) - \tau_{\mathrm{i}}\ (0\ \mathrm{nG}))$ at redshift $z = 4$.

LOFAR (Low-Frequency Array) and Square Kilometer Array (SKA) to attempt to detect cosmic magnetic fields. In particular, Blasi et al. (1999) considered the same physical setting (high redshift Lyα clouds) as in this paper. They computed the RM of Lyα density field and obtained bounds $\simeq 10^{-8}\,\mathrm{G}$ on magnetic fields with coherence length scales of the thermal Jeans length.

In addition to the upper bounds on the magnetic field strength obtained by these observables, recent results suggests that there might be a lower bound of $\simeq 10^{-15}\,\mathrm{G}$ on the magnetic field strength (e.g. Dolag (2010); Neronov & Vovk (2010); Tavecchio et al. (2010); Taylor et al. (2011)). Another lower bound is obtained from the study of echo emission from the blazar Mrk 501 (Takahashi et al. (2012)) which suggests magnetic field strength of $B_0 \gtrsim 10^{-20}G$ coherent over the length scale of ~ 1 kpc. This would suggest that the magnetic field strength could lie in the range $10^{-20} < B_0 <$ a few $10^{-9}\,\mathrm{G}$. This range is still too large for a better determination of the magnetic field strength.

In Figure 5.9, we show the constraints from the present study compare with similar constraints from cosmological gravitational lensing we obtained earlier (Pandey & Sethi (2012)). In Comparison to bounds on primordial magnetic fields from CMBR anisotropies (e.g. Figure 1 of Yamazaki et al. (2010)), for the entire range of spectral index, we obtain stronger limits on B_0. Other constraints from bispectrum and trispectrum analysis of

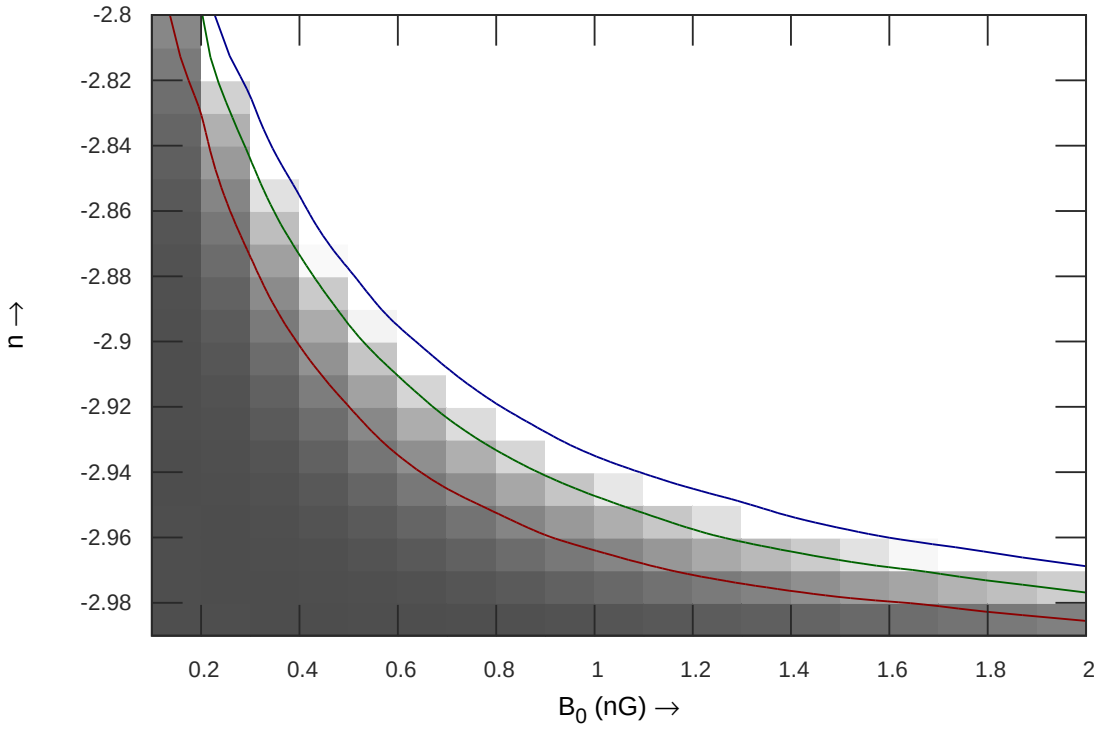

Figure 5.9: Allowed (the shaded) region in the (B_0, n) plane, based on the χ^2 analysis of $\tau_{\rm eff}$ against the data from Faucher-Giguère et al. (2008). The three curves (from top to bottom) are contours at the 5σ, 3σ and 1σ levels.

CMBR passive scalar modes Trivedi et al. (2010, 2012) are 2.4 nG and 0.7 nG, they have used spectral index value $n = -2.8$, whereas for $n = -2.8$ our analysis gives an upper bound on $B_0 \lesssim 0.3$ nG (Figure 5.9). As noted above, these bounds are even better than our previous analysis with the weak-lensing data (Figure 5.10).

In our present analysis, we consider four parameter: J, γ, B_0, and n but no other cosmological parameters. We also do not account for errors arising from different realizations of the density field. Our current bounds can be further improved by the inclusion of such effects. We note that even though the magnetic field signal could be degenerate with the overall normalization of the ΛCDM model as measured by σ_8, the current errors on the value of σ_8 (WMAP 7-year data give $\sigma_8 = 0.801 \pm 0.030$ (Larson et al., 2011)) are too small to sufficiently alter our conclusions.

In sum: Lyα clouds provide a sensitive probe of the matter power spectra at scales

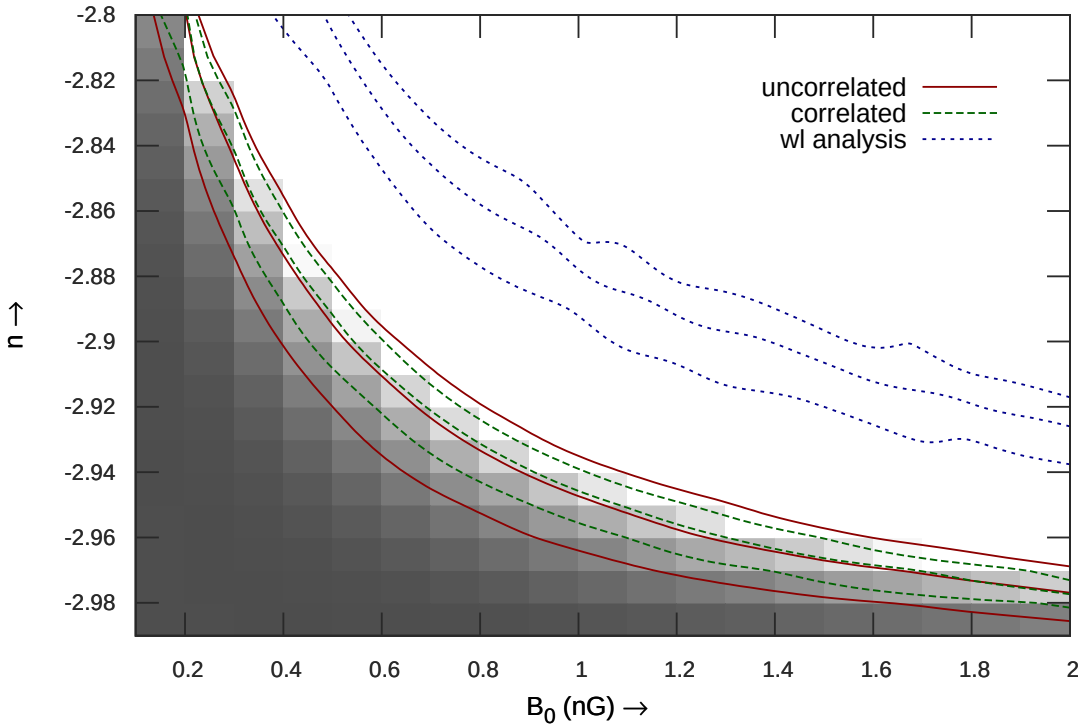

Figure 5.10: Contour of $\Delta\chi^2 = \chi^2_{\rm i} - \chi^2_{\rm min}$ for the present analysis (the lower triplets, solid ones correspond to 1 σ, 3 σ and 5 σ levels for the uncorrelated case, the dashed ones are the same for the correlated case) and the previous analysis (the upper triplet) on (B_0, n) plane.

$\lesssim 1\,\mathrm{Mpc}$. Primordial magnetic field induced matter perturbations give additional power at these scale which can be probed using the redshift evolution of $\tau_{\rm eff}$. Our results shows that this leads to one of the most stringent bounds on the parameters of primordial magnetic fields. These bounds can be further improved by more data on the evolution of $\tau_{\rm eff}$ at low redshifts and also more precise data at higher redshifts. Recently, Becker et al. (2012) have provided a measurement of the evolution $\tau_{\rm eff}$ which is in agreement with the data we have used (Faucher-Giguère et al. (2008)) for our analysis but claims better precision. In future, similar analysis with such data can give even more stringent constraints on the parameters of primordial magnetic fields.

6 Conclusion

The Following sections briefly describe the motivation, the groundworks, the main results of this thesis work and their relevance. This chapter also discuss the current status of this field of research and in particular the contribution and possible future prospects of this thesis work.

6.1 The Motivation And The Groundworks

From previous studies it is known that the presence of primordial magnetic fields during pre-recombination era could generate extra matter perturbations (over and above inflationary matter perturbations) in the universe. In the matter power spectrum this contributes appreciably as an additional power at smaller scales (k $\sim$ 1 - 10 h/Mpc) (Wasserman, 1978; Kim et al., 1996; Gopal & Sethi, 2003). Presence of sufficiently strong magnetic fields can even lead to heating of the ambient medium via ambipolar diffusion and magnetic field decay due to decaying turbulence (Sethi & Subramanian, 2005) and therefore affect the structure formation as thermal history plays a crucial role in structure formation processes. In other words primordial magnetic fields could play an important role in the formation of the first structures in the universe. The formation of the first structures in the universe has several other implications also, such as reionization Sethi & Subramanian (2005) of the universe. Moreover, since the existence of the primordial magnetic fields can influence the matter distribution in the universe, the cosmological probes of the matter distribution in the universe are expected to have signatures of the existence of primordial magnetic fields. Using these observables we can actually probe the existence of primordial magnetic fields or put bounds on the physical parameters related to them. To study

the effects of primordial magnetic fields quantitatively, one needs to know the strength and the other parameters of primordial magnetic fields with certain amount of accuracy. Therefore it is necessary to probe the magnetic fields with more and more accuracy. These were some of the main motivations behind this thesis work.

This thesis work is mostly based on the earlier works in this field of cosmology (effects of primordial magnetic fields on early structure formation) such as Wasserman (1978); Kim et al. (1996); Sethi (2003); Gopal & Sethi (2003, 2005); Sethi et al. (2008); Sethi & Subramanian (2005). My first project was to investigate the possible role of PMF in the formation of supermassive black holes (Chapter 2 of this thesis). Rest of thesis work was towards finding bounds on PMF from various cosmological observables (Chapter 3, 4 and 5 of this thesis). Chapter wise summary and results of my thesis work is as follows,

6.2 Thesis Work

6.2.1 Early formation of supermassive black holes

This work is about the investigation of possible role of primordial magnetic field to solve the puzzle of the formation of early super massive black holes posed by some SDSS observations of early ($z \simeq 6$) bright quasars. Many models have been proposed to solve this mystery based on super-Eddington accretion or hierarchal merger models. All the models make very optimistic assumptions and have their own share of problems. Presence of magnetic field also affects the course of thermal and dynamical evolution of collapsing gas because of ambipolar diffusion and dissipation of the magnetic fields. Our work suggests that if the magnetic field strength is above a critical value ($\sim$ 3.5 nG), it can actually lead to the formation of more massive stars $\simeq 10^4$ $M_\odot$. The black holes left behind after the death of these stars will have enough time to accrete gas to become a 10^8 $M_\odot$ SMBH by the redshift of 6-8. This model avoids many of the odd assumptions which are required in other models (Chapter 2). Though this model requires a larger magnetic field value than the available bounds on primordial magnetic fields and relies on metal-free primordial gas, these value of magnetic fields are allowed under $\sim$ 2-3 σ upward fluctuation of the Gaussian random PMF which is sufficient to account for the number high redshift quasars observed. Metal-free gas is not a bad assumption for the primordial gas at the redshift of $z \sim 15$. Over all this model presents a plausible novel mechanism to form high redshift supermassive black holes.

6.2.2 Primordial magnetic field limits from cosmological data

In this work we have studied the limits on primordial magnetic field coming from various cosmological probes such as, Faraday rotation of Cosmic Microwave Background (CMB) polarization plane and statistics of large scale structures in the universe. The presence of primordial magnetic field during recombination causes a rotation of the CMB polarization plane through the Faraday effect. The rotation angle is proportional to the magnetic field strength. Primordial magnetic field can also induce formation of structures in the Universe. Unlike the ΛCDM matter power spectrum, the magnetic field induced matter power spectrum increases at small scales (until a cut-off at magnetic Jeans scale) and it plays an important role in the formation of the first structures in the Universe also. The smallest structure to collapse at $z \simeq 10$ in the ΛCDM model are 2.5σ fluctuations of the density field as opposed to the magnetic field case where 1σ collapse is possible (Figure 3.3). This means the number of collapsed halo is more abundant in the later case. WMAP results suggests that the Universe reionized at z = 10. Comparing this with the results shown in the Figure 3.3 most of the model with different spectral index can be ruled out. Only the nearly scale invariant models with $n_B \simeq -3$ do not put strong constraint on the magnetic field strength. After doing all these analysis in this work we find that the range of the acceptable values of magnetic field strength is 1-3 nG. Figure 3.4 gives a rough sense of the acceptable range of $B_{\rm eff}$ over the entire range of n_B.

6.2.3 Probing primordial magnetic fields using weak lensing

In this work we have calculated a theoretical estimate of shear power spectrum and the shear correlation functions, taking into account the effect of primordial magnetic fields on matter power spectrum. Comparing this result with the CFHTLS weak lensing data (Fu et al., 2008), we have found limits on primordial magnetic fields which are much stronger ($\sim$ 0.5 nG for the spectral index value $n_B = -2.8$ under the confidence level of 5σ, Figure 4.7) in comparison to the existing limits on primordial magnetic fields coming from CMB data. Future proposed space missions are likely to improve the errors on these measurements, given that we can hope that SNAP would easily be able to probe magnetic fields with even greater precision.

6.2.4 Probing primordial magnetic fields using Lyα clouds

This work is an extension of the previous work, with the same motive but this time the observable is the line of sight distribution of Lyα clouds. We have simulated one dimensional

distribution of Lyα absorbers along the line of sight and calculated effective Lyα opacity as function of redshift. Using observed data of effective Lyα opacity from Faucher-Giguère et al. (2008) we have calculated bounds on primordial magnetic field, which turned out to be even stronger than our previous estimates ($B_0 \sim 0.2 - 0.3$ nG for n_B = -2.8 with the confidence level of 5σ). In this analysis we have considered two cases, one when the magnetic field induced perturbations are uncorrelated with inflationary perturbations, and the other is when they are correlated, though the final results (bounds on B_0) are not very different for both the cases (Figure 5.10). These bounds can be further improved by more data on the evolution of $\tau_{\rm eff}$ at low redshifts and also more precise data at high redshift. In this analysis we have consider four parameters namely, photoionization flux J, polytropic index γ, B_0 & n_B.

Overall this thesis investigates the possible role of primordial magnetic fields in early structure formation and attempts to constrain the primordial magnetic fields using several kinds of cosmological observables. The bounds coming from weak lensing and Lyα observables are stronger than the other bounds available in literature e.g., the bounds coming from the study of CMB anisotropies (Yamazaki et al., 2010; Kahniashvili & Ratra , 2005; Kahniashvili et al., 2010; Seshadri & Subramanian, 2009; Trivedi et al., 2010, 2012), and the bounds coming from the rotation measure (RM) of high redshift polarized radio sources (Kolatt, 1998; Sethi, 2003; Blasi et al., 1999). Most of these bounds are in the range of a few to a few tens of nano-Gauss, for example if we see the CMBR constraints shown in Figure 10 of Yamazaki et al. (2010) for entire range of spectral index $n_B > -2.95$ we obtain stronger upper limits on B_0. Similarly bispectrum and trispectrum analysis of CMBR passive scalar modes Trivedi et al. (2010, 2012) give upper bound values 2.4 nG and 0.7 nG ($n_B = -2.8$) respectively, whereas our weak lensing and Lyα analysis give stronger bounds such as 0.5 nG and 0.2 nG respectively.

In addition to the upper bounds on the magnetic field strength obtained by these observables, recent results suggests that there might be a lower bound of $\simeq 10^{-15}\,\mathrm{G}$ on the magnetic field strength (e.g. Dolag (2010); Neronov & Vovk (2010); Tavecchio et al. (2010); Taylor et al. (2011)). Another lower bound is obtained from the study of echo emission from the blazar Mrk 501 (Takahashi et al., 2012) which suggests magnetic field strength of $B_0 \gtrsim 10^{-20} G$ coherent over the length scale of ~ 1 kpc. This gives the cosmic magnetic field strength is in the range $10^{-20} < B_0 <$ a few $10^{-9}\,\mathrm{G}$. This range is still too large for a better quantitative determination of the impact of primordial magnetic field on cosmology.

A better understanding and measurement of early magnetic field is needed. We expect

that in future RM of radio sources obtained using the radio interferometers such as LOFAR and SKA will provide a better measurement of these magnetic fields Arshakian & Beck (2009). Future space missions such as SNAP can help providing better measurement of weak lensing shear and thus may provide a better probe for early magnetic fields. Similarly a better measurement of $\tau_{\rm eff}$ also can help improving the bounds on these magnetic fields.

Bibliography

Abel, T., Bryan, G. L., & Norman, M. L. 2002, Science, 295, 93

Albert, J. et al. 2005, astro-ph/0507460

Ando, S., & Kusenko, A. 2010, Astrophys. J. Lett., 722, L39

Arshakian, T. G., & Beck, R. 2009, The Low-Frequency Radio Universe, 407, 33

Athreya, R. M., Kapahi, V. K., McCarthy, P. J., & van Breugel, W. 1998, A&A, 329, 809

Barkana, R., Haiman, Z., & Ostriker, J. P. 2001, Astrophys. J., 558, 482

Barrow, J. D., Ferreira, P.G., & Silk, J. 1997, Phys. Rev. Lett., 78, 3610

Bartelmann, M., Schneider, P. 2001, Physics Reports, 340, 291-472

Beck, R. Brandenburg, A. Moss D., Shukurow, A., Ruzmaikin, A., & Skoloff, D. D. 1996, AARA, 34, 155

Becker, G. D., Hewett, P. C., Worseck, G., & Prochaska, J. X. 2012, arXiv:1208.2584

Begelman, M. C. 2002, Astrophys. J., 568, L97

Begelman, M. C., Volonteri, M., & Rees, M. J. 2006, MNRAS, 370, 289

Begelman, M. C., Rossi, E. M., & Armitage, P. J. 2008, MNRAS, 387, 1649

Bi, H., Ge, J., & Fang, L.-Z. 1995, Astrophys. J., 452, 90

Bi, H., Davidson, Arthur F. 1997, Astrophys. J.497, 523

Birnboim, Y. & Dekel, A. 2003, MNRAS, 345, 349

Blasi, P., Burles, S., & Olinto, A. V. 1999, Astrophys. J. Lett., 514, L79

Bond, J. R., Efstathiou, G. 1984, ApJ, 285, L45-L48.

Bromm, V., Coppi, P. S., & Larson, R. B. 2002, Astrophys. J., 564, 23

Bromm, V., & Loeb, A. 2003, Astrophys. J., 596, 34

Bromley, J. M., Somerville, R. S., & Fabian, A. C. 2004, MNRAS, 350, 456

Caldwell, Robert R. & Motta, Leonardo 2011, Phys. Rev. D, 84, 123525

Capitelli, M., Coppola, C. M., Diomede, P., & Longo, S. 2007, A&A, 470, 811

Cattaneo, F. & Vainshtein, S. I. 1991, Astrophys. J.376, L21

Cen, R., & Ostriker, J. P. 1994, Astrophys. J., 431, 451

Choudhury, T. R., Srianand, R., & Padmanabhan, T. 2001, Astrophys. J., 559, 29

Choudhury, T. R., Padmanabhan, T., & Srianand, R. 2001, MNRAS, 322, 561

Cowling, T. G. 1956, MNRAS, 116, 114

Croft, R. A. C., Weinberg, D. H., Katz, Neal et al. 1998, Astrophys. J., 495, 44

Croft, R. A. C., Weinberg, D. H., Pettini, Max et al. 1999, Astrophys. J., 520, 1

Croft, R. A. C., Weinberg, D. H., Bolte, M., et al. 2002, Astrophys. J., 581, 20

Demozzi, V., Mukhanov, V., & Rubinstein, H. 2009, JCAP, 8, 25

Dijkstra, M., Haiman, Z., Mesinger, A., & Wyithe, J. S. B. 2008, MNRAS, 391, 1961

Dolag, K. 2010, Highlights of Astronomy, 15, 461

Durrer, R., Ferreira, P. G., & Kahniashvili, T. 2000, Phys. Rev. D, 61, 043001

Fan, X. 2006, New Astron. Rev., 50, 665

Faucher-Giguère, C.-A., Prochaska, J. X., Lidz, A., Hernquist, L., & Zaldarriaga, M. 2008, Astrophys. J., 681, 831

Finelli, F., Paci, F., & Paoletti, D. 2008, Phys. Rev. D, 78, 023510

Fu, L., Semboloni, E., Hoekstra, H., et al. 2008, A&A, 479, 9

Galli, D., & Palla, F. 1998, A&A, 335, 403

Giovannini, M., & Kunze, K. E. 2008, Phys. Rev. D, 77, 063003

Gnedin, N. Y., Ferrara, A., & Zweibel, E. G. 2000, Astrophys. J., 539, 505

Gopal, R., & Sethi, S. K. 2003, J. Astrophys. Astron., 24, 51

Gopal, R., & Sethi, S. K. 2005, MNRAS, 363, 521

Greenfield, P. E., Roberts, D. H., & Bruke, B. F. 1985, Astrophys. J., 293, 370

Haiman, Z., & Loeb, A. 2001, Astrophys. J., 552, 459

Heger, A., Fryer, C. L., Woosley, S. E., Langer, N., & Hartmann, D. H. 2003, Astrophys. J., 591, 288

Hoekstra, H., & Jain, B. 2008, Annual Review of Nuclear and Particle Science, 58, 99

Howard, A. M., & Kulsurd, R. M. 1997, Astrophys. J., 483, 648

Hoyle, F. 1958, *La Structure et L'evolution de L'universe*, 53

Hui, L., Gnedin, N. Y., & Zhang, Y. 1997, Astrophys. J., 486, 599

Jedamzik, K., Katalinić, V., & Olinto, A. V. 1998, Phys. Rev. D, 57, 3264

Jenkins, A., Frenk, C. S., White, S. D. M., et al. 2001, MNRAS, 321, 372

Kahniashvili, T., & Ratra, B. 2005, Phys. Rev. D, 71, 103006

Kahniashvili, T., & Ratra, B. 2007, Phys. Rev. D, 75, 023002

Kahniashvili, Tina; Ratra, Bharat 2005, Phys. Rev. D, 71, 103006.

Kahniashvili, Tina; Tevzadze, Alexander G.; Sethi, Shiv K.; Pandey, Kanhaiya; Ratra, Bharat 2011, Phys. Rev. D, 82, 083005

Kahniashvili, T., Tevzadze, A. G., & Ratra, B. 2011, Astrophys. J., 726, 78

Kim, K.-T., Kronberg, P. P., Dewdney, Giovannini, G., & Venturi, T. 1989, Nature, 341, 720

Kim, K.-T., Kronberg, P. P., Dewdney, P. E., Landecker . T. L. 1990, Astrophys. J., 355, 29

Kim, K.-T., Tribble, P. C., & Kronberg, P. P. 1991, Astrophys. J., 379, 80

Kim, E.-J., Olinto, A. V., & Rosner, R. 1996, Astrophys. J., 468, 28

Kolatt, T. 1998, Astrophys. J., 495, 564

Komatsu, E., Dunkley, J., Nolta, M. R., et al. 2009, ApJS, 180, 330

Komatsu, E., Smith, K. M., Dunkley, J., et al. 2011, ApJS, 192, 18

Kosowsky, A., & Loeb, A. 1996, Astrophys. J., 469, 1

Kosowsky, A., Kahniashvili, T., Lavrelashvili, G., & Ratra, B. 2005, Phys. Rev. D, 71, 043006

Koushiappas, S. M., Bullock, J. S., & Dekel, A. 2004, MNRAS, 354, 292

Krause, F. & Rädler, K.-H. 1980, ”Mean Field Magnetohydrodynamics and Dynamo Theory” (Pergmon Press, Oxford)

Kronberg, P. P., Perry, J. P., & Zukowski, E. L. H. 1991, Astrophys. J., 379, 80

Kulsurd, R. M. 1999, AARA, 37, 37

Larson, D., Dunkley, J., Hinshaw, G., et al. 2011, ApJS, 192, 16

Lewis, A. 2004, Phys. Rev. D, 70, 043011

Li, Y., Hernquist, L., Robertson, B., et al. 2007, Astrophys. J., 665, 187

Lodato, G., & Natarajan, P. 2006, MNRAS, 371, 1813

Mack, A., Kahniashvili, T., & Kosowsky, A. 2002, Phys. Rev. D, 65, 123004

Maki, H., & Susa, H. 2004, Astrophys. J., 609, 467

Maki, H., & Susa, H. 2007, PASJ, 59, 787

Martin, P. G., Schwarz, D. H., & Mandy, M. E. 1996, Astrophys. J., 461, 265

Martini, P. 2004, Coevolution of Black Holes and Galaxies, 169

Mofatt, H. K. 1978, ”Magnetic Field Generation in Electrically Conducting Fluids, Cambridge Univ. Press, Cambridge”

Moss, D., & Shukurov, A. 1996, MNRAS, 279, 229

Munshi, D., Valageas, P., van Waerbeke, L., & Heavens, A. 2008, Phys. Rep., 462, 67

Neronov, A., & Vovk, I. 2010, Science, 328, 73

Oh, S. P., & Haiman, Z. 2002, Astrophys. J., 569, 558

Ohsuga, K., Mori, M., Nakamoto, T., & Mineshige, S. 2005, Astrophys. J., 628, 368

Omukai, K., Schneider, R., & Haiman, Z. 2008, Astrophys. J., 686, 801

Omukai, K. 2001, Astrophys. J., 546, 635

Pandey, Kanhaiya L. & Sethi, Shiv K. 2012, Astrophys. J., 748, 1

Parker, E. N. 1979, Cosmical Magnetic Fields (Oxford: Clarendon)

Piddington, J. H. 1964, MNRAS, 128, 345

Piddington, J. H. 1972, Cosmic Electrodynamics, 128, 345

Peacock, J. A., Dodds, S. J. 1996, MNRAS, 280, L19-L26.

Principles of Physical Cosmology by P.J.E. Peebles. Princeton University Press, 1993. ISBN: 978-0-691-01933-8

Ratra, B. 1992, Astrophys. J. Lett., 391, L1

Regan, J. A., & Haehnelt, M. G. 2009, MNRAS, 396, 343

Rephaeli, Y. Ulmer, M. & Gruber, D. 1994 Astrophys. J., 429, 554

Refregier, A. 2003, ARAA, 41, 645

Ruzmaikin, A. A., Shukurow, A. M., & Sokoloff, D. D. 1988, Magnetic Fields in Galaxies (Dordrecht: Kluwer)

Schaerer, D. 2002, A&A, 382, 28

Schleicher, D. R. G., Banerjee, R., Klessen R. S. 2009, ApJ, 692, 236

Schleicher, D. R. G., Galli, D., Glover, S. C. O., et al. 2009, Astrophys. J., 703, 1096

Schrabback, T., et al. 2010, A&A, 516, A63.

Schleicher, D. R. G., & Miniati, F. 2011, MNRAS, 418, L143

Seshadri, T. R., & Subramanian, K. 2001, Physical Review Letters, 87, 101301

Seshadri, T. R., Subramanian, K. 2009, Phys. Rev. Lett.103, 081303.

Sethi, S. K. 2003, MNRAS, 342, 962

Sethi, S. K. 2003, MNRAS, 342, 962

Sethi, S. K., & Subramanian, K. 2005, MNRAS, 356, 778

Sethi, S. K., Nath, B. B., Subramanian, K. 2008, MNRAS, 387, 1589.

Sethi, S. K., Subramanian, K. 2009, JCAP, 11, 21.

Sethi, Shiv, Haiman, Zoltan, Pandey, Kanhaiya 2010, ApJ, 721, 615.

Shang, C., Bryan, G. L., & Haiman, Z. 2010, MNRAS, 402, 1249

Shapiro, S. L. 2005, Astrophys. J., 620, 59

Shu, F. H. 1992, The physics of astrophysics. Volume II: Gas dynamics., by Shu, F. H.. University Science Books, Mill Valley, CA (USA), 1992, 493 p., ISBN 0-935702-65-2

Spaans, M., & Silk, J. 2006, Astrophys. J., 652, 902

Sreekumar, P. et al.1996, Astrophys. J., 464, 629

Steenback, M., Krause, F., & Rädler, K.-H. 1966, *Zs. f. Naturforschung* 21, 369

Subramanian, K. , & Barrow, J. D. 1998, Phys. Rev. D, 58, 083502

Subramanian, K., & Barrow, J. D. 2002, MNRAS, 335, L57

Takahashi, K., Mori, M., Ichiki, K., Inoue, S. 2012, Astrophys. J., 744, L7.

Tanaka, T., & Haiman, Z. 2009, Astrophys. J., 696, 1798

Tashiro, H., Sugiyama, N. 2006, MNRAS, 368, 965.

Tavecchio, F., Ghisellini, G., Foschini, L., et al. 2010, MNRAS, 406, L70

Taylor, A. M., Vovk, I., & Neronov, A. 2011, A&A, 529, A144

Trivedi, Pranjal, Subramaniyan, K., Seshadri, T. R. 2010, Phys. Rev. D, 82, 123006

Trivedi, Pranjal, Seshadri, T. R., Subramaniyan, K. 2012, Phys. Rev. Lett., 108, 23

Turk, M. J., Abel, T., & O'Shea, B. 2009, Science, 325, 601

Turner, M. S., & Widrow, L. M. 1988, Phys. Rev. D, 37, 2743

Volonteri, M., & Rees, M. J. 2005, Astrophys. J., 633, 624

Volonteri, M., & Rees, M. J. 2006, Astrophys. J., 650, 669

Volonteri, M., Lodato, G., & Natarajan, P. 2008, MNRAS, 383, 1079

Volonteri, M. 2010, A&A Rev., 18, 279

Wasserman, I. 1978, Astrophys. J., 224, 337

Widrow, L. M. 2002, Reviews of Modern Physics, 74, 775

Wise, J. H., Turk, M. J., & Abel, T. 2008, Astrophys. J., 682, 745

Yamazaki, D. G., Ichiki, K., Kajino, T., & Mathews, G. J. 2006, Astrophys. J., 646, 719

Yamazaki, D. G., Ichiki, K., Kajino, T., & Mathews, G. J. 2008, Phys. Rev. D, 77, 043005

Yamazaki, D. G., Ichiki, K., Kajino, T., & Mathews, G. J. 2008, Phys. Rev. D, 78, 123001

Yamazaki, D. G., Ichiki, K., Kajino, T., & Mathews, G. J. 2010, Phys. Rev. D, 81, 023008

Yamazaki, D. G., Ichiki, K., Kajino, T., Mathews, G. J. 2010, Advances in Astronomy, 2010, 586590

Yoo, J., & Miralda-Escudé, J. 2004, Astrophys. J. Lett., 614, L25

Yoshida, N., Omukai, K., & Hernquist, L. 2008, Science, 321, 669

Zel'dovich, Ya. B., Ruzmaikin, A. A., & Sokoloff, D. D. 1983, "Magnetic Fields in Astrophysics, Gordon & Breach, New York

Zweibel, E. G., & Heiles, C. 1997, Nature, 385, 131